Design and Fabrication of Organic Radical Battery with TEMPO-Bearing Polymethacrylate Cathode for a New Power Source

新規電源創出のための TEMPO側鎖ポリメタクリレート正極を用いた 有機ラジカル電池の設計と作製

July 2011

Waseda University
Graduate School of Advanced Science and Engineering
Major in Applied Chemistry, Research on Polymer Science

Kentaro NAKAHARA

中原 謙太郎

Preface

Rechargeable batteries are one of the great successes of modern chemistry. These batteries have enriched people's life by offering convenient, easily usable, and mobile energy sources during a century. For the green and sustainable society in the future, the batteries will soon widen their appeals as the clean automotive energy sources and the core of renewable energy systems. Furthermore, the potential of the batteries make it possible to expand their application fields to space, robotics, and medical technologies.

However, on March 11th 2011, a big earthquake suddenly destroyed our peaceful life. The followed nuclear plant crisis threatened our nation. I deeply express my regret over the many persons who lost lives in the natural disaster. At the same time, the disaster let me learn the powerlessness of human's wisdom. Coincidentally, it is decided to make the year 2011 "The International Chemistry Year" in commemoration of madam curie's 100th Nobel Prize winning anniversary. The theme of the event is "Chemistry - our life, our future". It is a good chance for looking back modestly the greatness of chemistry. I believe that chemistry will play important roles for creating ideal society for the future.

This thesis mainly describes the performances of the rechargeable battery using a nitroxyl radical polymer as a cathode active material. The author first proposed the applicability of organic polymers bearing robust unpaired electrons for the electrochemical redox reactions of rechargeable batteries. Such an "Organic Radical Battery" would be environmentally friendly and have high-power characteristics. The electron transfer mechanism and recent developments that should lead to the practical application of the organic radical battery are also reviewed in the thesis. I desire to let this study contribute to the advancement of the chemistry even a little.

Kentaro Nakahara

Index

5. Cell Performances of Organic Radical Battery with PTMA/Carbon Composite Cathode

6. Improvement of High-Rate Capability in Organic Radical Battery

7. Fabrication of Organic Radical Batteries for Practical Applications

8. Future Perspectives

Chapter 1
General Introduction

1.1. Lithium-ion Battery

1.1.1. Lithium-ion Battery for Sustainable Society

Market of lithium-ion battery

Lithium-ion batteries are widely used power sources for consumer electronics such as cellular phones and laptop computers because of their high specific energy, high efficiency, and long life.[1,2,3,4,5] Markets of these batteries are recently expanding to the applications of electric vehicles and renewable energy resources (Fig. 1.1)[4]. However, scale-up technologies of lithium-ion battery used for these huge markets are holding many problems, such as safety, quality, and cost. The science underlying lithium-ion battery is extremely important for the future, because sustainable society will be achieved only by using clean energy sources, which is brought by spreading lithium-ion batteries.

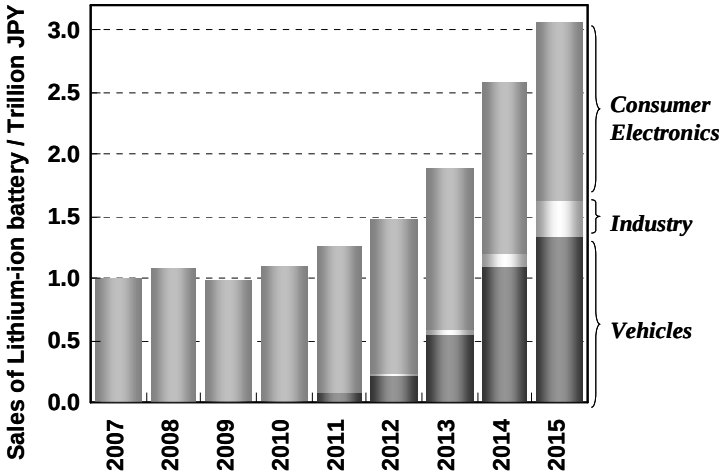

Figure 1.1 World sales of the lithium-ion battery.

General chemistry of lithium-ion battery

A lithium-ion battery typically contains a graphite anode (e.g. artificial graphite, natural graphite), a cathode formed by a lithium transition metal oxide (e.g. $LiCoO_2$, $Li_{1+x}Mn_2O_4$), and an electrolyte consisting of a solution of a lithium salt (e.g. $LiPF_6$, $LiBF_4$) in a mixed organic solvent (e.g. ethylene carbonate/diethyl carbonate, EC/DEC, propylene carbonate/ethylene carbonate/dimethyl carbonate, PC/EC/DMC) imbedding in a micro-pored film separator (Fig. 1.2). The electrochemical process of lithium-ion battery is based on the reversible exchange of lithium ion between the two

electrodes. The process involves the reversible extraction and insertion of lithium ions between two electrodes with a concomitant removal and addition of electrons as shown below chemical equation:

$yC + LiCoO_2 \leftrightarrow Li_xC_y + Li_{1-x}CoO_2$, x~0.5, y=6

Lithium-ion batteries are characterized by light, compact and work with a voltage of the order of 4V with a specific density around 200 W h kg^{-1}.

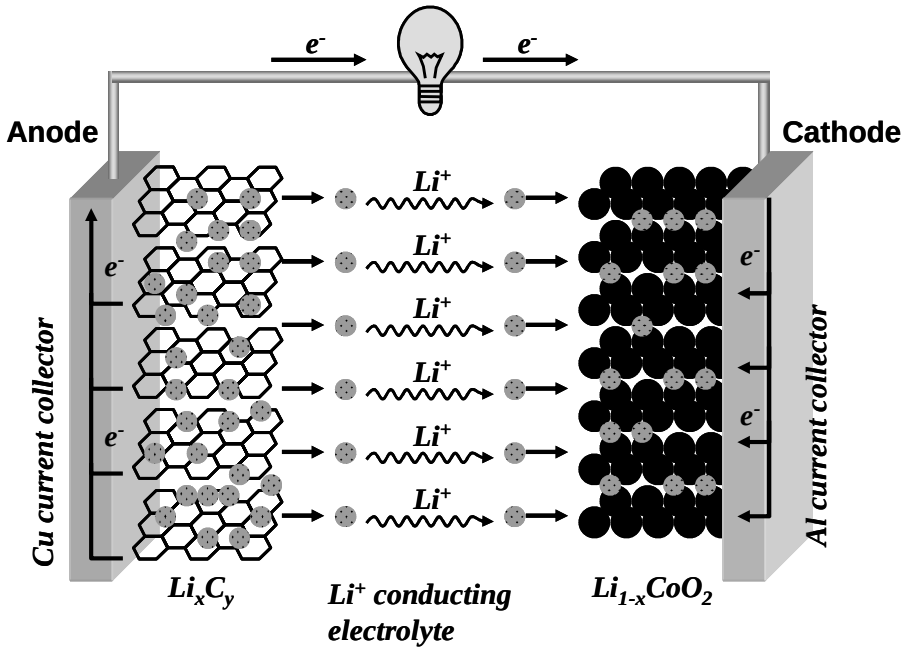

Figure 1.2 Scheme of a common lithium-ion battery.[4]

1.1.2. Anode active materials

Carbon-based materials

Since the electrochemical window of a carbonate-based electrolyte was known to be 0.8-4.5 V vs. Li/Li^+, the lithium-ion battery with a graphite anode, which reacts at 0.1 V vs. Li/Li^+, was concluded to be thermodynamically unstable (Fig. 1.3).[4] However, it was found that the initial decomposition of carbonate-based electrolyte results in the formation of a protective solid electrolyte interphase (SEI) on the graphite anode surface. In June 1991, Sony Corporation commercialized the first lithium-ion battery having the voltage of 3.6 V with gravimetric energy density of 120-150 W h kg^{-1}. A key technology for the commercialization is known as the combination of a carbonate-based electrolyte and a carbon-based anode supported by the SEI formation.

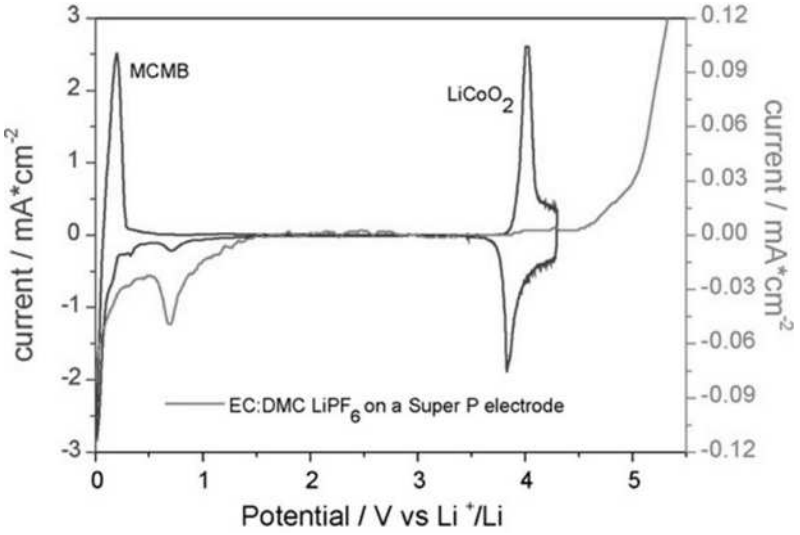

Figure 1.3 Cyclic voltammetry profiles (potential vs. Li/Li^+) of lithium ion battery components: artificial graphite anode, lithium cobalt oxide cathode, and carbonate-based electrolyte.[4]

Billion of lithium-ion batteries are today being manufactured per year. In the batteries, three types of carbon-based materials are mainly employed as anode active materials: artificial graphite, natural graphite, and hard carbon materials. Artificial graphite (e.g. mesocarbon microbeads, MCMB) is expensive though it demonstrates good performance. Natural graphite is cheaper than artificial graphite, though it shows worse performance. Hard carbon materials bring large irreversible capacity although the materials achieve higher specific capacity and rate capability than graphite. It is today very important to employ or mix them properly according to the application.

Lithium alloys

Lithium metal alloys, such as lithium-silicon (Li-Si) and lithium-tin (Li-Sn) are the most promising anode active materials to replace conventional carbon-based materials (Table 1.1).[6] These alloys have a theoretical capacity of 4200 mA h g^{-1} (Li-Si) and 994 mA h g^{-1} (Li-Sn), those largely exceed that of 372 mA h g^{-1} for graphite. Unfortunately, because both Li-Si and Li-Sn alloys cause large volume change which occurs during extraction and insertion of lithium ions, these alloys can not demonstrate applicable cyclability.

Table 1.1 Comparison of the specific capacity, volume change, and onset potential of various anode materials.[6]

Materials	-	Li	C	$Li_4Ti_5O_{12}$	Si	Sn	Sb	Al
Density	g/cm^3	0.53	2.25	3.5	2.23	7.29	6.7	2.7
Lithiated phase	-	Li	LiC_6	$Li_7Ti_5O_{12}$	$Li_{4.4}Si$	$Li_{4.4}Sn$	Li_3Sb	LiAl
Specific capacity	mAh/g	3826	372	175	4200	994	660	993
Volume change	%	100	12	1	320	260	200	96
Potential vs Li	V	0	0.05	1.6	0.4	0.6	0.9	0.3

Lithium-silicon anode fabricated by a vacuum deposited process is reported to achieve a specific capacity over 2000 mA h g^{-1} with 500 cyclability.[7] Mesoporous lithium-tin anode is reported to be effective for the accommodation of volume change during charge/discharge process.[8] As the next step, it is recently requested for these lithium alloys to be demonstrated higher volumetric energy density, lower initial irreversible capacity, and cheaper material cost than graphite as a totally designed cell with the acceptable cyclability.

1.1.3. Inorganic cathode active materials

Conventional materials

So far, five materials have been commercialized mainly as a cathode active material for a lithium-ion battery: lithium cobalt oxide ($LiCoO_2$), cobalt-doped lithium nickel-manganese oxide ($LiNi_{0.5-x}Co_{2x}Mn_{0.5-x}O_2$), cobalt-, aluminum-co-doped lithium nickel oxide ($LiNi_{1-x-y}Co_xAl_yO_2$), lithium manganese oxide ($LiMn_2O_4$), and lithium iron phosphate ($LiFePO_4$). Lithium transition metal oxides with layered rock salt crystal structure, such as $LiCoO_2$, $LiNi_{0.5-x}Co_{2x}Mn_{0.5-x}O_2$, and $LiNi_{1-x-y}Co_xAl_yO_2$, are normally used for consumer electronics applications because of their high specific density over 140 mA h g^{-1} with good cell performances. However, these lithium metal oxides are not suitable for electric vehicle applications because they are expensive. Lithium manganese oxide with spinel structure ($LiMn_2O_4$) is today being used for electric vehicles. Although the lithium manganese oxide causes poor cyclability and thermal stability, the lower cost and higher safety than the other lithium oxides are promising.

Lithium iron phosphate with olivine structure is attractive especially in US and China, though it has lower energy density.

High voltage materials

The energy density of lithium-ion battery has been increased mainly by the optimization of the cell design such as to increase the loading of active materials. However, since such a manufacturing improvement is facing to the limit of the energy density, innovations of the cell chemistry are today widely required. Lithium nickel manganese oxide with spinel structure ($LiNi_{0.5}Mn_{1.5}O_4$) is characterized by a high flat voltage around 4.5 V vs. Li/Li^+ with the specific capacity of 146 mA h g^{-1} (Fig. 1.4).[9] The high operational voltage potentially increases the energy density by 30% more than that of conventional lithium manganese oxide with spinel structure. Similar attention is also focuses on alternate olivine phosphate such as $LiMnPO_4$ and $LiCoPO_4$.[10] The practical use of these high voltage cathodes may be prevented by the lack of suitable electrolyte, since the conventional carbonate-based electrolytes are not totally compatible with the voltage over 4.5 V vs. Li/Li^+. Development of a stable electrolyte against high voltage is also required so that to make the innovative cathode acceptable for commercial use.

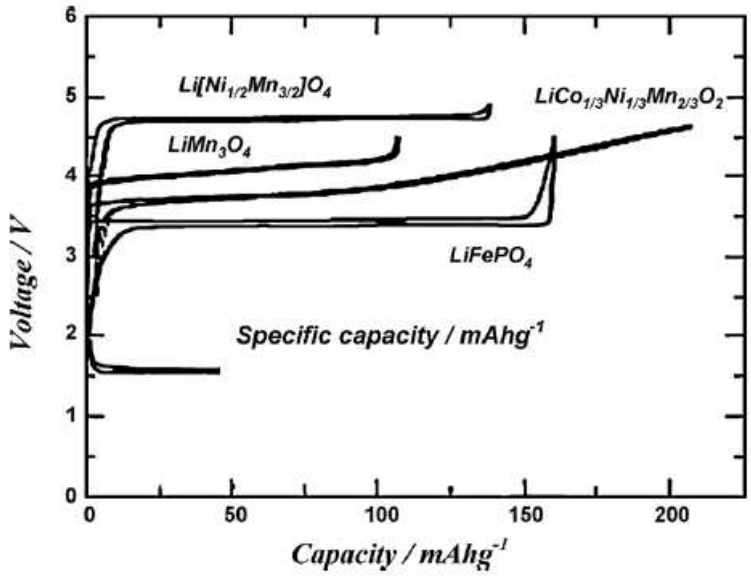

Figure 1.4 Charge-discharge profiles of various lithium metal oxides and a lithium iron phosphate.[4]

High specific capacity materials

Lithium-rich layered oxide such as Li_2MnO_3 and its solid solutions are attractive candidate for replacing conventional cathode active materials.[11,12,13] It is recently reported that Li_2MnO_3-$LiMO_2$ (M=Ni, Mn, Co etc.) exhibits a high specific capacity of more than 200 mA h g^{-1} with the operational voltage of 4.6 V vs. Li/Li^+ (Fig. 1.5). Although this kind of large capacity oxide still has poor cyclability problems, many efforts are making the durability high for practical applications.

New research directions of cathode active materials are recently reported for high specific capacity. Lithium fluorophosphates[14] (e.g. Li_2MPO_4F) and lithium silicates[15] (e.g. Li_2MSiO_4) are expected to exchange two electrons per mole of transition metal. In addition, conversion process is proposed to achieve from two to six electron transfer per mole of transition metals. Although these multi-electron reactions have not been realistic today, a constant development of the materials is necessary for the high energy density of the future.

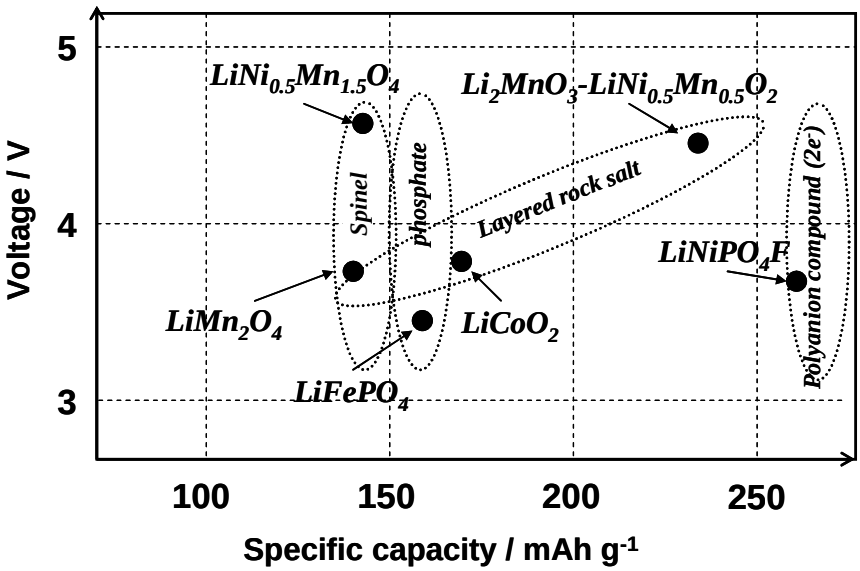

Figure 1.5 Operating voltage vs. specific capacity of inorganic cathode active materials.

1.1.4. Organic cathode active materials

Conducting polymers

The use of organic materials as a cathode active material appears promising to design environmentally friendly rechargeable battery. Conducting polymers, such as polyacetylene, polypyrol, and polyaniline, were examined as a cathode active material of a lithium battery (Fig. 1.6). These polymers demonstrate reversible doping/undoping redox reaction with the theoretical energy density of 200-400 mW h g^{-1}.[16] However, the excitons of conducting polymers generated by the electrochemical redox reaction are generally delocalized over a wide –electron conjugated system, interacting with one another, which causes problems with limiting the doping level. For example, the doping level of polyacetylene is known to be only 7%. Polyaniline exhibits the highest doping level among conducting polymers, around 50% during reactions.

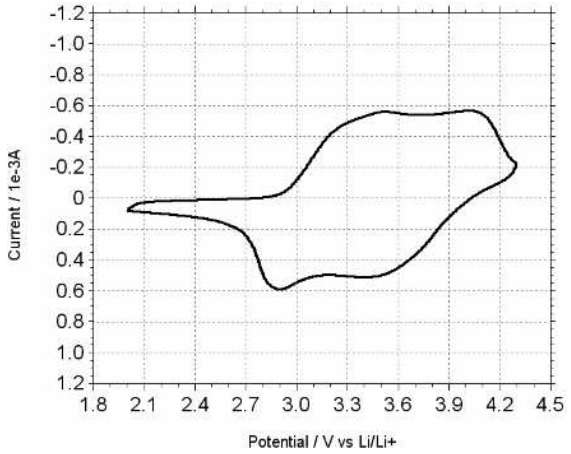

Figure 1.6 Cyclic voltammogram of polyaniline.

Disulfide compounds

A different approach for an organic cathode active material is the use of reversible redox cleavage of disulfide bond to give lithium thiolate (Fig. 1.7) [17]:

$$-SS- + 2Li^+ + 2e^- \leftrightarrow -SLi + LiS-$$

Depending on the molecular structure, the voltage can be up to 3V vs. Li/Li^+. The voltage is much higher than that of sulfur itself (2.4 V vs. Li/Li^+). It is reported that 2,5-dimercapto-1,3,4-thiadiazole (DMcT) has a theoretical capacity of 331 mA h g^{-1}. (Fig. 1.7) 17 In addition, the disulfide compound is low-cost and low-toxicity like conducting polymers. Furthermore, DMcT-polyaniline composite electrode is reported

to be effective for improving kinetics of the electrochemical reaction, which results in exhibiting initial operating voltage of 3.7 V vs. Li/Li^+.[18] Although promising in principle in terms of capacity and cost, disulfide compounds are presently prevented the practical use from the relative low density of the compounds and solubility of resulting thiolate into the electrolyte, leading to self-discharge.

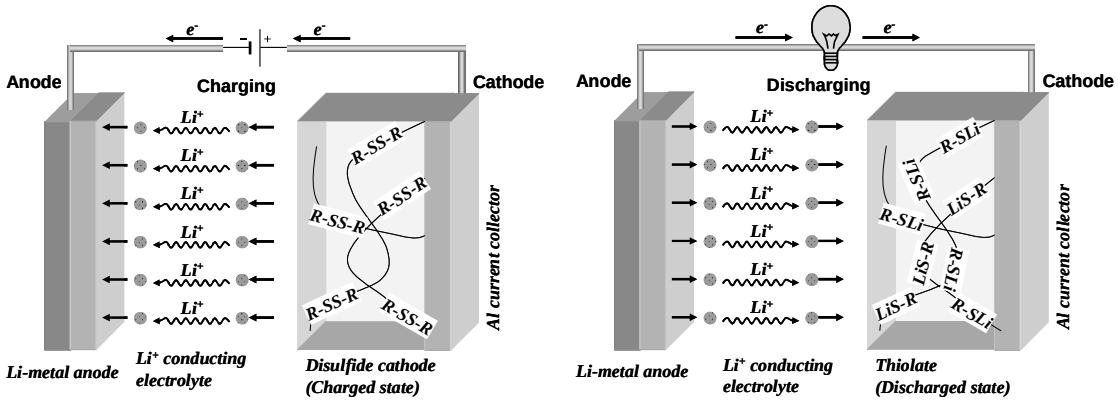

Figure 1.7 Scheme of a lithium-ion battery with disulfide cathode.

1.1.5. Electrolyte materials

Conventional materials

The electrolyte is the third component critical for the safety and durability of lithium-ion battery.[4] Carbonate-based conventional electrolyte is considered to have the problems, such as low stability, flammability, and incompatibility with the environment and human body. Many additives have been developed to improve safety by building-up stable SEI. Ionic liquids, such as 1-ethyl-3-methylimidazolium tetrafluoroborate ($EMIBF_4$), *N*-butyl-*N*-methylpipelidinium bis(trifluoromethanesulfonyl)imide (BMPTFSI), are examined as a nonflammable and non volatile electrolyte solvents for applying to decrease flammability. Lithium salts as an alternative to $LiPF_6$ are considered to reduce toxicity.

Solvent-free polymer electrolyte

Other approaches using lithium conducting polymer electrolytes are considered for improving safety and durability. Polymer electrolytes are expected to reduce flammability and prevent electrolyte from leaking. An ideal possibility is obviously that

the use of an all solid, solvent free-electrolyte. Although various polymers have been proposed, interest today concentrates on poly(ethylene oxide), PEO, hosting a lithium salt (Fig. 1.8). Chemical inertness and reasonably good lithium transport make PEO meet in principle the main requirements as efficient polymer electrolyte. Unfortunately, the ionic conductivity and electrochemical stability on the cathode surface have so far prevented their practical use.

Polymer gel electrolyte

As a realistic solution of intrinsic issues of solvent-free polymer electrolyte, solid-liquid hybrid electrolytes have been adopted for practical applications. In the system, typical liquid electrolyte, e.g. $LiPF_6$-mixed carbonates, is trapped in a polymer matrix, e.g. poly(acrylo nitrile), PAN or poly(vinylidene fluoride), PVdF, to form gel-type polymer electrolytes. The poly(vinylidene fluoride)-hexafluoropropylene, PVdF-HFP, based gel electrolyte pioneer the way of lithium-ion battery with polymer gel electrolytes. Polymer gel electrolytes achieved high conductivity, nearly matching that of liquid electrolyte, although the issues typically associated with the presence of the liquid can not be completely avoided. Nevertheless, Polymer gel electrolyte are practically applied by some battery manufactures for the fabrication of the so called "lithium-ion polymer battery".

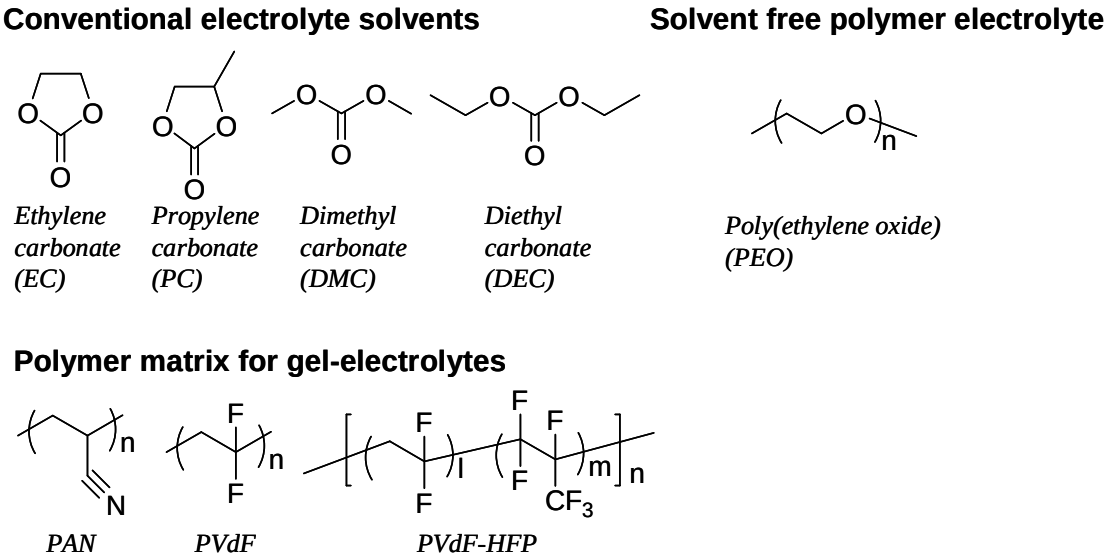

Figure 1.8 Electrolyte materials applied for lithium-ion battery.

1.2. Organic Radical Battery

1.2.1. Radical polymers

Radical polymers are the candidates for replacing the lithium transition metal oxide cathodes of the lithium-ion battery.[19,20,21,22] We call a polymer which has unpaired electrons the radical polymer. The disappearance of the unpaired electrons due to chemical bond formation can be suppressed by the precisely designed chemical structure through a combination of the resonance effect of the electrons and the sterically hindered effect of the substituent groups. Chemical groups such as nitroxyl, phenoxyl, and hydrazyl are robust structures with less-reactive unpaired electrons in the uncharged state.

Radical polymers show reversible redox electrochemical reactions in aprotic solutions.[19] Preparing a polymer composite electrode with carbon materials significantly enhances the electrochemical activity.[19,20] A previous study[19] showed that a lithium battery with a radical polymer composite cathode has an operating voltage of 3.5 V with cyclability comparable to that of a conventional lithium ion battery. We named this new battery "organic radical battery" (Fig. 1.9). The highest theoretical capacity of the radical polymers is 147 $mA \cdot h \cdot g^{-1}$,[23,24] which is comparable to the practical specific capacity of $LiCoO_2$ (140 $mA \cdot h \cdot g^{-1}$ [1,2]). The organic radical battery is a promising environmentally friendly and high-power rechargeable battery.[25]

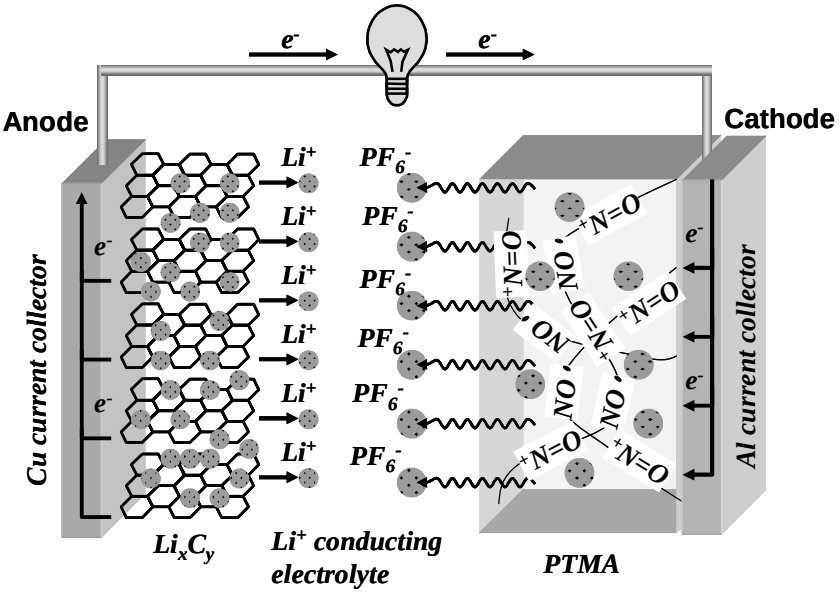

Figure 1.9 Scheme of a typical organic radical battery.

1.2.2. Nitroxyl radical polymers as cathode active materials

Most radical polymers consist of two main components: a robust radical pendant and a backbone polymer. For use in rechargeable batteries, a radical polymer must be robust over a long period of time, possess insolubility in but affinity to electrolyte, and support high energy density.

To be robust in an electrochemical cell for a long period of time, the unpaired electrons in the polymer must be less-reactive sufficiently in the electrolyte. This is an essential and difficult-to-achieve requirement for molecular design. Typical structures of the radical pendants are alicyclic nitroxyls such as TEMPO and PROXYL. For example, unpaired electrons in the TEMPO structure can survive for more than a year in aprotic solution containing 1.0 M lithium hexafluorophosphate ($LiPF_6$).

The structures of the backbone polymer affect insolubility in and affinity to the electrolyte. To prevent the radical polymer from contacting the opposite electrode, the polymer should be insoluble in the electrolyte. The polymer should also have affinity for the electrolyte to support the ionic conductivity. To date, various backbone polymers, such as polymethacrylate,[19,20] poly(vinyl ether),[36] polystyrene,[26,27] polyether,[23] polynorbornene,[28,29,30] polysiloxane,[31] polyacetylene,[32,33] cellulose,[34] and DNA complexes[35] have been reported. The polymer used must be dense in a thick electrode to obtain sufficient capacity. From the viewpoints of processability and mechanical strength, backbone polymers such as polymethacrylate, poly(vinyl ether), and polyether, are promising backbone structures for the radical polymers.

Radical polymers with alicyclic nitroxyl such as 2,2,6,6-tetramethylpiperidine-1-oxy (TEMPO) and 2,2,5,5-tetramethylpyrrolidine-1-oxy (PROXYL) in particular have been studied in detail.[19,20,21,22,36] Two previously synthesized nitroxyl radical polymers, poly (2,2,6,6-tetramethylpiperidine-4-yl-1-oxy methacrylate) (PTMA)[19,20] and poly(2,2,6,6-tetramethylpiperidine-4-yl-1-oxy vinyl ether) (PTVE)[36], are promising candidates because they provide sufficient stability, high voltage, and high specific capacity for battery use (figure 1.10).[19,20]

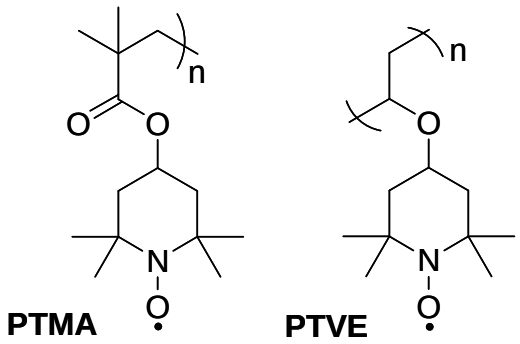

Figure 1.10 Molecular structures of PTMA and PTVE.

The energy density of a battery is represented by the product of the voltage and the capacity. The reaction voltage of radical polymers is affected by a type of redox reaction. Radical polymers cause two types of redox reactions, between a radical and a cation (p-type) and between a radical and an anion (n-type).[19,20,21,22] Although both types of the reactions can be used as an alternative to the reaction of lithium transition metal oxide, the voltage of a p-type reaction tends to be higher than that of an n-type reaction. Using a p-type reaction is thus better for obtaining high energy density.

The theoretical capacity of a radical polymer is inversely proportional to the molecular weight of the monomer unit. High theoretical capacity is obtained from a compact unit structure. A polyether bearing 2,2,5,5-tetramethyl-2,5-dihydro-1H-pyrrol-1-oxyl-3-yl has a theoretical capacity of 147 mA·h·g-1,[23,24] the highest theoretical capacity for radical polymers to date, when a one-electron redox reaction is assumed.

The energy density of an organic radical battery can be calculated by assuming that it has a radical polymer cathode and a lithium metal anode. Such calculation shows that the p-type reaction of nitroxyl radical polymers has an energy density of 400–550 $mW \cdot h \cdot g^{-1}$ (figure 1.11). In contrast, the energy density of an n-type reaction in a modified nitroxyl radical polymer and in a poly(galvinoxylstyrene) is 250 and 150 $mW \cdot h \cdot g^{-1}$, respectively. The p-type reaction of nitroxyl radical polymers means that they are now considered to be the material closest to being a practical alternative to lithium transition metal oxides.

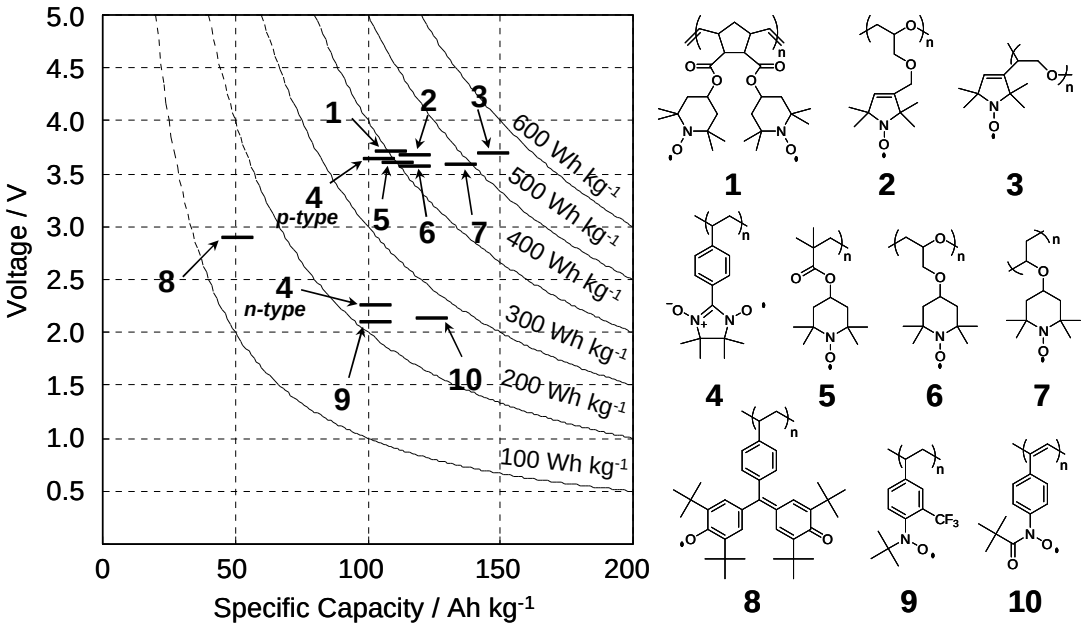

Figure 1.11 Operating voltage vs. specific capacity of radical polymers.

This thesis mainly describes the performances of an organic radical battery using a nitroxyl radical polymer as the cathode active material. The redox reactions of the radical polymer, the electron transfer mechanism in the composite electrode, and recent developments in its practical use are also described.

References

1) J. -M. Tarascon, M. Armand, *Nature* **2001**, 414, 359.

2) A. S. Arico, P. Bruce, B. Scrosati, J. -M. Tarascon, W. V. Schalkwijk, *Nature Mater*. **2005**, 4, 366.

3) P. Bruce, B. Scrosati, J. -M. Tarascon, *Angew. Chem. Int. Ed.* **2008**, 47, 2930.

4) B. Scrosati, J. Garche, *J. Power Sources* **2010**, 195, 2419.

5) M. Wakihara, *Mater Sci Eng.* **2001**, R33, 109.

6) W.-J. Zhang, *J. Power Sources* **2011**, 196, 13.

7) T. Takamura, S. Ohara, M. Uehara, J. Suzuki, K. Sekine, *J. Power Sources* **2004**, 129, 96.

8) H. Nara, Y. Fukuhara, A. Takai, M. Komatsu, H. Mukaibo, Y. Yamauchi, T. Momma, K. Kuroda, T. Osaka, *Chem. Lett.* **2008**, 37, 2, 142.

9) G. Q. Liu, L. Wen, Y. M. Liu, *J. Solid State Electrochem.* **2010**, 14, 2191.

10) M. Nakayama, S. Goto, Y. Uchimoto, M. Wakihara, Y. Kitajima, *Chem. Mater.*, **2004**, 16, 18, 3399.

11) C. S. Johnson, N. Li, C. Lefief, J. T. Vaughey, M. M. Thackeray, *Chem. Mater.* **2008**, 20, 6095.

12) M. Tabuchi, Y. Nabeshima, T. Takeuchi, K. Tatsumi, J. Imaizumi, Y. Nitta, *J. Power Sources* **2010**, 195, 834.

13) A. Ito, D. Li, Y. Sato, M. Arao, M. Watanabe, M. Hatano, H. Horie, Y. Ohsawa, *J. Power Sources* **2010**, 195, 567.

14) E. Dumont-Botto, C. Bourbon, S. Patoux,P. Rozier, M. Dolle, *J. Power Sources* **2011**, 196, 2274.

15) M. E. Arroyo y de Dompablo, U. Amador, J. M. Gallardo-Amores, E. Moran, H. Ehrenberg, L. Dupont, R. Dominko, *J. Power Sources* **2009**, 189, 638.

16) P. J. Nigrey, D. Maclnnes Jr., D. P. Nairns, A. G. MacDiarmid, *J. Electrochem. Soc.* **1981**, 1651.

17) S. J. Visco, M. Liu, L. C. De Jonghe, *J. Electrochem. Soc.* **1990**, 137, 1191.

18) N. Oyama, T. Tatsuma, T. Sato, T. Sotomura, *Nature* **1995**, 373, 598.

19) K. Nakahara, S. Iwasa, M. Satoh, Y. Morioka, J. Iriyama, M. Suguro, E. Hasegawa, *Chem. Phys. Lett.* **2002**, 359, 351.

20) H. Nishide, S. Iwasa, Y.-J. Pu, T. Suga, K. Nakahara, M. Satoh, *Electrochim. Acta* **2004**, 50, 827.

21) J. Iriyama, K. Nakahara, S. Iwasa, Y. Morioka, M. Suguro, M. Satoh, *IEICE Trans.* **2002**, E85-C, 6, 1256.

22) H. Nishide, T. Suga, *Electrochem. Soc. Interface* **2005**, 14, 32.

23) K. Oyaizu, T. Suga, K. Yoshimura, H. Nishide, *Macromolecules* **2008**, 41, 6646.

24) K. Oyaizu, T. Kawamoto, T. Suga, H. Nishide, *Macromolecules*, **2010**, 43, 10382.

25) K. Nakahara, J. Iriyama, S. Iwasa, M. Suguro, M. Satoh, E. J. Cairns, *J. Power Sources* **2007**, 163, 1110.

26) T. Suga, Y.-J. Pu, S. Kasatori, H. Nishide, *Macromolecules* **2007**, 40, 3167.

27) T. Suga, S. Sugita, H. Ohshiro, K. Oyaizu, H. Nishide, *Adv. Mater.*, in press.

28) T. Suga, H. Konishi, H. Nishide, Chem. Commun. **2007**, 1730.

29) J. Qu, T. Katsumata, M. Satoh, J. Wada, T. Masuda, *Polymer* **2009**, 50, 391.

30) T. Katsumata, M. Satoh, J. Wada, M. Shiotsuki, F. Sanda, T. Masuda, *Macromol. Rapid. Commun.* **2006**, 27, 1206.

31) M. Suguro, A. Mori, S. Iwasa, K. Nakahara, K. Nakano, *Macromol. Chem. Phys.* **2009**, 210, 1402.

32) J. Qu, T. Katsumata, M. Satoh, J. Wada, J. Igarashi, K. Mizoguchi, T. Masuda, *Chem. Eur. J.* **2007**, 13, 7965.

33) K. Oyaizu, T. Sukegawa, H. Nishide, *Chem. Lett.* **2011**, 40, 184.

34) J. Qu, R. Morita, M. Satoh, J. Wada, F. Terakura, K. Mizoguchi, N. Ogata, T. Masuda, *Chem. Eur. J.* **2008**, 14, 3250.

35) J. Qu, F. Z. Khan, M. Satoh, J. Wada, H. Hayashi, K. Mizoguchi, T. Masuda, *Polymer* **2008**, 49, 1490.

36) M. Suguro, S. Iwasa, Y. Kusachi, Y. Morioka, K. Nakahara, *Macromol. Rapid Commun.* **2007**, 28, 1929.

Chapter 2

Electrochemical and Spectroscopic Properties of Nitroxyl Radicals

2.1. Introduction of Chapter 2

A stable radical compound was first synthesized in 1961.[1] Since then, a series of stable radical compounds with various structures, such as nitroxyl, phenoxyl and hydrazyl, have been successfully synthesized. Because stable radical compounds have an electron spin in spite of organic materials, the compounds have been considered to have potential to be ferromagnets. Numerous efforts aimed at developing higher spin multiple numbers brought the first organic ferromagnet in the 90's.[2] Stable radical compounds are now in practical use as protective oxidation reagents on plastic materials and spin-labeling reagents for electron-spin resonance spectroscopy. In addition, stable radical compounds are considered to have future applications as medicinal drugs, catalysts and optical nonlinearity materials.[3]

In chapter 2, we reported on the electrochemical and spectroscopic properties of nitroxyl radicals. The cyclic voltammograms, ultraviolet-visible spectra, and electron spin resonance spectra of the nitroxyl radicals with various structures, such as alicyclic, aromatic, aliphatic, and nitroxyl nitroxide, were investigated. Comparing the electrochemical and spectroscopic properties of various nitroxyl radicals, it is expected that molecular design for a cathode active material would be progressed. In the chapter, we also reported that the redox potential of nitroxyl radicals are various by the range of 0.5 V and predictable approximately by quantum calculations.

2.2. Experimental

Materials

Nitroxyl radical compounds were prepared as below (Fig. 2.1). A nitroxyl free radical, 2,2,6,6-tetramethylpiperidine-1-oxyl (TEMPO, **1**), was obtained from WAKO inc. Some of the others, 4-amino-2,2,6,6-tetramethylpiperidine-1-oxyl (4-amino-TEMPO, **2**), 3-carbamoyl-2,2,5,5-tetramethylpyrrolidine-1-oxyl (**3**), 3-carbamoyl-2,2,5,5-tetramethylpyrroline-1-oxyl (**4**), and di-tert-butyl aminyloxy (**5**) was obtained from Aldrich. Bis [4-(2-phenyl-2-propyl)phenyl] aminyloxy (**6**) was synthesized ourselves by oxidation of related amine compound using 3-chloroperoxybenzoic acid (m-CPBA). Dianisylaminyloxy (**7**) and

anisyl-tert-butylaminyloxy (**8**) were also synthesized ourselves by oxidation of related hydroxyl amine compounds using PbO_2. A nitroxyl nitroxide compound, 2-phenyl-4,4,5,5-tetramethyl-1-imidazolinyloxy-3-oxide (PTIO, **9**), was obtained from Aldrich. All electrolytes were obtained from Tomiyama pure chemical industries, Ltd.

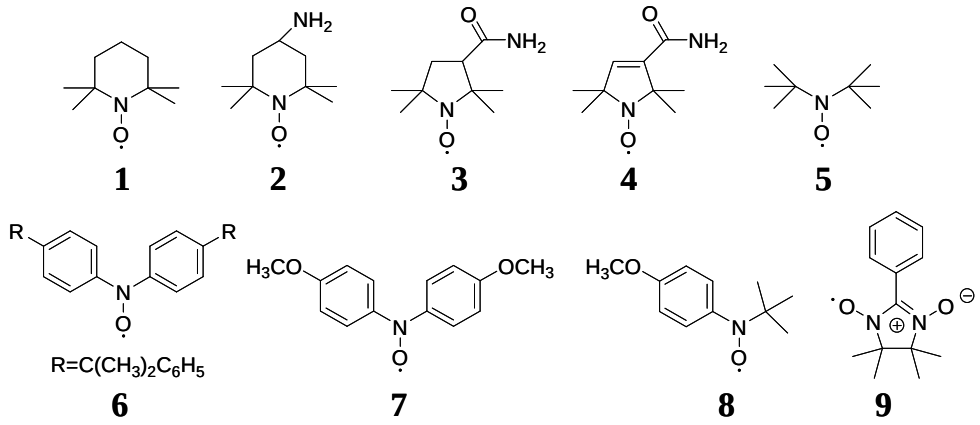

Figure 2.1. Chemical formula of nitroxyl radical compounds.

Cyclic voltammogram

Cyclic voltammogram (CV) measurements were carried out by a standard three-electrode cell in dry argon atmosphere at room temperature using an Electrochemical Analyzer 604, CH Instruments, potensiostat system. The electrolyte consists of 1.0 M tetraethylammonium tetrafluoroborate ($TEABF_4$) in propylene carbonate (PC). The concentration of sample was fixed to be 10 mM. A graphite plate was used as the working electrode, and a platinum wire with sufficient surface area was used as the counter electrode. The reference electrode, a silver wire in electrolyte containing silver nitrate ($AgNO_3$) salt, was set through a porous glass salt bridge. Every sample was evaluated by scan speed of 10, 20, 30, 50 and 100 mV sec^{-1}.

ESR, UV-Vis, and Quantum calculation

Electron spin resonance (ESR) spectra were obtained using JES-FR30, JEOL, X-band (9.48 GHz) spectrometer with MnO marker. We measured the sample at the state of 1 mM acetnitrile solution. We calculated their g-value by using Mn^{2+} signals as a standard. Hyperfine splitting constant (a_N) was obtained from the split width of hyperfine structure. Ultraviolet-visible (UV-vis) spectra were measured using a

UV-3150, Shimadzu, spectrometer in room temperature. Wavelength range was set from 200 to 800 nm. We prepared acetonitrile solutions of samples by concentration of 0.1, 1.0 and 10 mM. Semi-empirical molecular orbital calculations were performed by using MOPAC2000^{TM} (PM3) software.

2.3. Results and Discussion

2.3.1. Cyclic voltammograms of TEMPO

Cyclic voltammograms of TEMPO (**1**) in 1.0M-$TEABF_4$ contained PC electrolyte is shown in Fig. 2.2 Each voltammogram was obtained by different scan speeds. Electrochemical parameters are summarized in Table 2.1. Typical redox couples were seen at around -0.026 V vs. Ag/Ag^+. The peak separation was very small, 72 mV at a scan speed of 10 mV s^{-1}, and it is closed to theoretical value (59.5 mV, 25^{o}C) based on a reversible redox reaction. The anodic ($I_{p.a.}$) and cathodic ($I_{p.c.}$) peak current densities were almost the same value ($I_{p.a.}/I_{p.c.}$= 0.98-1.01) independent of scan speed. Therefore, it is considered to be sure that PTMA shows reversible redox reaction.

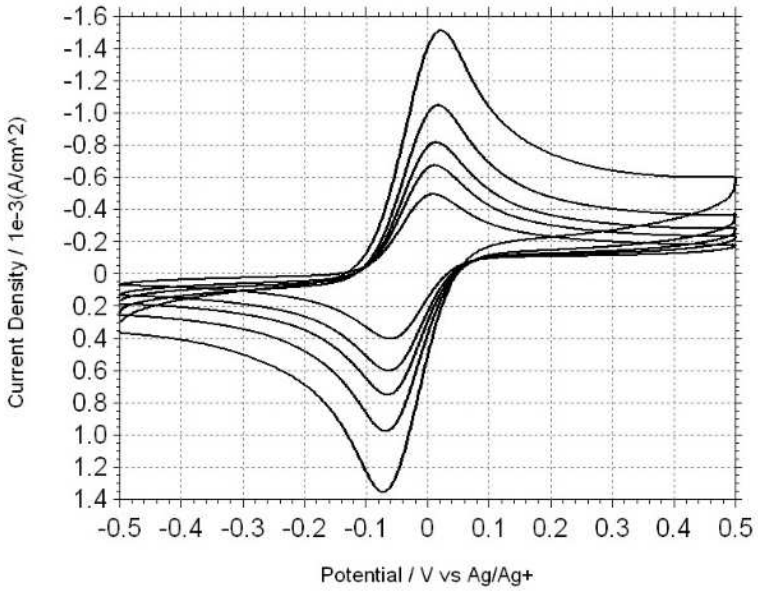

Figure 2.2. Cyclic voltammograms for TEMPO in PC/1.0M-$TEABF_4$ electrolyte. Each scan speed corresponds to 10, 20, 30, 50 and 100 mV sec^{-1}, respectively.

Table 2.1. Electrochemical parameters for nitroxyl radical compounds.

		1	**2**	**3**	**4**	**5**
$E_{p.a.}$	[V vs. Ag/Ag^+]	0.011	0.185	0.106	0.230	-0.074
$E_{p.a.}$	[V vs. Ag/Ag^+]	-0.061	0.116	0.038	0.163	-
$(E_{p.a.}+E_{p.c.})/2$	[V vs. Ag/Ag^+]	-0.025	0.151	0.072	0.197	-
$E_{p.a} - E_{p.c.}$	[mV]	72	69	68	67	-
$I_{p.a.}$	[mA/cm^2]	0.448	0.229	0.436	0.374	0.446
$I_{p.c.}$	[mA/cm^2]	0.496	0.326	0.437	0.369	-
$I_{p.a.}/I_{p.c.}$	[-]	0.98	0.70	1.00	1.01	-
D_R	[$cm^2\ s^{-1}$]	2.8×10^{-6}	1.7×10^{-6}	2.3×10^{-6}	1.5×10^{-6}	-

		6	**7**	**8**	**9**
$E_{p.a.}$	[V vs. Ag/Ag^+]	-0.077	0.176	-0.087	0.113
$E_{p.a.}$	[V vs. Ag/Ag^+]	-0.144	0.109	-0.152	0.046
$(E_{p.a.}+E_{p.c.})/2$	[V vs. Ag/Ag^+]	-0.111	0.143	-0.120	0.080
$E_{p.a} - E_{p.c.}$	[mV]	67	67	65	67
$I_{p.a.}$	[mA/cm^2]	0.205	0.160	0.173	0.304
$I_{p.c.}$	[mA/cm^2]	0.187	0.174	0.211	0.300
$I_{p.a.}/I_{p.c.}$	[-]	1.10	0.92	0.82	1.01
D_R	[$cm^2\ s^{-1}$]	2.8×10^{-6}	2.8×10^{-6}	2.8×10^{-6}	2.8×10^{-6}

2.3.2. Cyclic voltammograms of alicyclic, aromatic, and aliphatic nitroxyl radicals

Similar to TEMPO, the other alicyclic nitroxyl radical compounds (**2**, **3**, **4**) showed reversible redox reactions. However, as shown in Table 2.1, their redox potentials are a little bit different. It would be made clear that substituent groups can affect their redox potentials. Aromatic nitroxyl radical compounds (**6**, **7**, **8**) and a nitronyl nitroxide radical (**9**) also showed reversible redox reactions. Examples of the CV for an aromatic and a nitronyl nitroxide are displayed in Fig. 2.3 and 2.4. Although their redox potential was various, there was no significant difference in electrochemical behavior among them. Nevertheless, only aliphatic nitroxyl radical (**5**) didn't show a redox couple. The CV is shown in Fig. 2.5. Sharp anodic peaks are observed, but there is no cathodic

peak at any scan speed. We considered that a related oxoammonium cation is so unstable that it decomposed immediately after oxidation.

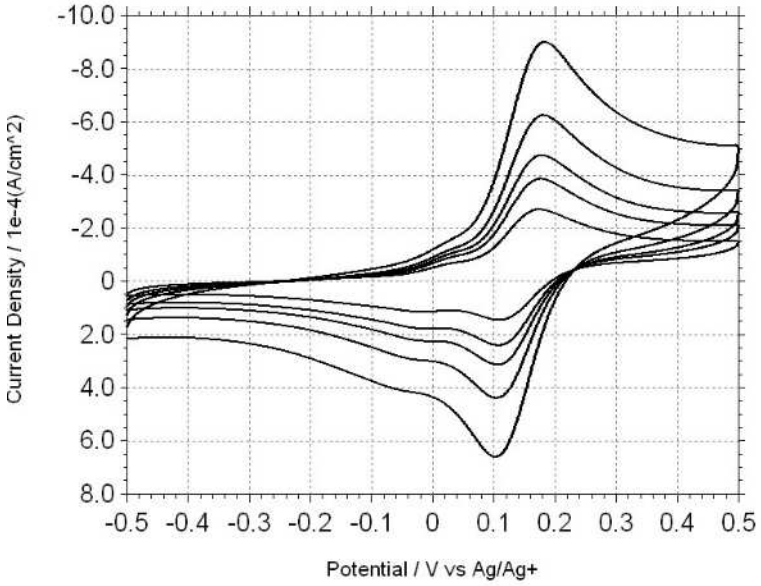

Figure 2.3. A Cyclic voltammogram for **6** in 1.0M-$TEABF_4$ PC electrolyte. Each scan speed corresponds to 10, 20, 30, 50 and 100 mV sec^{-1}, respectively.

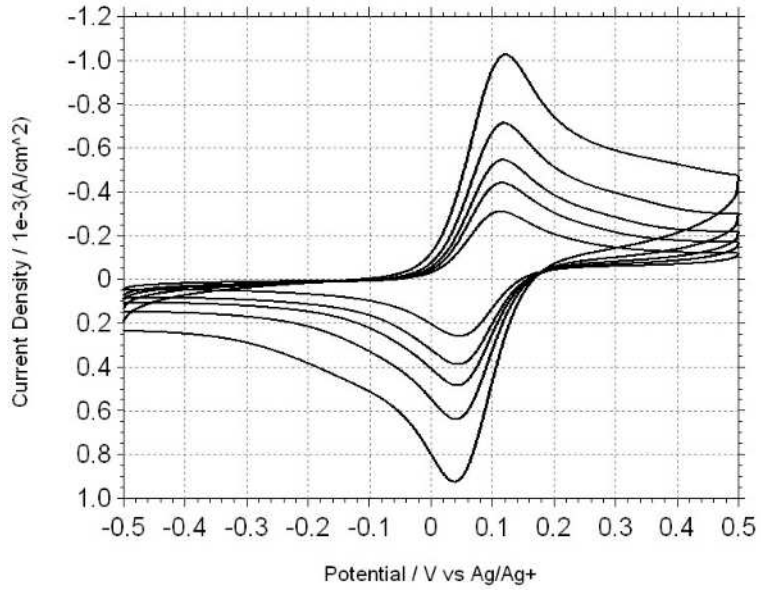

Figure 2.4. A Cyclic voltammogram for **9** in 1.0M-$TEABF_4$ PC electrolyte. Each scan speed corresponds to 10, 20, 30, 50 and 100 mV sec^{-1}, respectively.

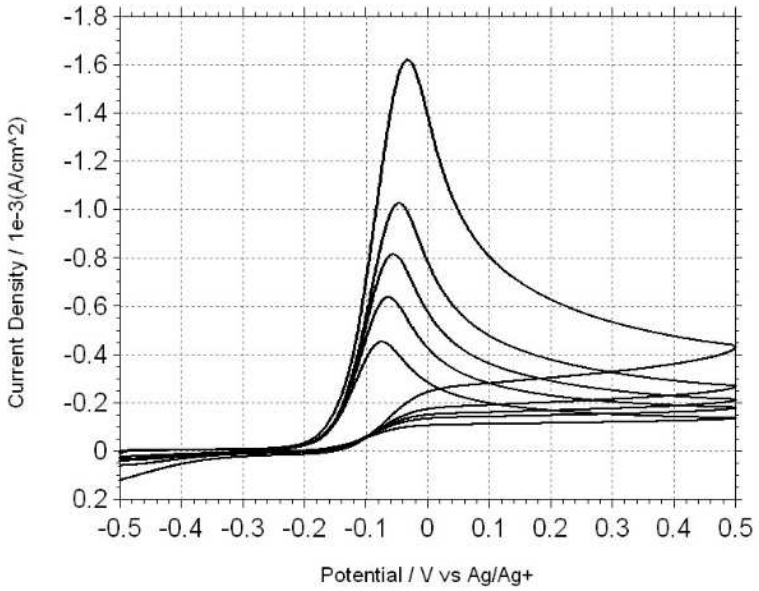

Figure 2.5. A Cyclic voltammogram for 5 in 1.0M-$TEABF_4$ PC electrolyte. Each scan speed corresponds to 10, 20, 30, 50 and 100 mV sec^{-1}, respectively.

2.3.3. Diffusion constants of nitroxyl radicals

Figure 2.6 shows a relationship between anodic peak current densities and the square root of scan speeds for alicyclic, aromatic and nitronyl nitroxide compounds. It is confirmed that peak current densities increased in proportion to the square root of scan speeds. It is already known theoretically that a peak current density of reversible redox reaction is given by the following equation.

$$i_p = 0.4463 \times n^{3/2} \times F^{3/2} \times C_R \times \sqrt{\frac{D_R v}{RT}} \qquad (1)$$

where n is the number of electrons transferred, F is a Faraday constant, C_R is the bulk concentration of reductant, R is a universal gas constant, T is the absolute temperature, D_R is the diffusion coefficient for redactant and v denotes scan speed. According to this equation, we can calculate their diffusion coefficient. Evaluated values are in the order between 10^{-7} and 10^{-6} $cm^2 \cdot s^{-1}$, as displayed in Table 2.1. We found that there is a tendency that the diffusion coefficients of alicyclic compounds are the biggest, that of nitronyl nitroxide is the next and those of aromatic compounds are the last. We considered that the

affinities between these compounds and polar solvent molecules would be increased in this turn.

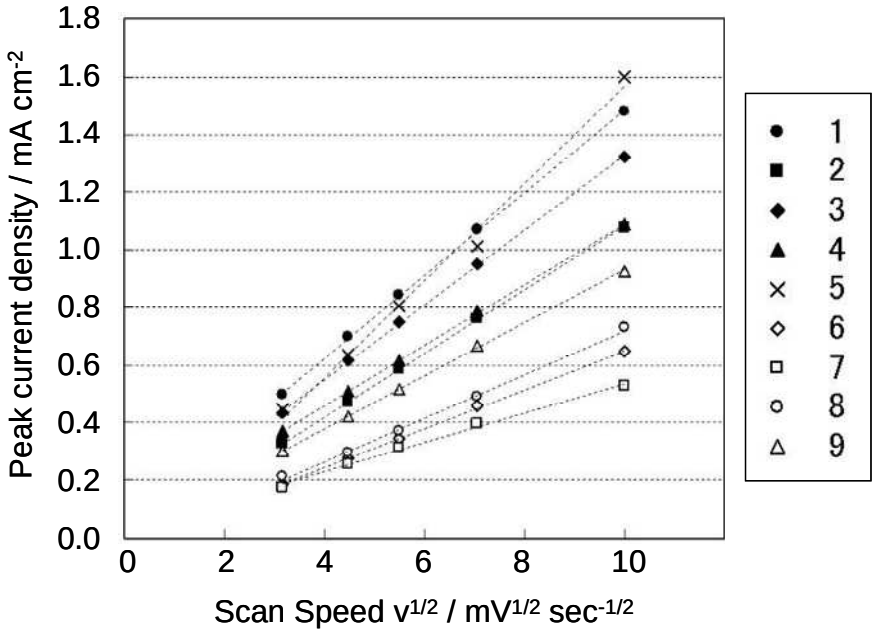

Figure 2.6. The relationship between scan speed and peak current density.

2.3.4. Electron spin resonance spectra of nitroxyl radicals

Electron spin resonance (ESR) spectra are shown in Fig. 2.7. It is already known that a nitroxy radical shows triplet hyperfine structure, because of the interaction between a nuclear spin of ^{14}N (I=1) and an electron spin of free radical (s=1/2). In all cases of alicyclic (**1**, **2**, **3**, **4**), aromatic (**6**, **7**, **8**) and aliphatic (**5**) compounds, triplet hyper fine structure with the same intensity was found as shown in Fig. 2.7. The small peaks shown at 332 and 341 mT, result from MnO standard marker. Nitronyl nitroxide (**9**) has quintuple signal with an intensity of 1:2:3:2:1 respectively. According to previous works, it is reported that this quintuple hyperfine structure originates from the interaction between two equivalent nuclear spins of ^{14}N (I=1) and an electron spin (s=1/2). The g-values and hyperfine splitting constants (a_N) are shown in Table 2.2. All compounds had almost same g-values (g~2.007) as that of previously reported for nitroxyl radicals. On the other hand, they have various hyperfine coupling constant (a_N). It is already known that hyperfine coupling constant (a_N) is an index of interaction between nuclear

spins and electron spins, and this value is directly proportional to the π-electron spin density around the nitrogen atom as shown in following McConnell equation.

$$a_N = Q\rho_N$$

where Q has the semiempirical value of 2.3 mT and ρ_N is π-electron spin density around the nitrogen atom. Based on this equation, π-electron spin density was calculated and shown in Table 2.2. In case of alicyclic and aliphatic compounds, these values were between 0.64-0.70. However aromatic compounds had the value between 0.44-0.60, and a nitronyl nitroxide showed 0.33. These results indicate that a free radical electron of alicyclic and aliphatic compounds is relatively localized in nitroxyl group, however, that of aromatic and nitronyl nitroxide compound is delocalized. The degree of free radical localization is related to their stabilities. Therefore, it is considered that aromatic radical compounds are less stable than the other compounds.

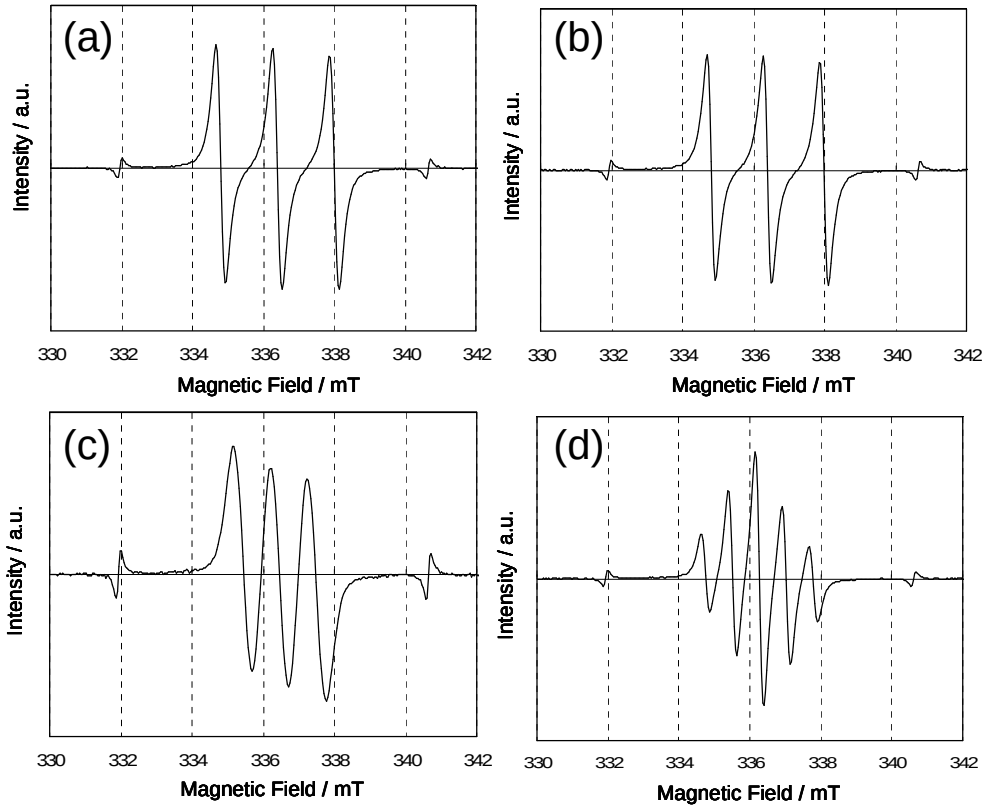

Figure 2.7. Electron Spin Resonance Spectra of 1 mM acetnitrile solution for (a) **1**, (b) **5**, (c) **6** and (d) **9** obtained by X-band (9.48 GHz) spectrometer with MnO marker.

2.3.5. Ultraviolet-visible spectra of nitroxyl radicals

Ultraviolet-visible (UV-vis) spectra are shown in Fig. 2.8. We especially focused on the weak absorption peak of visible region (400-600 nm), because this is considered to be mainly contributed to free radical electrons located on the non-bonding singly occupied molecular orbitals (SOMOs). The wavelength of maximum absorbance (λ_{max}) and the molar extinction coefficient (ε) are summarized in Table 2.2. We found that λ_{max} of aromatic compounds (490-502 nm) is slightly longer than that of alicyclic and aliphatic compounds (428-468 nm). Nitronyl nitroxide showed relatively longer λ_{max} (583 nm) than the others. That is why only nitronyl nitroxide solution looks violet color, in spite of the other solutions are yellow or orange. The values of the molar extinction coefficient (ε) have wide variety. Alicyclic and aliphatic compounds have much smaller ε (4-10) compared with those of aromatic and nitronyl nitroxide compounds (124-920). It is generally known that the optical transition from non-bonding molecular orbitals (n→π*, n→σ*) are forbidden because of highly symmetry. However, in case of aromatic and nitronyl nitroxide compounds, it is considered that the symmetry of non-bonding molecular orbital is slightly broken by delocalization of free electrons.

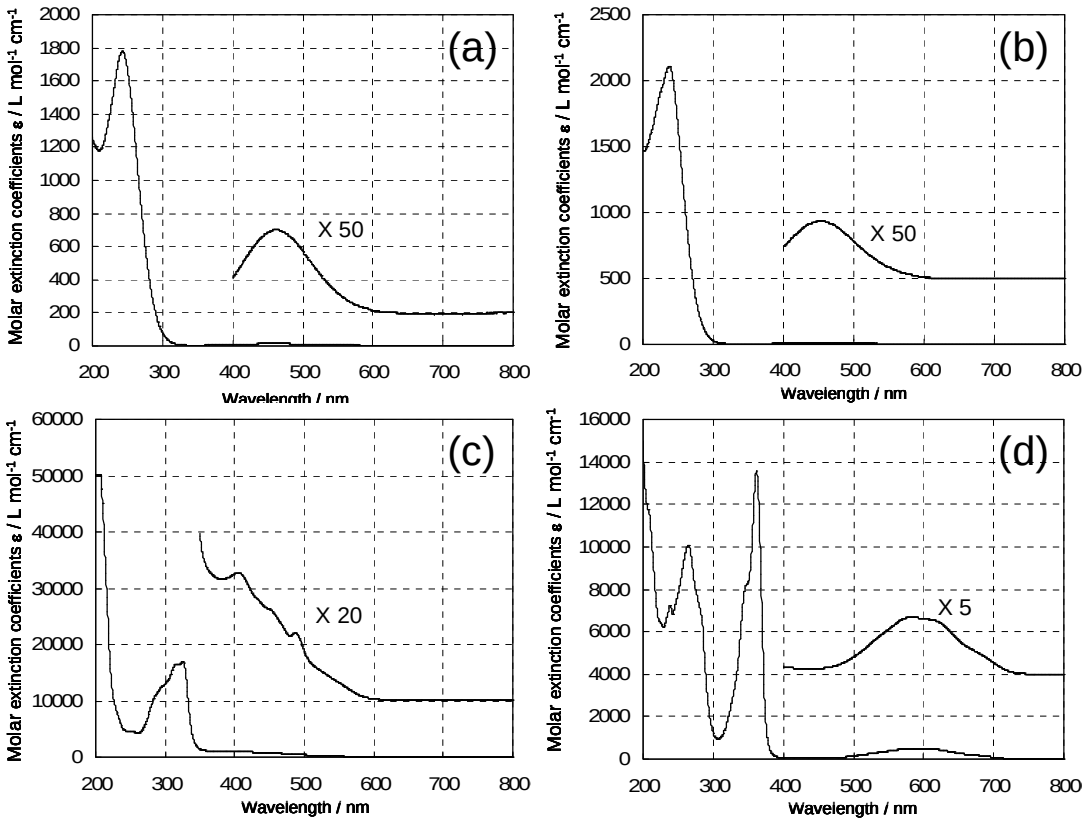

Figure 2.8. Ultraviolet-visible spectra for (a) **1**, (b) **5**, (c) **6** and (d) **9**.

Table 2.2. Electron Spin Resonance spectra parameters and Ultraviolet-visible spectra parameters for nitroxyl radical compounds.

		1	**2**	**3**	**4**	**5**
g-value	[-]	2.007	2.007	2.007	2.007	2.007
aN	[mT]	1.60	1.59	1.47	1.48	1.58
ρN	[-]	0.70	0.69	0.64	0.64	0.69
λmax	[nm]	463	468	428	438	453
ε	[L mol^{-1} cm^{-1}]	10	8	6	4	9

		6	**7**	**8**	**9**
g-value	[-]	2.006	2.007	2.007	2.008
aN	[mT]	1.01	1.03	1.38	0.75
ρN	[-]	0.44	0.45	0.60	0.33
λmax	[nm]	491	502	490	583
ε	[L mol^{-1} cm^{-1}]	580	920	124	537

2.3.6. Semi-empirical molecular orbital calculation of nitroxyl radicals

The space distributions of the SOMO were calculated and illustrated in Fig 2.9. It is quite obvious that the radical electrons of alicyclic and aliphatic compounds are located in nitroxyl groups and those of aromatic and nitronyl nitroxide compounds are delocalized over molecules. Therefore, there is a considerable difference in the hyperfine coupling constant (a_N) of ESR spectra and the molar extinction coefficient (ε) of UV-vis spectra between them. On the other hand, the electrochemical behaviors have another tendency. There was no significant difference among alicyclic, aromatic and nitrony nitroxide compounds, however, only alicyclic compound showed strange behavior. That indicates electrochemical properties are affected by not only the properties of nitroxyl radicals but also those of oxidized compounds, oxoammonium cations.

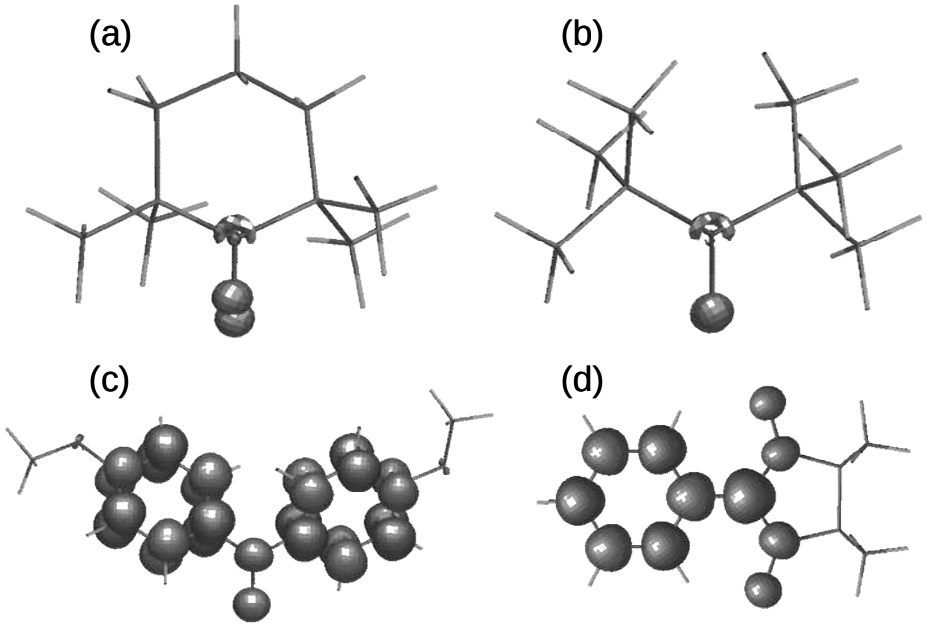

Figure 2.9. Space distributions of the SOMO for (a) **1**, (b) **5**, (c) **7** and (d) **9** evaluated via semi-empirical molecular orbital calculations by using MOPAC2000^{TM} (PM3) software.

Figure 2.10 shows relationship between calculated energy level of SOMO and experimentally obtained redox potentials of alicyclic, aromatic and nitronyl-nitroxide compounds. There is a tendency that deeper energy level causes higher redox potential. According to the following basic equation, it is natural that the difference of energy level between lithium metal and SOMO roughly indicates the reaction potential.

$$\Delta G = -nF\Delta E$$

where ΔG is the change of Gibbs free energy, ΔE is electrical potential of the reaction. The experimentally obtained potentials expanded while the range about -0.1-0.2 V vs. Ag/Ag^{+}. Considered from the viewpoint of application for a cathode active material of lithium batteries, the voltage would be 3.5-3.8 V. It is already well known that electron withdrawing groups, such as $–CF_3$ (σ_p: 0.53) and $–NO_2$ (σ_p: 0.81), are effective in deepening the energy level and electron donating groups, such as –OMe (σ_p: -0.28) and –tBu (σ_p: -0.15) works on making shallow it. So in the future, we may be able to predict and control the potential of lithium batteries with organic radical cathode.

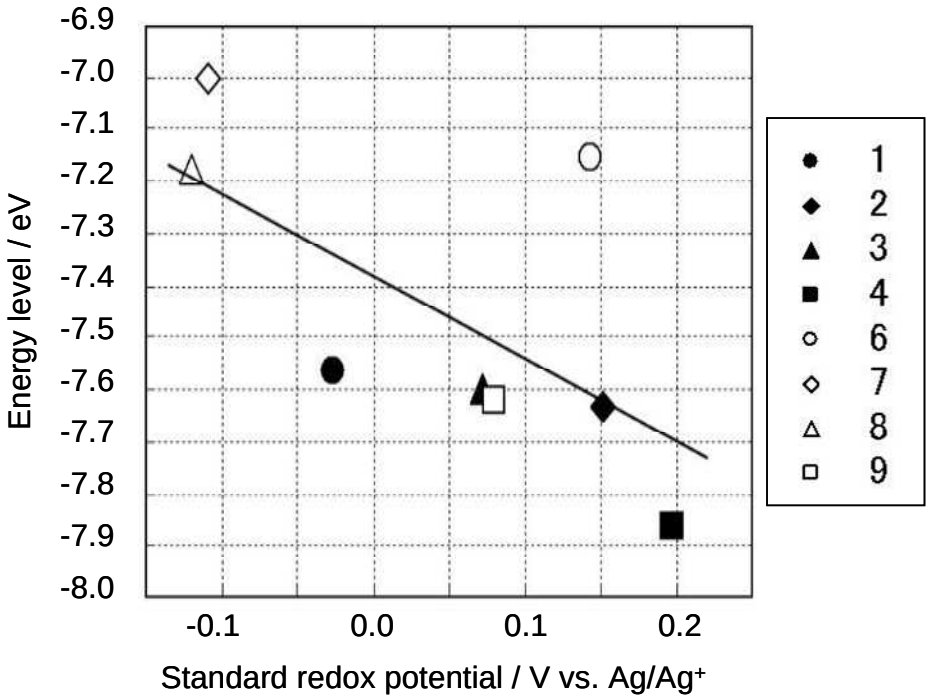

Figure 2.10. The relationship between standard redox potential and calculated energy level. Energy level of HOMO for radical compounds and that of LUMO for oxoammonium cation were calculated by semi-empirical MP3 method using MOPAC2000^{TM} software, and the average of them was used as the energy level here.

2.4. Conclusion of Chapter 2

Electrochemical properties of nitroxyl radical compounds in aprotic electrolyte were measured and it was found that most compounds show reversible redox behavior independent of their structures. Their redox potential are various by the range of 0.5 V and found to be predictable approximately by quantum calculations. That means various molecular designs would be possible as an active materials for lithium rechargeable batteries. On the other hand, their absorption spectra were significantly different from each other as their electron distribution. So we might be able to control the capacity, voltage, mechanical strength and color of active materials for lithium batteries in the future. That would be useful for spreading the application of the batteries.

References

1) A. K. Hoffman and A. T. Henderson, *J. Am. Chem. Soc.* **1961**, 83, 4671.

2) Yu. V. Korshak, T. V. Medvedeva, A. A. Ovchinnikov and V. N. Spector, *Nature*, **1987**, 326, 370.

3) M. Takahashi, S. Yamada, H. Matsuda, H. Nakanishi, E. Tsuchida and H. Nishide, *Chem. Commun.* **1997**, 1853.

Chapter 3

Electrolyte Anion-Assisted Charge Transportation in Nitroxyl Radical Polymer/Electrolyte Gels

3.1. Introduction of Chapter 3

Organic radical battery is a new type of rechargeable battery which utilized stable radical polymers as the active material.[1,2,3,4,5] Nitroxyl radical polymers, such as poly (2,2,6,6-tetramethylpiperidinoxyl-4-yl methacrylate) (PTMA) and poly(2,2,6,6-tetramethylpiperidine-4-yl-1-oxy vinyl ether) (PTVE) are the candidates as alternatives of transition-metal oxides in aprotic rechargeable batteries. It is reported that the highest theoretical capacity of the nitroxyl radical polymers is 147 $mA \cdot h \cdot g^{-1}$, [6,7] which is comparable to the practical specific capacity of $LiCoO_2$ (140 $mA \cdot h \cdot g^{-1}$ [8,9]). The organic radical battery which using a PTMA/carbon composite cathode has an operating voltage of 3.5 V with good cyclability comparable to that of conventional lithium ion battery.[10,11] The battery is attractive as an environmentally friendly, high power, and high energy density battery.

The charge transportaion through the nitroxyl radical polymer is considered to have two steps: the heterogeneous charge transportations from a current collector to the redox sites, and the homogeneous charge transportation among the redox sites (Fig. 3.1.).[5,12] The standard rate constant (k_0) of heterogeneous charge transportation from a platinum surface to 2,2,6,6-tetramethylpiperidine-1-oxyl (TEMPO) was investigated to be ca. 10^{-1} $cm \cdot s^{-1}$ by electrochemical measurements such as cyclic voltammetry, chronoamperometry, and AC impedance spectroscopy[13] The rate constant is thus almost of the same order as that for the redox reactions of transition metal ions (Co^{2+}/Co^{3+}: ca. 10^{-2} $cm \cdot s^{-1}$ [14]) and is several orders larger than that of disulfide compounds (ca. 10^{-8} $cm \cdot s^{-1}$ [14]) The conformation of the molecule is almost unchanged during the charge transportation process, which promotes fast charge transportation. The rate of the electrochemical reaction is determined completely by the diffusion rate of the molecules onto the platinum surface.

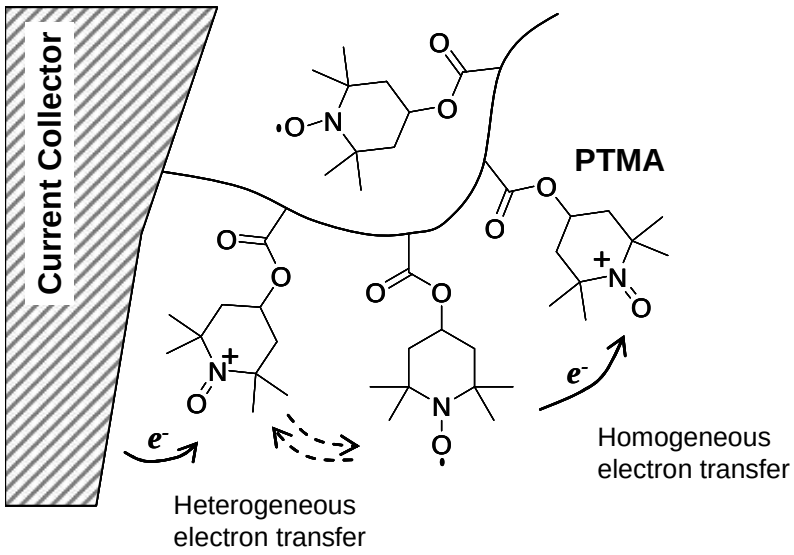

Figure 3.1. Charge transportation profile in a radical polymer electrode.

Mechanisms of the homogeneous charge transportation in a cross-linked polynorbornene bearing TEMPO have been investigated.[15] The transportation is apparently driven by the charge concentration gradient through an electron self-exchange reaction among neighboring redox sites. The diffusion constant of the charge transportation is reported to be 5.3×10^{-10} $cm^2 \cdot s^{-1}$.[15] The bimolecular rate constant (k_{ex}) of the self-exchange reaction was estimated to be 1.8×10^5 $M^{-1} \cdot s^{-1}$.[15] It is also reported that the relatively fast self-exchange reaction causes the hundreds nanometer thick Nernstian adsorbate-like bulk layer for the ideal finite-diffusion behavior.[15] However, the effect of electrolyte, swelling condition, and cross-linking of the polymers to the charge transportation in nitroxyl radical polymers are still unknown. In this report, we describe the charge transportation behavior in various PTMA/electrolyte gels to investigate the details of the charge transportation mechanisms. Chronoamperometry study on the basis of infinite-diffusion model reveals that the electrolyte anion strongly assisted the charge transportation in the PTMA/electrolyte gels.

3.2. Experimental

Materials

PTMAs were synthesized by the previously reported process.[1,2,3,4] The cross-linking was carried out by adding ethylene glycol dimethacrylate as the cross-linking agent. Propylene carbonate (PC) and electrolyte salts, such as lithium hexafluorophosphate ($LiPF_6$), lithium tetrafluoroborate ($LiBF_4$), and tetrabutylammonium tetrafluoroborato ($TBABF_4$) were employed in purified battery grade materials.

Measurements

Potential-step chronoamperometry of the PTMA/electrolyte gels were carried out by the potential from OCV to 4.2 V vs. Li/Li^+. A Pt working electrode and a Pt wire current electrode were set into the gels with a Li/Li^+ reference electrode. Ionic conductivity was obtained from the x-intercept of the Nyquist plots of AC impedance measurements. The PTMA/electrolyte gels were formed between two gold plate electrodes (20 mmφ) with the gap of 1 mm. The frequency was set from 10^5 to 10^2 Hz, and the amplitude was 10 mV.

The rheological properties of PTMA/electrolyte gels were investigated. Dynamic viscosity measurements were carried out to determine the strain dependence of the storage modules (*G'*) and the loss modules (*G"*) by applying oscillating shear stresses at angular frequency of 10 sec^{-1}.

3.3. Results and Discussion

3.3.1. Chronoamperometry for PTMA/electrolyte gel

A PTMA/electrolyte gel was prepared according to the following way. Straight chain PTMA powder (532.3 mg) was dispersed into 1.0M-$LiPF_6$ contained propylene carbonate (PC) electrolyte (2.209 ml), and kept in ambient condition through over night to swelling it enough. The molar ratio of the nitroxyl radical component against that of the electrolyte salt, $[NO]/[LiPF_6]$, were controlled to be 1.0. The volume of

PTMA/electrolyte gel was found to be 2.89 ml. The concentration of redox sites and electrolyte salt was both 0.76 M in the PTMA/electrolyte gel.

Chronoamperometry measurements were carried out by the potential from OCV to 4.2 V vs. Li/Li^+ at 20°C, 30°C, 40°C and 50°C. In the potential over 3.6 V vs. Li/Li^+, it is known that nitroxyl radical components were completely oxidized to form oxo-ammonium salt.[2,3] Chronoamperometric curves show logarithmic decay of the current density until 120 second (Fig. 3.2a). The Cottrell plots showed an accurate linear relationship in all the observation points (Fig. 3.2b). According to the Nernst-Planck equation, the flux of ions is divided into the origin of an ionic concentration gradient and an electric field. However, since y-intercept of Cottrell plots was 0.08 mA/cm^2 approximately, it is considered that the influence of electric field can be roughly disregarded in this experiment. The result indicates that the charge transportation in the PTMA/electrolyte gel is driven by the concentrate-gradient of the charge on the infinite-diffusion model. According to the Cottrell equation, diffusion constant were estimated to be 3.5×10^{-9} $cm^2 \cdot s^{-1}$ at 20°C, 7.9×10^{-9} $cm^2 \cdot s^{-1}$ at 50°C. Arrhenius plot of diffusion constant revealed the activation energy of 26 $kJ \cdot mol^{-1}$.

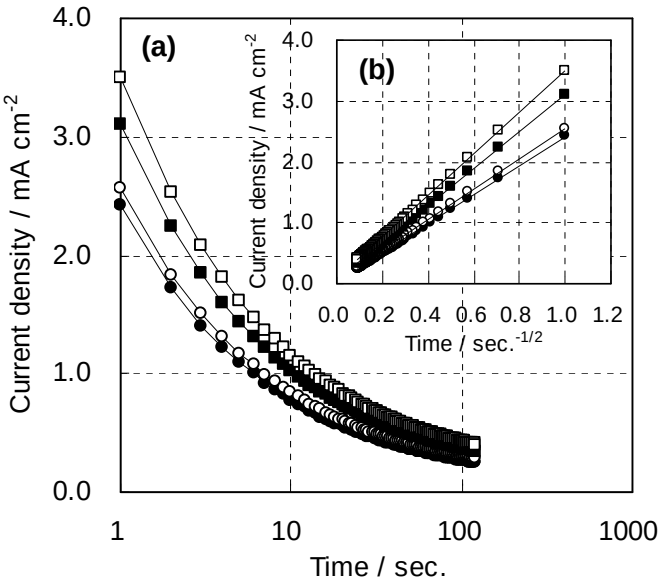

Figure 3.2. Chronoamperometric curves (a) and Cottrell plots (b) of a PTMA/electrolyte gel at 20°C(●), 30°C(○), 40°C(■) and 50°C(□). The molar ratio of the gel: [NO]/[LiPF6] = 1.0.

Charge transportation in the PTMA/Electrolyte gel occurs based on the self-exchange reaction of redox sites. The bimolecular rate constant (k_{ex}) of the self-exchange reaction is obtained from the diffusion constant according to Dahms-Ruff equation: $D = k_{ex}\delta^2 C^*/6$, where δ is the average distance of the neighboring redox sites, which is estimated by the redox site concentration in the PTMA/Electrolyte gel. The estimated bimolecular rate constant (k_{ex}) of the PTMA/electrolyte gel was 1.4×10^6 $M^{-1}\cdot s^{-1}$ at 20°C, and about one order larger than that of cross-linked polynorbornene bearing TEMPO (1.8×10^5 $M^{-1}\cdot s^{-1}$) and poly(vinyl ferrocene) (ca. 10^5 $M^{-1}\cdot s^{-1}$).

3.3.2. Redox site concentration dependence of chronoamperometry

Chronoamperometry measurements of PTMA/electrolyte gels with various redox site concentrations were investigated (Fig. 3.3). The molar ratio of the redox sites against that of electrolyte salt, [NO]/[$LiPF_6$], were 0.6, 1.0, 1.4 and 1.8. All the gels were prepared by the electrolyte of 1.0M-$LiPF_6$ containing PC.

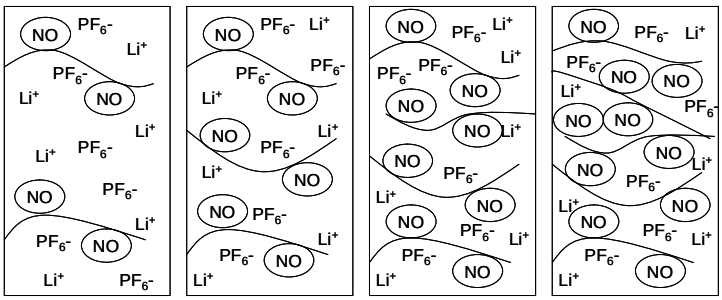

Figure 3.3. Schematic Images for PTMA/electrolyte gels with various redox site concentrations

Diffusion constant, bimolecular rate constant were estimated according to Cottrell equation and Dahms-Ruff equation, and the activation energy was obtained from Arrhenius plots (Fig. 3.4) of the diffusion constants (Table 3.1). According to the equations, charge transportation based on the self-exchange reaction between two redox sites should be enhanced by increasing redox site concentration. However, it was surprised that the diffusion current densities are almost independent on the concentration. Therefore, the lower redox site concentration resulted in the higher diffusion constant and bimolecular rate constant. The result means charge transportation in the

PTMA/Electrolyte gel would be not determined by the neighboring distance and concentration of redox sites.

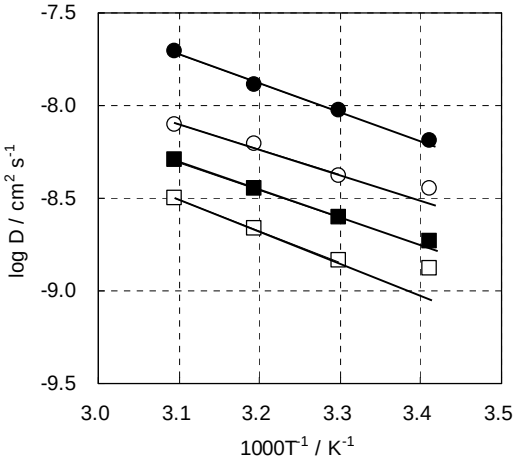

Figure 3.4. Arrhenius plots of diffusion constants for PTMA/electrolyte gels with various redox site concentrations: [NO]/[$LiPF_6$] = 0.6 (●), 1.0 (○), 1.4 (■) and 1.8 (□).

Table 3.1. Diffusion constant, bimolecular rate constant, and activation energy for PTMA/electrolyte gels with various redox site concentrations

Experiments	**#1**	**#2**	**#3**	**#4**
Radical polymer	PTMA	PTMA	PTMA	PTMA
Electrolyte	1.0M $LiPF_6$ PC	1.0M $LiPF_6$ PC	1.0M $LiPF_6$ PC	1.0M $LiPF_6$ PC
[NO]/[$LiPF_6$]	0.6	1.0	1.4	1.8
[NO] in the gel	0.50 M	0.76 M	1.06 M	1.31 M
[$LiPF_6$] in the gel	0.84 M	0.76 M	0.76 M	0.73 M
D at 20°C	6.4×10^{-9} cm^2•s^{-1}	3.5×10^{-9} cm^2•s^{-1}	1.9×10^{-9} cm^2•s^{-1}	1.3×10^{-9} cm^2•s^{-1}
D at 50°C	2.0×10^{-8} cm^2•s^{-1}	7.9×10^{-9} cm^2•s^{-1}	5.0×10^{-9} cm^2•s^{-1}	3.2×10^{-9} cm^2•s^{-1}
k_{ex} at 20°C	2.2×10^{6} M^{-1}•s^{-1}	1.4×10^{6} M^{-1}•s^{-1}	8.2×10^{5} M^{-1}•s^{-1}	6.2×10^{5} M^{-1}•s^{-1}
k_{ex} at 50°C	6.6×10^{6} M^{-1}•s^{-1}	3.1×10^{6} M^{-1}•s^{-1}	2.2×10^{6} M^{-1}•s^{-1}	1.5×10^{6} M^{-1}•s^{-1}
Activation energy	30 kJ/mol	26 kJ/mol	29 kJ/mol	32 kJ/mol

3.3.3. Electrolyte salt concentration dependence of chronoamperometry

PTMA/electrolyte gels were prepared by using straight chain PTMA and the PC electrolyte with various electrolyte salt concentrations, 0.5M-, 1.0M- 1.5M-$LiPF_6$. Concentrations of redox sites in the gels were controlled to be almost same. The molar ratio of the redox sites against that of electrolyte salt, [NO]/[$LiPF_6$], were 2.0, 1.0, and 0.7, respectively.

Diffusion constant and bimolecular rate constant were estimated from chronoamperometric curves of the PTMA/electrolyte gels (Table 3.2). The activation energy was obtained from Arrhenius plots of the diffusion constants (Fig. 3.5). It is found that the current density significantly depends on the electrolyte salt concentration. The lower concentration brought the larger diffusion constant. Arrhenius plots reveal the activation energy of the PTMA/Electrolyte gels using PC electrolyte with 0.5M-, 1.0M-1.5M-$LiPF_6$ to be 18, 26, 42 kJ/mol, respectively. The results strongly suggest that the charge transportation in the PTMA/Electrolyte gels is significantly depended on the mobility of ions in the gels.

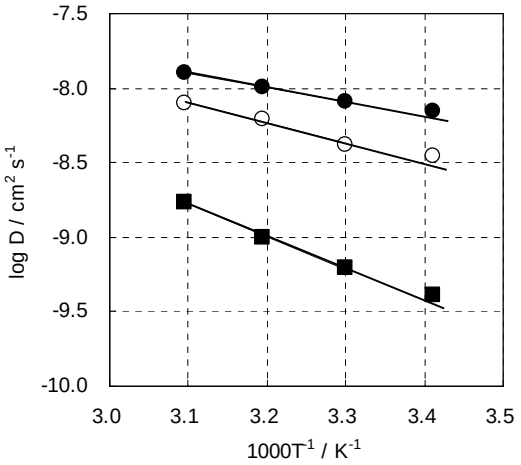

Figure 3.5. Arrhenius plots of diffusion constants for PTMA/electrolyte gels using PC electrolyte with various salt concentrations, 0.5M-(●), 1.0M-(○) 1.5M-(■) $LiPF_6$.

Table 3.2. Diffusion constant, bimolecular rate constant, and activation energy for PTMA/electrolyte gels using PC electrolyte with various salt concentrations

Experiments	**#5**	**#1**	**#6**
Radical polymer	PTMA	PTMA	PTMA
Electrolyte	0.5M $LiPF_6$ PC	1.0M $LiPF_6$ PC	1.5M $LiPF_6$ PC
[NO]/[$LiPF_6$]	2.0	1.0	0.67
[NO] in the gel	0.80 M	0.76 M	0.78 M
[$LiPF_6$] in the gel	0.40 M	0.76 M	1.31 M
D at 20°C	6.9×10^{-9} cm^2•s^{-1}	3.5×10^{-9} cm^2•s^{-1}	4.1×10^{-10} cm^2•s^{-1}
D at 50°C	1.3×10^{-8} cm^2•s^{-1}	7.9×10^{-9} cm^2•s^{-1}	1.7×10^{-9} cm^2•s^{-1}
k_{ex} at 20°C	2.8×10^{6} M^{-1}•s^{-1}	1.4×10^{6} M^{-1}•s^{-1}	1.6×10^{5} M^{-1}•s^{-1}
k_{ex} at 50°C	5.1×10^{6} M^{-1}•s^{-1}	3.1×10^{6} M^{-1}•s^{-1}	6.8×10^{5} M^{-1}•s^{-1}
Activation energy	18 kJ/mol	26 kJ/mol	42 kJ/mol

3.3.4. Electrolyte salt type dependence of chronoamperometry

Three types of electrolyte salts, $LiPF_6$, $LiBF_4$, $TBABF_4$, were employed for preparing PTMA/Electrolyte gels. Concentrations of redox sites, and electrolyte salts were controlled to be almost the same as the molar ratios of 1.0. Diffusion constant, bimolecular rate constant and activation energy estimated by chronoamperometric curves indicate that charge transportation in the PTMA/Electrolyte gels were affected by anion type rather than cation type (Table 3.3). It is considered that charge transportation between two redox sites is mainly assisted by the mobility of electrolyte anion (Fig. 3.6).

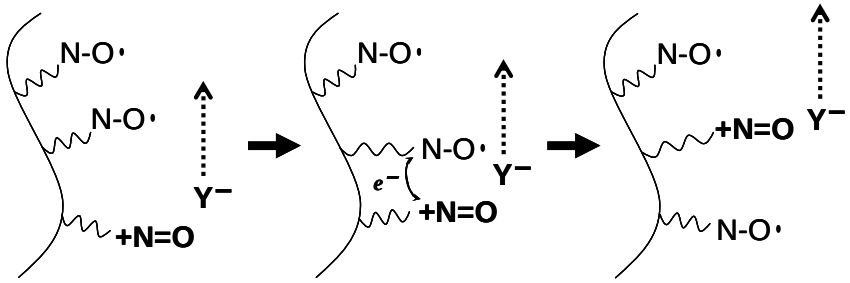

Figure 3.6 Schematic images for electrolyte anion assisted charge transportation in PTMA/electrolyte gel

Table 3.3. Diffusion constant, bimolecular rate constant, and activation energy for PTMA/electrolyte gels using PC electrolyte with 1.0M-$LiPF_6$, $LiBF_4$, $TBABF_4$ as the electrolyte salts

Experiments	**#1**	**#8**	**#9**
Radical polymer	PTMA	PTMA	PTMA
Electrolyte	1.0M $LiPF_6$ PC	1.0M $LiBF_4$ PC	1.0M $TEABF_4$ PC
[NO]/[$LiPF_6$]	1.0	1.0	1.0
[NO] in the gel	0.76 M	0.81 M	0.79 M
[$LiPF_6$] in the gel	0.76 M	0.81 M	0.79 M
D at 20°C	3.5×10^{-9} $cm^2 \cdot s^{-1}$	2.0×10^{-9} $cm^2 \cdot s^{-1}$	2.6×10^{-9} $cm^2 \cdot s^{-1}$
D at 50°C	7.9×10^{-9} $cm^2 \cdot s^{-1}$	6.0×10^{-9} $cm^2 \cdot s^{-1}$	7.2×10^{-9} $cm^2 \cdot s^{-1}$
k_{ex} at 20°C	1.4×10^6 $M^{-1} \cdot s^{-1}$	8.0×10^5 $M^{-1} \cdot s^{-1}$	1.0×10^6 $M^{-1} \cdot s^{-1}$
k_{ex} at 50°C	3.1×10^6 $M^{-1} \cdot s^{-1}$	2.4×10^6 $M^{-1} \cdot s^{-1}$	2.8×10^6 $M^{-1} \cdot s^{-1}$
Activation energy	26 kJ/mol	32 kJ/mol	34 kJ/mol

3.3.5. Ionic conductivity of a PTMA/electrolyte gel

Ionic conductivity of a PTMA/electrolyte gel (1.0M-$LiPF_6$ PC, [NO]/[$LiPF_6$] = 1.0) was measured by AC impedance method at the temperature of 20°C, 30°C, 40°C and 50oC. The ionic resistances were estimated from the x-intercept of the Nyquist plots. The

ionic conductivity of the PTMA/Electrolyte gel was almost one third of that of the liquid electrolyte. Arrhenius plots of the conductivities reveal that the activation energy for the PTMA/Electrolyte gel and the liquid electrolyte were 10 and 13 kJ/mol, respectively (Fig. 3.7). The result indicates that there is strong interaction between nitroxyl polymer and electrolyte salts.

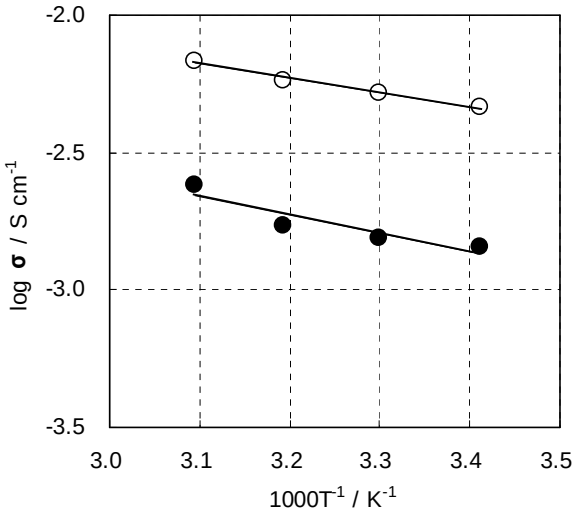

Figure 3.7 Arrhenius plots of ionic conductivities for a PTMA/electrolyte gel (●), and liquid electrolyte, 1.0M-$LiPF_6$ PC (○).

3.3.6. PTMA/electrolyte gels with cross-linked polymers

Cross-linked PTMAs were employed for PTMA/electrolyte gels preparation. The cross-linked PTMA was synthesized by adding 1%- and 4%- ethylene glycol dimethacrylate as a cross-linking reagent while polymerization. The cross-linked polymers have the limitation of swellable electrolyte volume. If the swelling electrolyte is insufficient, air remains in the gels. And if the swelling electrolyte is too much, the liquid phase is appeared. The critical amount of the swelling electrolyte volume was optimized for each gel before measurements. The concentrations of redox sites at the optimized gels were 0.66 and 0.77 M for 1%- and 4%- cross-linked PTMAs, respectively.

The rheological properties of the cross-linked PTMA/electrolyte gels were investigated. A strain dependence of the storage modules (*G'*) and the loss modules (*G"*) indicated the gel points of the gels to be around 10% strain region (Fig. 3.8). Straight-chain PTMA kept gel state (*G'*>*G"*) in entire strain range examined. At the

linear strain region around 0.1 %, it was found that dynamic viscosity was increased by cross-linking. The dynamic viscosity reveals that the cross-linked PTMA/electrolyte gels were not homogeneous. The particle boundary is still remained in the gel state contrasting to straight-chain PTMA/Electrolyte gels.

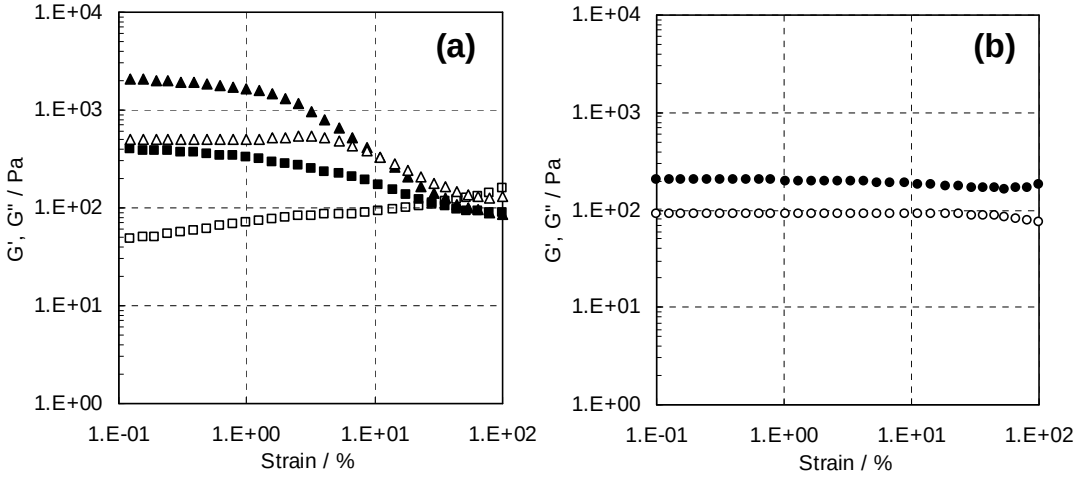

Figure 3.8 A strain dependence of dynamic viscosity (a) for a 1%-(*G'*:■, *G''*:□), 4%-(*G'*:▲, *G''*:Δ) cross-linked PTMA/electrolyte gels, and (b) straight-chain (*G'*:●, *G''*:○) PTMA/electrolyte gel.

3.3.7. Chronoamperometry for cross-linked PTMA/electrolyte gels

Diffusion constants, bimolecular rate constants, and activation energy were obtained by chronoamperometry measurements of optimized cross-linked PTMA/electrolyte gels (Table 3.4). Diffusion constants of cross-linked PTMA/electrolyte gels were 1-2 orders smaller than that of straight-chain PTMA/electrolyte gels. Arrhenius plots show the activation energy of charge diffusion for the gel with 4% cross-linked PTMA was significantly bigger than that of straight-chain PTMA. Since the relaxation of redox sites is limited by the cross-linking, the charge transportation would be significantly suppressed compare to straight-chain PTMA/electrolyte gels.

Table 3.4. Diffusion constant, bimolecular rate constant, and activation energy for PTMA/electrolyte gels using 1%-, and 4%-cross-linked PTMA

Experiments	**#10**	**#11**
Radical polymer	1%-CL PTMA	4%-CL PTMA
Electrolyte	1.0M $LiPF_6$ PC	1.0M $LiPF_6$ PC
[NO]/[$LiPF_6$]	0.77	0.99
[NO] in the gel	0.61 M	0.79 M
[$LiPF_6$] in the gel	0.79 M	0.79 M
D at 20°C	8.3×10^{-10} $cm^2 \cdot s^{-1}$	6.7×10^{-11} $cm^2 \cdot s^{-1}$
D at 50°C	2.1×10^{-9} $cm^2 \cdot s^{-1}$	3.1×10^{-10} $cm^2 \cdot s^{-1}$
k_{ex} at 20°C	3.0×10^{5} $M^{-1} \cdot s^{-1}$	2.5×10^{4} $M^{-1} \cdot s^{-1}$
k_{ex} at 50°C	7.8×10^{5} $M^{-1} \cdot s^{-1}$	1.2×10^{5} $M^{-1} \cdot s^{-1}$
Activation energy	30 kJ/mol	43 kJ/mol

3.3.8. Ionic conductivity of cross-linked PTMA/electrolyte gels

Ionic conductivities of the cross-linked PTMA/electrolyte gels were investigated (Fig. 3.9). It is noted that the conductivities and the activation energy were almost same as that of the liquid electrolyte, and twice larger than that of straight-chain polymer. Though the cross-linked PTMA/electrolyte gels showed slower charge transportation than that with straight-chain PTMA, they demonstrated the higher ionic conductivity. It is considered that the suppressed relaxation of redox sites in cross-linked PTMA brings weak interaction between a redox site and an electrolyte anion. The weaker interaction results in causing slower charge transportation than PTMA/electrolyte gels using straight-chain PTMA/electrolyte gels. Therefore, it would be considered that the stronger interaction would contribute to the faster charge transportation according to electrolyte anion assisted charge transportation in PTMA/Electrolyte gels.

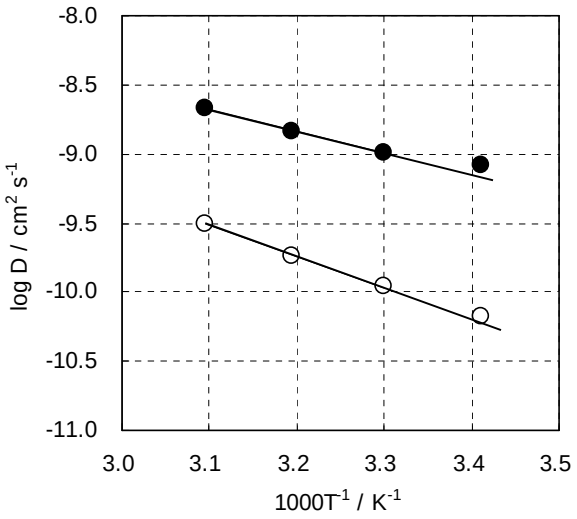

Figure 3.9 Arrhenius plots of ionic conductivities for a 1%-(●), and 4%-(○) cross-linked PTMA/electrolyte gels

3.4. Conclusion of Chapter 3

Charge transportation in PTMA/electrolyte gels is strongly assisted by the mobility of anion in the electrolytes. Diffusion constant of charge in a straight-chain PTMA/electrolyte gel with the [NO]/[$LiPF_6$] ratio of 0.6 achieved to be 3.5×10^{-9} $cm^2 \cdot s^{-1}$ at 20^{o}C, because of stronger interaction between redox site and electrolyte anion, and higher mobility of anion in the gel. Bimolecular rate constant (k_{ex}) of the gel was estimated to be 2.8×10^6 $M^{-1} \cdot s^{-1}$ from Dahms-Ruff equation. The fast charge transportation would bring high-rate capability of organic radical battery with PTMA cathode.

———————————————————————————————

References

1) H. Nishide, K. Oyaizu, *Science* **2008**, 319, 737.

2) K. Nakahara, S. Iwasa, M. Satoh, Y. Morioka, J. Iriyama, M. Suguro, E. Hasegawa, *Chem. Phys. Lett.* **2002**, 359, 351.

3) H. Nishide, S. Iwasa, Y.-J. Pu, T. Suga, K. Nakahara, M. Satoh, *Electrochim. Acta* **2004**, 50, 827.

4) H. Nishide, T. Suga, *Electrochem. Soc. Interface* **2005**, 14, 32.

5) K. Nakahara, K. Oyaizu, H. Nishide, *Chem. Lett.* **2011**, 40, 222.

6) K. Oyaizu, T. Suga, K. Yoshimura, H. Nishide, *Macromolecules* **2008**, 41, 6646.

7) K. Oyaizu, T. Kawamoto, T. Suga, H. Nishide, *Macromolecules* **2010**, 43, 10382.

8) J. -M. Tarascon, M. Armand, *Nature* **2001**, 414, 359.

9) A. S. Arico, P. Bruce, B. Scrosati, J. -M. Tarascon, W. V. Schalkwijk, *Nature Mater.* **2005**, 4, 366.

10) K. Nakahara, J. Iriyama, S. Iwasa, M. Suguro, M. Satoh, E. J. Cairns, *J. Power Sources* **2007,** 165, 398.

11) K. Nakahara, J. Iriyama, S. Iwasa, M. Suguro, M. Satoh, E. J. Cairns, *J. Power Sources* **2007**, 165, 870.

12) K. Oyaizu, H. Nishide, *Adv. Mater.* **2009**, 21, 2339.

13) T. Suga, Y.-J. Pu, K.Oyaizu, H.Nishide, *Bull. Chem. Soc. Jpn.* **2004**, 77, 2203.

14) M. Satoh, K. Nakahara, J. Iriyama, S. Iwasa, M. Suguro, *IEICE Trans.* **2004**, E87-C, 12, 2076.

15) K. Oyaizu, Y. Ando, H. Konishi, H. Nishide, *J. Am. Chem. Soc.* **2008**, 130, 14459.

Chapter 4

Fabrication of Organic Radical Battery as a New Energy Device

4.1. Introduction of Chapter 4

Polymer material is one of the most important masterpieces of modern society. Almost all personal belongings, such as stationeries, household goods and electric products use polymer materials in them. Without these materials, we couldn't get a rubber tire, a plastic bag and a chemical fiber. They are practically used because of their insulating properties and mechanical features. However in 1980s, conducting polymers were first reported and their electronic activities started to be attracted.[1] It is known that conducting polymers with π-conjugated electronic structure show over 10^4 $S \cdot cm^{-1}$ of conductivity when they oxidized or reduced. And it was also reported that it can be oxidized or reduced electrochemically, so they were used as active materials for rechargeable batteries.[2]

Polyradicals have been used as one-dimensional throw-bond organic ferromagnets, and considerable effort has been made to increase their values of spin quantum number (*S*) in an electronic ground state[3,4] In addition to that, many polyradicals are known to be oxidized and reduced electrochemically,[5,6] and it is characteristic that radical-cation/anion is not produced in any stage of the redox process. If polymers did not have radical electrons in a charged/discharged state, they would stabilize. We initially found that these redox processes would be suitable for a reaction of cathode active materials in aprotic rechargeable batteries. The use of organic materials as an active material in cathodes appears promising to design environmentally friendly, high energy-density rechargeable batteries. In this chapter, we describe the electrochemical properties of a stable nitroxyl polyradical, poly (2,2,6,6-tetramethylpiperidine-1-1oxyl methacrylate) (PTMA), and the performance of the prototype lithium battery using this design.

4.2. Experimental

Materials

PTMA was synthesized by a radical polymerization of 2,2,6,6-tetramethylpiperidine methacrylate monomer (ASAHI denka, LA-87) with 2,2'-azobisisobutyronitrile (AIBN), followed by oxidizing it with 3-chloroperoxybenzoic

acid (*m*-CPBA) (Fig. 4.1). A pale orange polymer was purified using re-precipitation with methanol.

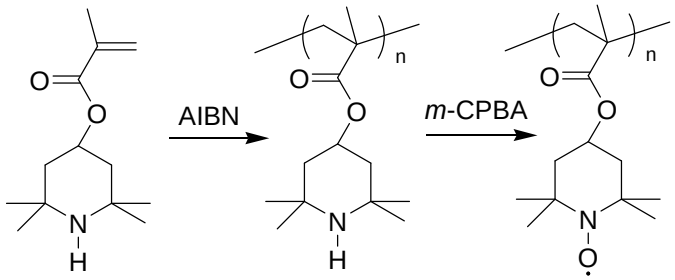

Figure 4.1. Synthesis procedure of PTMA

Measurements

Cyclic voltammetry was performed using the standard three-electrode method. To prepare a working electrode, PTMA was mixed and tempered with graphite and binding powder, then pressed into an aluminum current collector. A Platinum wire counter electrode and a Li/Li^+ reference electrode were used in an electrolyte mixture solution of diethyl carbonate (DEC) and ethylene carbonate (EC) [DEC/EC=7/3], into which 1.0M-$LiPF_6$ had been dissolved. A normal potensiostat system (Electrochemical Analyzer 604, CH Instruments) was used to measure it. All experiments were run under an argon atmosphere at room temperature. Electron spin resonance (ESR) spectroscopy was performed using a JES-FR30 type X-band (9.48 GHz) spectrometer.

Cell fabrications

The coin-type cell was fabricated by the stacking of electrodes with separator film. Pulverized PTMA (specific density 1.15 g cm^{-3}, 100 mg) and graphite powders (800 mg) were mixed and tempered with polytetrafluoroethylene powder (DAIKIN industries, F-104, 100 mg). The resulting clay was spread out in a board-like shape, and a composite cathode 12 mm in diameter was stamped out of it. This cathode (150-250 μm thick, 9-15 mg) was dried under a high vacuum at 80^{o}C and impregnated with an electrolyte solution of DEC (7.0 g) and EC (3.0 g), into which $LiPF_6$ (1.5 g) had been dissolved. We put the composite cathode on a current collector. On top of the collector, we put a porous polyethylene film separator suffused with liquid electrolyte. Over these, we then stacked an over-sized lithium metal anode (1.4 mm thick) and another current collector, thus

forming a prototype battery. The battery was charged and discharged at a constant current. The upper charge voltage was limited to 4.0 V. The discharge was cut off when the potential reached 3.0 V. All the charge-discharge experiments were carried out at room temperature using a computer-controlled automatic battery charge-discharge instrument labelled BTS-2004 (NAGANO).

4.3. Results and discussion

4.3.1. PTMA as a new cathode active material

Using gel permiation chromatography, we estimated the weight-average molecular weight of PTMA to be 89,000. The obtained PTMA was insoluble in such nonaqueous solutions such as DEC. ESR spectroscopy showed the radical concentration of PTMA to be approximately 2.5×10^{21} spins/g, which nearly matches with a theoretically calculated value of one radical per monomer unit. The radicals on the PTMA are stable up to the thermal decomposition temperature of the polymer (240^{o}C). Furthermore, the radical concentration remained unchanged over 5 months under ambient laboratory conditions.

4.3.2. Cyclic voltammogram of a PTMA/carbon composite cathode

A cyclic voltammogram of PTMA electrode is shown in Fig. 4.2. A half-wave potential ($E_{1/2}$) of PTMA is 3.58 V vs. Li/Li^{+}. It is noted that the difference of ration of the anodic ($E_{a,p}$: 3.66 V) and cathodic ($E_{c,p}$: 3.50 V) peak potentials is estimated as 0.16 V at a sweep rate of 10 mV/sec, which is extremely smaller than that of the other electroactive organic materials such as disulfide compounds. The small gap of the anodic and cathodic peaks corresponds with its fast electrode reaction rate of the present polyradicals, which leads to a capability for high power rate in the charge and discharge process of the battery. Both of an anodic and a cathodic capacities of this electrode tested between 3.0 and 4.0 V were estimated, to be much the same, 1.06 C and 1.07 C respectively. This indicates the Coulomb efficient is regarded as nearly equaling 100 %.

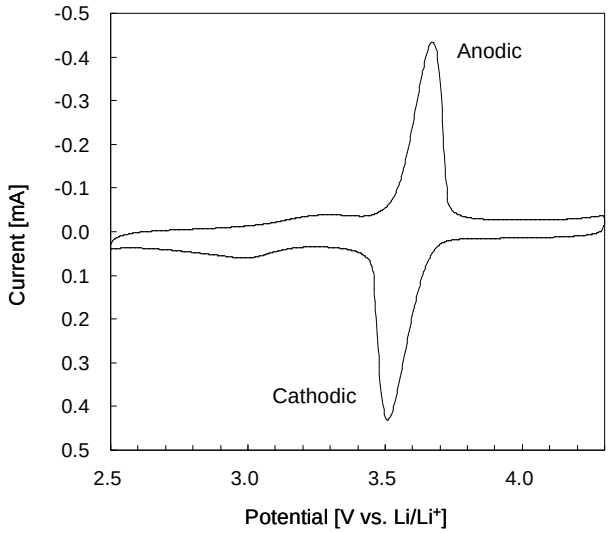

Figure 4.2. Cyclic Voltammogram of PTMA contained a composite electrode at sweep rate of 10 mV/s. Composite electrode contains PTMA/Graphite/binder at the ratio of 1/8/1. Platinum wire counter electrode and Li/Li^+ reference electrode were used in an electrolyte mixture solution of EC/DEC, into which 1.0M-$LiPF_6$ had been dissolved.

4.3.3. ESR spectra of a PTMA/carbon composite cathode

Figure 4.3 shows the ESR spectra of electrochemically oxidized (4.3 V vs. Li/Li^+) and reduced (3.3 V vs. Li/Li^+) PTMA electrodes. A significantly large peak (*g*-value: 2.0076) was observed in the spectrum of the reduced electrode. On the contrary, the small and broad peak could be seen in that of oxidized one. The radical concentration of oxidized electrode, which is calculated by double integrations of the ESR spectra, is estimated to be only 26% of that of reduced one. This indicates that the anodic process of PTMA eliminates some radical electrons, which later regenerate during the cathodic process. More precisely, we considered that the nitroxyl radical is oxidized to form a cation and joins an electrolyte anion to form oxoammonium salt during the anodic process, and its reverse reaction occurs during the cathodic process.

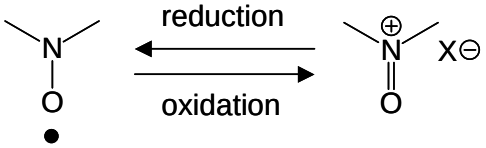

The three abnormalities, observed in the ESR spectra at magnetic fields of 334.33, 335.95, and 337.57 mT, are considered to be an influence of peak separations caused by the nuclear spin of a nitrogen atom.

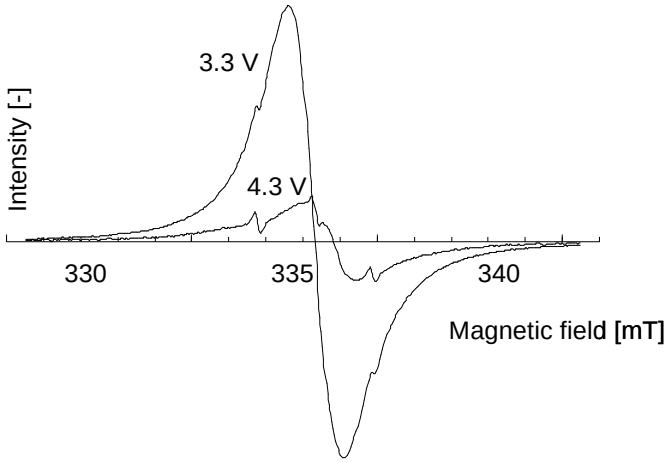

Figure 4.3. Electron spin resonance spectra for pieces of composite electrodes, which are picked up at potentials of 3.3 and 4.3 V vs. Li/Li^+.

4.3.4. Charge/discharge profile of Li/PTMA half-cell

The fabricated PTMA/Li battery was charged at constant current densities of 0.1 and 1.0 mA/cm^2 until its voltage reached 4.0 V. Figure 4.4 shows the charge-discharge curves. An obvious voltage plateau is evident in both curves. The found plateau voltage of nearly 3.5 V is comparable to the redox potential of PTMA, which indicates that the charge process at the cathode consists of PTMA oxidizing to oxoammonium salt, and that the discharge process consists of a reduction in salt. The initial discharge capacity was 77 mAh/g of the PTMA weight at a current density of 0.1 mA/cm^2. Assuming one electron per monomer unit in the redox process, we estimate the theoretical capacity of the PTMA to be 111 mAh/g. The experimentally obtained discharge capacity was 70 % of the theoretical capacity. At the current density of 1.0 mA/cm^2, the discharge capacity retained 91% of that found for the 0.1 mA/cm^2 measurement. It should be noted that a current density of 1.0 mA/cm^2 is much larger than that of conventional battery and suggests that only 5 minutes was needed to fully charge the battery.

4.3.5. Cyclability of Li/PTMA half-cell

Figure 4.5 shows the cycle performance of the fabricated Li/PTMA battery. Charging and discharging were repeated at a current density of 1.0 mA/cm^2 for cell

voltages ranging from 3.0 to 4.0 V. As shown in this figure, no significant deterioration in the capacity is observed at up to 500 cycles. Because the capacity of the PTMA composite cathode is significantly less than that of the lithium metal anode, its use did not result in the usual decrease in battery capacity. The increase in capacity observed during the initial 30 cycles appears to arise from the newness of the contact between the electrode and electrolyte. It should be noted, however, that the cathode contains only 10 wt% of active material, and it is necessary to increase this percentage for the practical use.

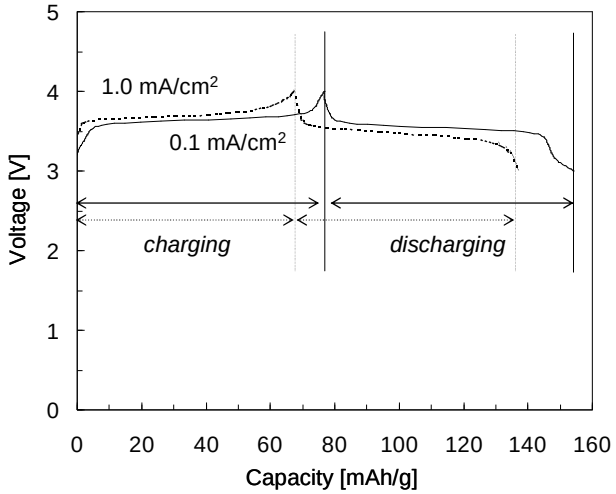

Figure 4.4. Charge-discharge curves for PTMA/Li battery at the charge-discharge current density of 0.1 and 1.0 mA/cm^2.

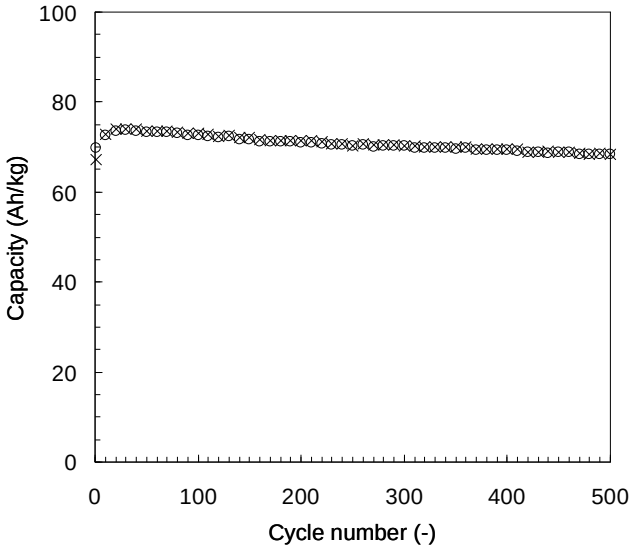

Figure 4.5. Changes in charge (x) and discharge capacities (o) of PTMA/Li battery during repeated cycles (1.0 mA/cm^2, 3.0-4.0 V).

4.4. Conclusion of Chapter 4

A space distribution of non-bonding molecular orbital for nitroxyl radicals is considered to be localized in the nitroxyl group. The locality of the energy storage component promises to offer a variety of molecular design possibilities for use in cathode active materials. It might be possible to produce flexible, adhesive, electro-conductive, or even liquid cathode active materials. Further, because their localized nature restrains the interaction between energy storage components, these systems enable overcoming the capacity limitations, which are seen in conductive polymers. By packing radical components together for a high density, producing organic materials with a capacity of >300 A/kg may be possible. However, because many types of radicals are insulators, the composition of the electrodes needs to be refined. Using molecular design to give conductivity to the radicals is also necessary. The future of the organic radical cathode appears to depend on the progress in organic synthesis technologies.

References

1) P. J. Nigrey, D. Maclnnes Jr., D. P. Nairns, A. G. MacDiarmid, *J. Electrochem. Soc.* **1981**, 1651.

2) P. J. Nigrey, A. G. MacDiarmid and A. J. Heeger, *J. Chem. Soc. Chem. Commun.*, **1979**, 14, 594.

3). H. Nishide and T. Kaneko, in: P. M. Lahti (Eds.), *Magn. Prop. Org. Mater.*, **1999**, 285.

4) Y. Miura, in: P. M. Lahti (Eds.), *Magn. Prop. Org. Mater.*, **1999**, 267.

5) M. F. Semmelhack, C. S. Chou, and D. A. Cortes, *J. Am. Chem. Soc.*, **1985**, 105, 4492.

6). A. Merz and H. Bachmann, *J. Am. Chem. Soc.*, **1995**, 117, 901.

Chapter 5

Cell Performances of Organic Radical Battery with PTMA/Carbon Composite Cathode

5.1. Introduction of Chapter 5

An organic radical battery is a new type of lithium rechargeable battery which utilizes the reversible redox reaction of stable radical compounds as a cathode reaction. So far, a number of stable nitroxyl radical polymers, such as poly (2,2,6,6-tetramethyl-1-piperidinyloxy-4-yl methacrylate) (PTMA)[1,2,3] and poly (*N*-tert-butylnitroxy-3,5-phenylene), have been synthesized and utilized for cathode active materials in lithium batteries.[2,3] Among them, Li/PTMA battery has been intensively investigated as a rechargeable battery with long cycle life[2,3,4,5] and its reaction mechanism was being made clear by some of analytical experiments.[3,6,7]

It had been considered that PTMA lacks electronic conductivity, so in previous work, we have made a PTMA-carbon composite cathode by mixing and solidifing PTMA powder, carbon black and PTFE binder in dry condition simply. Using a composite cathode made by this process, we achieved rechargeable battery with long cycle life. However, it is thought that the homogeneousness of this electrode was so insufficient that we couldn't achieve high capacity. The obtained capacity was less than 80% of theoretical capacity.[2]

In chapter 5, a cathode making process using doctor blade method with water based slurry was employed. As a result, we succeeded in making homogeneous electrode with PTMA powder and achieved high utilization of active material. The obtained capacity was almost equal to theoretical one. In addition to that, half cell properties such as cycle ability, temperature dependence, rate capability and self-discharge rate were measured in detail. This chapter also suggests that graphite anode was available against for PTMA based cathode. This result is very important for thinking commercialization of the battery.

5.2. Experimental

Materials

PTMA was synthesized ourselves by a radical polymerization of 2,2,6,6-tetramethylpiperidine-4-yl methacrylate monomer (LA-87, Asahi-denka) using 2'-azobisisobutyronitrile (AIBN) followed by oxidizing it with 3-chloroperoxybenzoic acid (m-CPBA). The synthesis procedure was described somewhere else in detail.[2,3] All electrolytes were obtained from Ube Industries Ltd.

Electrode fabrication

PTMA cathode was prepared by following procedure. In order to make viscous solution, we added 5.0 g of Carboxy methyl Cellulose, CMC, (HB9, ZEON Corp.) into 500 g of pure water, and stirred until it was dissolved completely. Then, 1.25 g of PTFE fine powder (60% water dispersion, D-1B, DAIKIN) and 56.25 g of vapor grown carbon fibers (VGCF^{TM}, Showa-Denko) were added into the CMC solution, and kept stirring intensively for 1 hour. We completed to make slurry by adding 62.5 g of PTMA fine powder into well dispersed carbon ink and mixing it well. Resulted slurry was spread on carbon coated Aluminum foil by Doctor Blade method. And after evaporation of solvent water by heating (100^{o}C, 10 min.), PTMA cathode was prepared. This cathode contained PTMA (50 wt.%), VGCF (45 wt.%), CMC (4 wt.%) and PTFE (1 wt.%). The thickness was 130-180 μm. Graphite, mesocarbon microbeads (MCMB#3, Osaka-gas) anode was prepared by normal process using NMP slurry and Doctor Blade method. This anode contained graphite (90 wt.%), conductive carbon black (1.0 wt.%) and PVdF (9.0 wt.%). The thickness was adjusted to be 10-20 μm. Scanning Electron Microscope (SEM) observation was performed by using an S-2400, HITACHI, SEM apparatus.

Cyclic voltammogram

Cyclic voltammogram was obtained by a standard three-electrode cell in dry argon atmosphere at room temperature using an Electrochemical Analyzer 604, CHInstruments, potensiostat system. A platinum wire with sufficient surface area was used as the counter electrode and lithium metal was used as the reference electrode. The electrolyte was 1.0 M lithium hexafluorophosphate ($LiPF_6$) in ethylene carbonate (EC) and diethyl carbonate (DEC) mixed solvent (EC/DEC=3/7, v/v). The sweep speed was set to be 1 mV sec^{-1}.

Cell fabrication

Coin cells (2320-type) were assembled using microporous film separators, Celgard 2400, in dry room (dew point < -50^{o}C). In half-cell experiments, 1.4 mm thick lithium metal ingot was used as anodes. As a liquid electrolyte, we used 1.0 M $LiPF_6$ in mixed carbonate solvent (EC/DEC=3/7, v/v). Charging and discharging control was

carried out by using a BLS, Tabai espec, automatic battery measurement system under controlled temperature.

Cell evaluations

Self-discharge tests were carried out by the following method. After coin cells were charged at 1 C constant current up to 4.5 V, they had been left at open circuit state for various periods. And then, the cells were discharged at 0.2 C down to 2.6 V. By comparing with the charging capacities and discharging capacities, we calculated their self-discharge rate. Continuously, we charged them at 1 C up to 4.5 V again, and discharged them at 0.2 C down to 2.6 V without time break. Based on the values of discharge capacities with and without time break, we evaluated their recovery rate.

Li^+ pre-doped grapite anode for thin-type battery

Thin-type batteries with Al-laminated film were fabricated and used for the stability evaluations. Active-polymer composite cathodes were made by 70%-PTMA, 21%-conducting carbon (VGCF + SuperP) and 9%-binder (CMC + PTFE). The thickness of the cathode was 132 μm and electrode density was found to be 0.69 g/cm^3. Electrochemically Li^+ pre-doped graphite (MCMB#6-28) were applied as anode. Doping depth was controlled to be 90% of the capacity. A mixture of 1M-$LiPF_6$ EC/DEC (3/7 by vol.) was used as an electrolyte. Measurements were normally carried out by cc-cv charging (UCV: 3.9V, from 1C=0.57 mA/cm^2 to 0.1C) and cc discharging (LCV: 3.0V, 1C) processes.

5.3. Result and Discussions

5.3.1. PTMA/carbon composite cathode fabricated by slurry coating process

Figure 5.1 shows a surface image of PTMA-carbon composite electrode. PTMA particles with the several tens micron diameter are buried under the carbon fiber conductive additives. There are many void spaces in the electrode surface. The deposited density of the electrode was 0.4-0.5 g cm^{-1}.

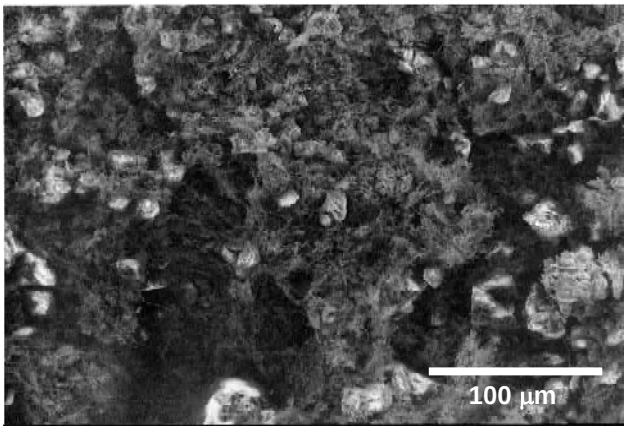

Figure 5.1. A Scanning Electron Microscope (SEM) image of PTMA-carbon composite electrode made from water based slurry.

The electrochemical properties of a PTMA-carbon composite electrode were investigated by using a platinum wire as a counter electrode and a lithium metal as a reference electrode. As shown in Fig. 5.2., the cyclic voltammogram obtained for the electrode in an aprotic electrolyte displayed a pair of current peaks at the standard redox potential of 3.58 V vs. Li/Li^+. The peaks were remarkably sharp, and their separation was quite narrow. This indicates that the redox reaction of PTMA was homogenous and that the redox reaction at each site was almost independent. The densely populated radical components brought about high capacity without any limitations. The area of oxidation capacity was almost equal to that of the reduction capacity. That indicates excellent redox efficiency. Compared with the previous reports, the peak height ratio to background was considerably increased because of homogeneousness improvement of active material.

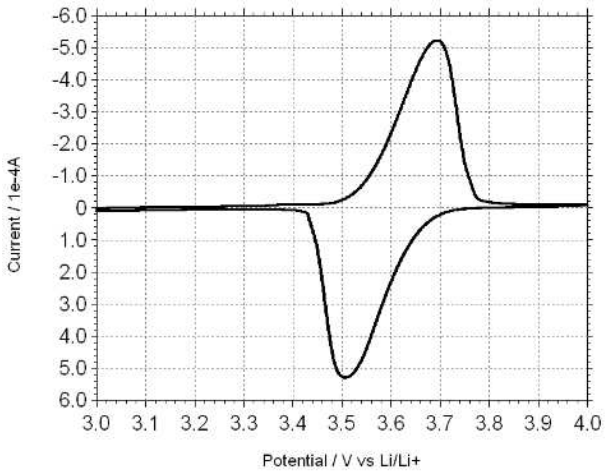

Figure 5.2. A Cyclic voltammogram of PTMA-carbon composite electrode made from water based slurry in EC/DEC=3/7, 1.0M-$LiPF_6$ electrolyte.

5.3.2. Charge/discharge profiles of a Li/PTMA half-cell

The charging and discharging curves obtained for the voltage range 2.6–4.5 V displayed obvious plateaus (Fig. 5.3). The discharge plateau showed average discharge voltage of 3.51 V. The specific capacity of the PTMA was 110 $mA \cdot h \cdot g^{-1}$, nearly equal to the theoretical capacity (111 $mA \cdot h \cdot g^{-1}$), indicating that almost all the nitroxyl radical components contributed to the charge storage. This is evidence that the composite electrode allowed delivering of electrons to all radical components in the oxidized state during discharge and that electro-neutralization with electrolyte counterions occurred throughout the radical polymers.

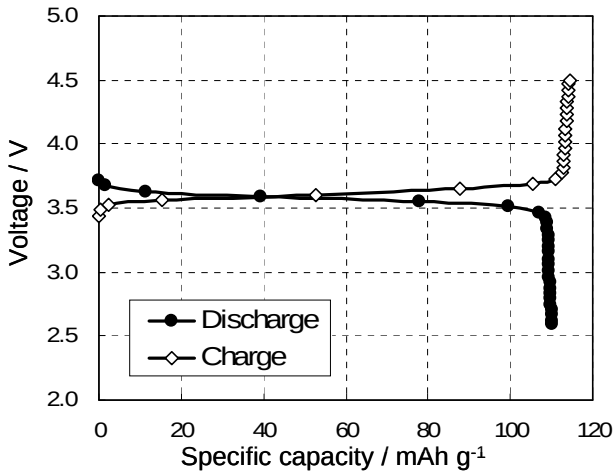

Figure 5.3. Charging and discharging curves of Li/PTMA half cell (45°C, 2.6-4.5 V). Charging and discharging current was set to be 0.3 mA and it corresponds to about 1 C rate.

5.3.3. Cyclability of a Li/PTMA half-cell

Li/PTMA coin cells were cycled by charging and discharging them at a temperature of 20, 45, or 60°C, a voltage of 2.6–4.5 V, and 1 C rate (Fig. 5.4a). As shown in the Fig. 5.4b, at 20°C, the capacity after 100 cycles was 91% of the initial capacity. Another test[2] showed that a composite electrode with highly dispersed PTMA retained 98% of its initial capacity after 500 cycles. These results demonstrate that PTMA is sufficiently stable during cycling at 20°C. The higher temperatures, however, caused faster deterioration of the cell capacity. In particular, at 60°C, almost 50% of the initial capacity was lost during the first 100 cycles. Side reactions such as decomposition of

electrolyte or inactivation of lithium anode surface caused by moisture might be accelerated by high temperature.

Cyclability at 1 C and 5 C rates are shown in Fig. 5.5. Charging rates were set as same as discharging rates. Compared with 1 C rate cycles, a slightly large degradation of capacity was seen at 5 C. It is considered that an increase in the impedance during cycles caused degradation of the charging capacity at a higher rate. We considered that the degradation caused by repeating cycle was more effective than that caused by time progress.

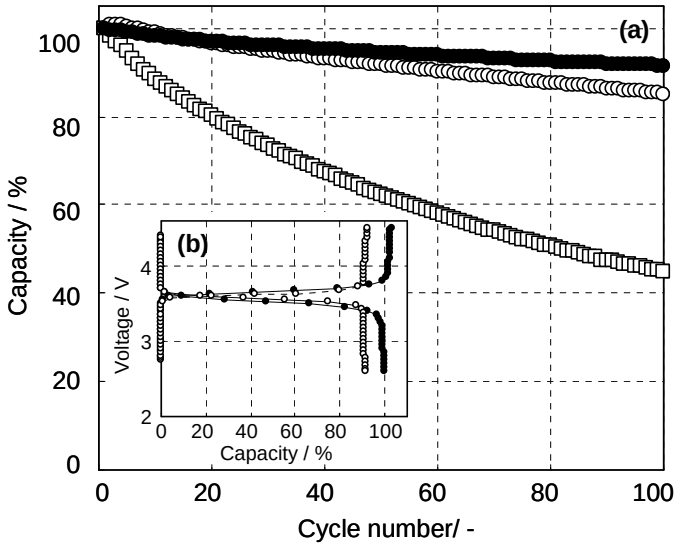

Figure 5.4. (a) Cycling performance of half-cell measured for 2.6-4.5 V (●: 20°C, ○: 45°C, □: 60°C). (b) Charge and discharge curves for 1st(●) and 100th(○) cycle obtained at 20°C.

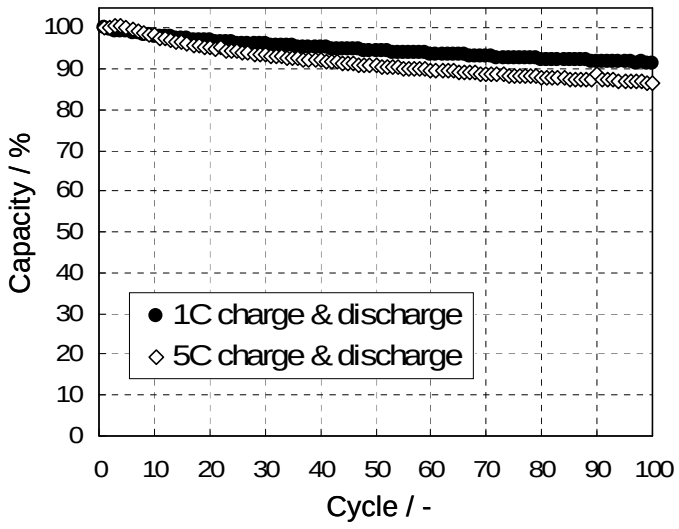

Figure 5.5. Cycle abilities of Li/PTMA half cell at 1 C and 5 C rates.

5.3.4. Discharge rate capability of a Li/PTMA half-cell

Rate dependence of discharge curves in the range from 0.5 to 20 C at 20°C and 45°C are shown is Fig. 5.6. All charging processes were operated at 1 C. A discharge current of 1 C rate corresponded to a current density of 0.27 $mA \cdot cm^{-2}$. We found that the higher discharge rate caused a drop of the discharging voltage and a degradation of the capacity. The voltage drop is considered to be mainly caused by the ionic resistance of the electrolyte, because the dropping ratio of the voltage was directly proportional to the discharge rate. Therefore, compared the results obtained at 20°C with 45°C, the higher temperature resulted in the smaller decrease of the discharging voltage.

On the other hand, behavior of capacity degradation obtained at 20°C was similar to that at 45°C. The discharge capacity at a 20 C was 78% that at a 1 C (45°C). The capacity decrease at a high discharge rate was caused by an increase in the number of inert radical components in the radical polymers rather than an increase in the direct current resistance. The increase in the number of inert radical components was due to the limitation of the kinetics of the self-exchange reaction between neighboring radical components. The capacity decrease at the high rate can be reduced by improving dispersivity in the composite electrode by using an effective dispersing solvent for the PTMA, such as N-methyl-2-pyrrolidone. A composite electrode with highly dispersed PTMA should thus be effective for reducing the thickness of the homogeneous electron transfer layer.[8] This indicates that Li/PTMA half cell has a possibility to be a high-power energy sources.

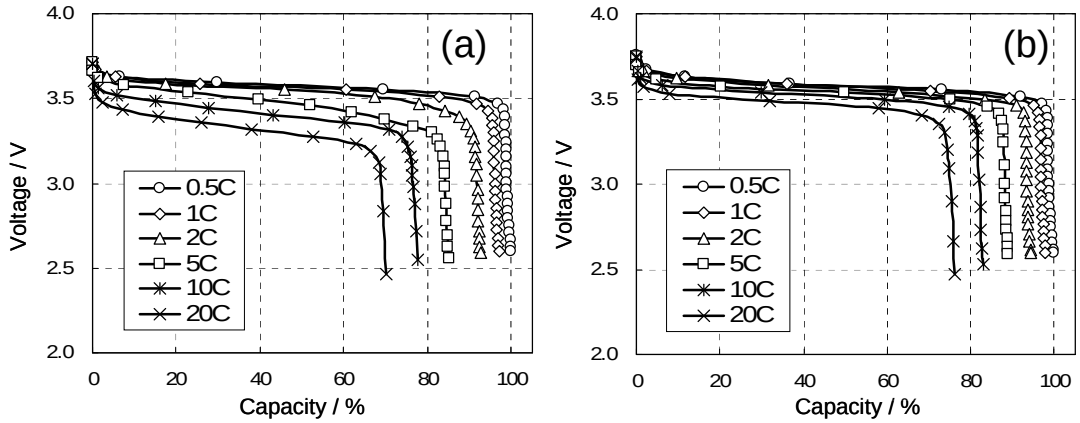

Figure 5.6. Discharge rate capabilities of Li/PTMA half cell at (a) 20°C and (b) 45°C.

5.3.5. Storage evaluation of a Li/PTMA half-cell

Self discharge rate was evaluated at 20°C and shown in Fig. 5.7. Large self-discharge was observed and it was found to be proportional to the square root of time progress. After 1 week preservation, 38% of the charging capacity was disappeared. However, it recovered well (>98.5%) at the next cycle. That indicates that material itself was not damaged by preservation. We are considering the self discharge caused by redox shuttle mechanism. Resolved PTMA to the electrolyte might work as a redox species. Cross-linking and purification of the radical polymers effectively suppressed the self-discharge.

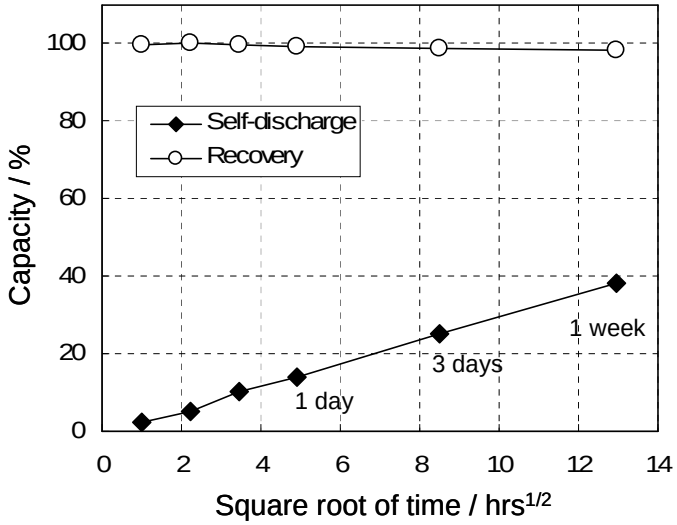

Figure 5.7. Self-discharge rate of Li/PTMA half cell at 20°C.

5.3.6. Battery design for a graphite/PTMA rechargeable cell

A graphite anode was prepared for assembling a coin cell with a PTMA cathode. First charging capacity of the anode was adjusted to be same as that of PTMA cathode with the value of 0.30-0.35 mAh. Figure 5.8. shows an example of first charging and discharging curves of Li/Graphite half cells. First charging and discharging capacities were 0.34 and 0.26 mAh, respectively. That means 24% of initial charging capacity was irreversible. Average voltage was 0.15-0.20 V.

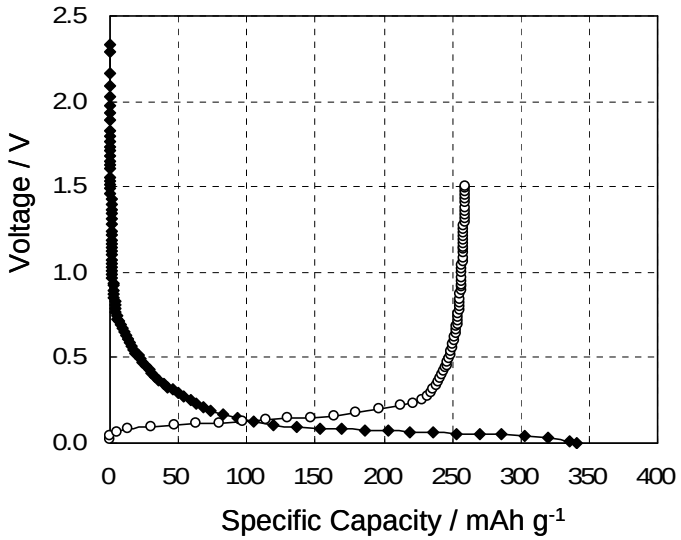

Figure 5.8. The first charging and discharging curves of Li/Graphite half cell at 20°C.

5.3.7. Charge/discharge profiles of a graphite/PTMA cell

Figure 5.9 shows the first charging and discharging curves for Graphite/PTMA cell. First charging and discharging was carried out at the constant current of 0.1 mA, it corresponds to about 1/3 C rate of first charging capacity. Upper and lower limit voltage was 4.0 and 2.6 V, respectively. Open circuit voltage of as prepared cell was about 0.2 V, however, the voltage increased gradually while charging. The charging voltage plateau was seen at around 3.5 V, and the voltage rose suddenly after the plateau. The first charging capacity was 0.35 mAh, and its average voltage was 3.4 V. And then, the first discharging curve also had a good shape. The discharging voltage plateau was seen at around 3.5 V, and the capacity was 0.23 mAh. That means 0.11 mAh (33%) of the first charging capacity was irreversible. As described before, graphite anode itself had 24% of irreversible capacity, so this percentage went up by assembling with PTMA cathode. If we use a PTMA cathode, lithium salt ($LiPF_6$) concentration in the electrolyte solution would be changed continuously during charging and discharging process. At the completely discharged state (DOD=100%), the concentration was set to be 1.0 M, however, at the charging state, it would be lower than 1.0 M. So we considered that the component of solid electrolyte interface (SEI) layer on graphite of Graphite/PTMA cell was different from that of Li/Graphite cell. That might caused an increase of first irreversible capacity.

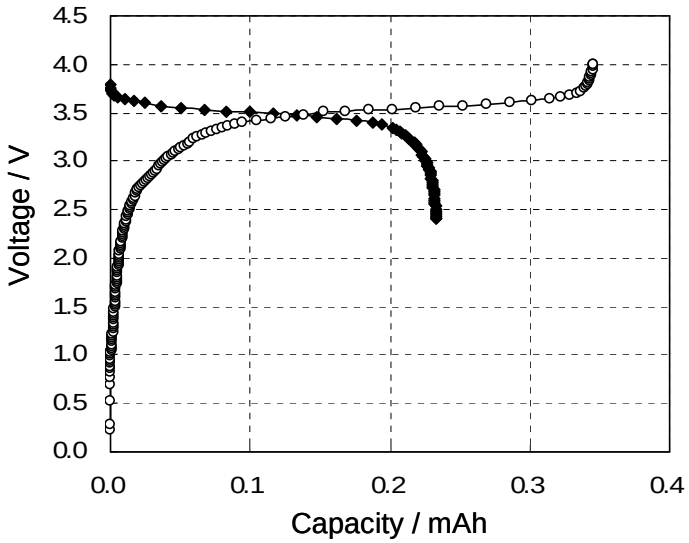

Figure 5.9. The first charging and discharging curves of Graphite / PTMA cell at 20oC. Charging and discharging current was 0.1 mA.

Figure 5.10 shows the second charging and discharging curves. Charging and discharging was carried out at the constant current of 0.2 mA, it corresponds to roughly about 1.1 C rate of reversible capacity. Upper and lower limit voltage was 4.0 and 2.6 V, respectively. We found that Graphite/PTMA cell entered the stable state after the second cycle. Charging and discharging voltage plateau were observed around 3.5 V and their capacity were 0.23 and 0.22 mAh, respectively.

5.3.8. Cyclability of a graphite/PTMA cell

Cycle ability was shown in Fig. 5.11. The cycle was repeated at constant current of 0.2 mA between 2.6-4.0 V. Discharge capacity was decreased gradually, and at 25th cycle, 87 % of initial capacity was obtained. Although a large irreversible capacity was observed at first cycle, it almost disappeared after that. After 10th cycle, over 97% of coulomb efficiency was achieved and it was also improving more during cycles.

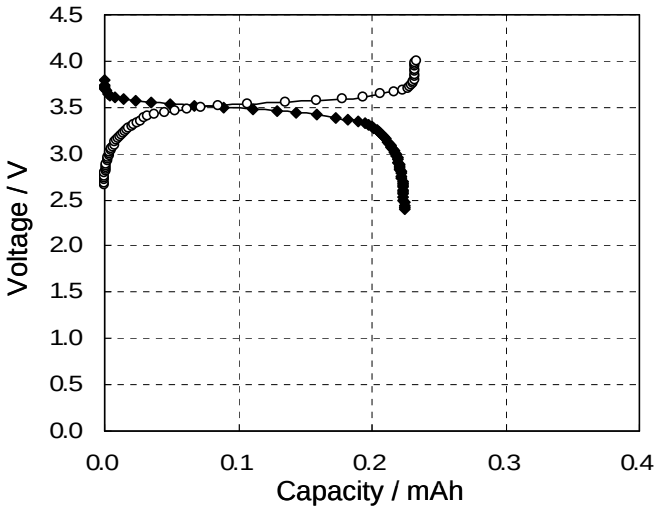

Figure 5.10. Second charging and discharging curves of Graphite/PTMA half cell at 20°C. Charging and discharging current was 0.2 mA.

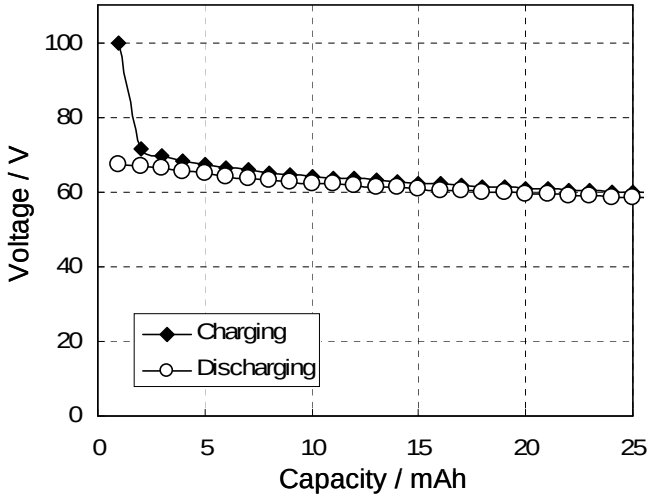

Figure 5.11. Cycle abilities of Graphite/PTMA half cell at 20°C. Charging and discharging current was 0.2 mA.

5.3.9. Stability evaluations with Li^+ pre-doped graphite anode

Thin-type batteries with Al-laminated film were fabricated and used for the stability evaluations. A composite cathode which consists of 70%-PTMA and electrochemically Li^+ pre-doped graphite anode were applied for the evaluations. The PTMA was cross-linked by adding ethylene glycol dimethacrylate as the cross-linking agent. The cross-linkage has the effect of preventing PTMA from dissolving into the electrolyte. As a result of optimization, the degree of cross-linkage was selected to be 1%. The higher degree of cross-linkage brought the higher resistivity. The lower one

exhibited the lower insolubility. Figure 5.12 shows utilized region of the anode and cathode. One third of the anode capacity with deep state of charge area was used for the experiment.

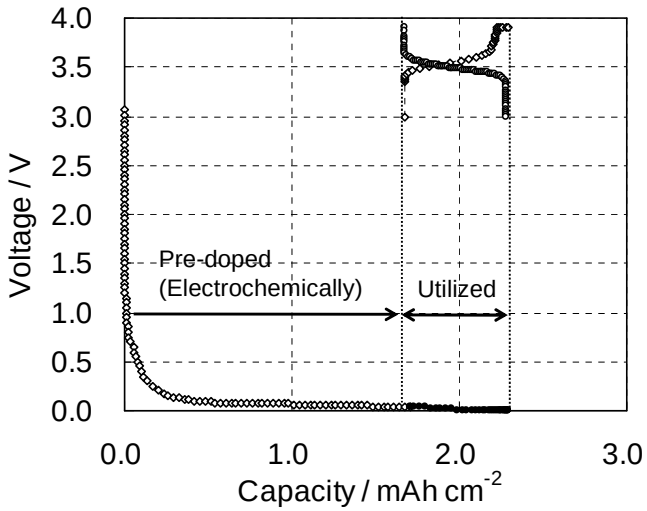

Figure 5.12. The utilized region of Li^+ pre-doped graphite anode

Initial specific capacity of PTMA measured at 0.1C under 20°C was 96 mAh/g, and discharging voltage was 3.49V in the average (Fig. 5.13). Specific capacity measured at 10C discharge was 66 mAh/g, which corresponds to 69% of 0.1C capacity (Fig. 5.14).DC resistance was estimated to be 33 Ω/cm^2 (Fig. 5.15). These cell properties of thin-type batteries were demonstrated similar with those of coin-type cells.

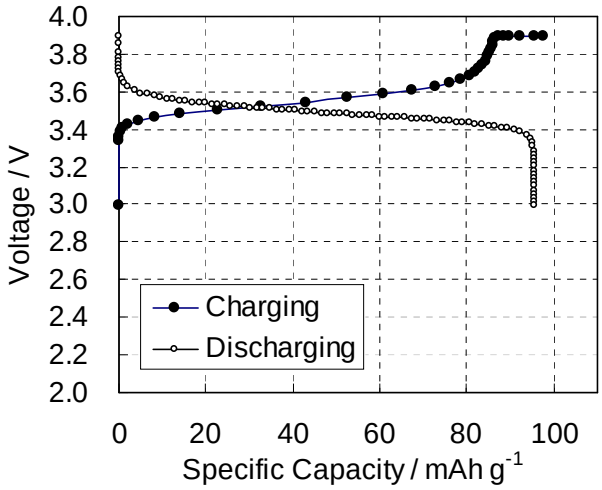

Figure 5.13. Charge/discharge profiles for thin-type organic radical battery with Li^+ pre-doped graphite anode.

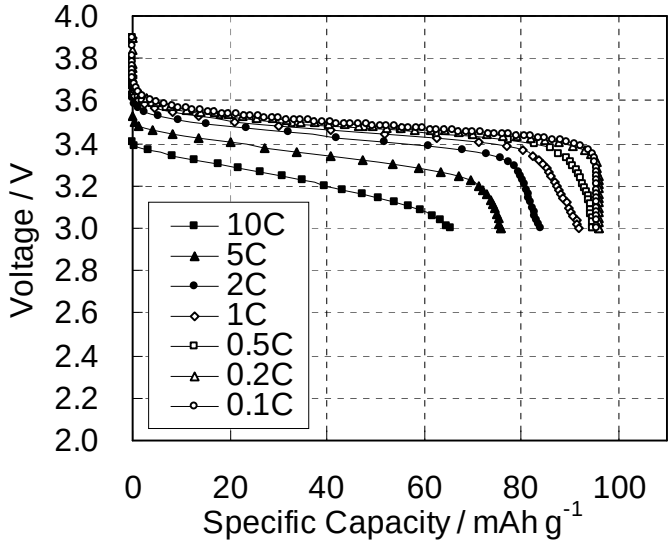

Figure 5.14. Discharge profiles for thin-type organic radical battery with Li^+ pre-doped graphite anode at various C-rate (20°C).

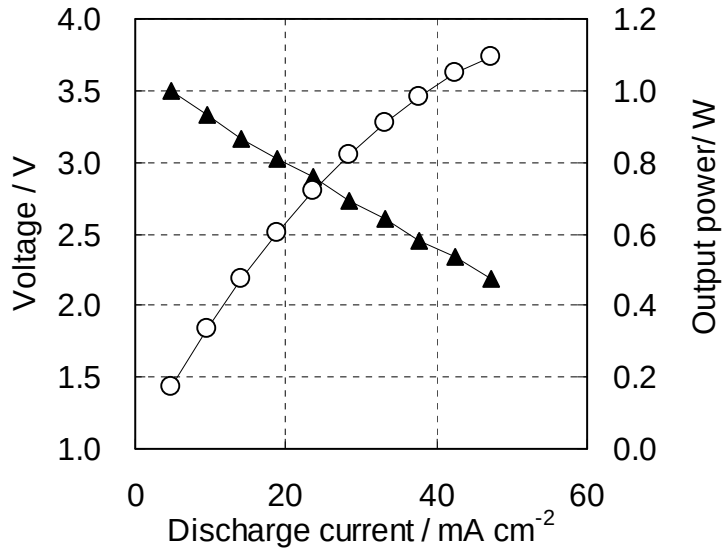

Figure 5.15. Charge/discharge profiles for thin-type organic radical battery with Li^+ pre-doped graphite anode.

Cyclability of the cell measured at 20°C is shown in Fig. 5.16. Specific capacities of PTMA were around 90 mAh/g through 200 cycles. The capacity degradation was less than 5%. The reversible capacity corresponds to 0.55 mAh/cm^2. The discharge profiles exhibited almost no raise of resistance.

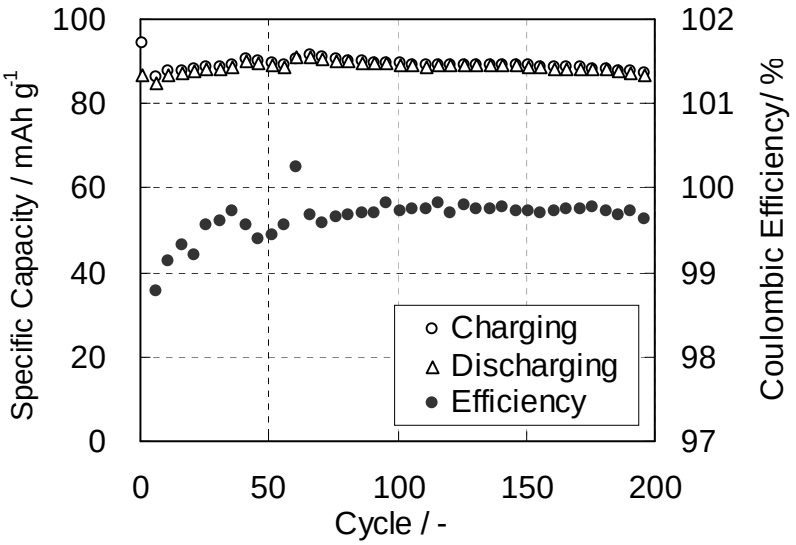

Figure 5.16. Cyclability evaluation for thin-type organic radical battery with Li^+ pre-doped graphite anode.

Charge and discharge profiles those were measured before and after 1 month storage at 20^{o}C are shown in Fig. 5.17. The cell was stored at fully charged state. Self-discharge rate was 14%. However, it has recovered up to 97% of the former capacity. These results indicate that deterioration of the cathode is hardly caused in usual operation. The use of Li^+ pre-doped graphite anode reduced self-discharge rate from 38 %/week to 14 %/month. This might be a promising technology for the practical use of environmentally friendly and low-cost organic radical battery.

The temperature dependence of the initial charge discharge profiles was evaluated at 0.1C (Fig. 5.18). The storage evaluation was also carried out at various temperature (Fig. 5.19). At high temperature over 50oC, the initial capacity was lost gradually during storage, and that was not recovered after re-charging. It was considered that some side reaction, which only occurred at high temperatures, caused irreversible deterioration of the battery.

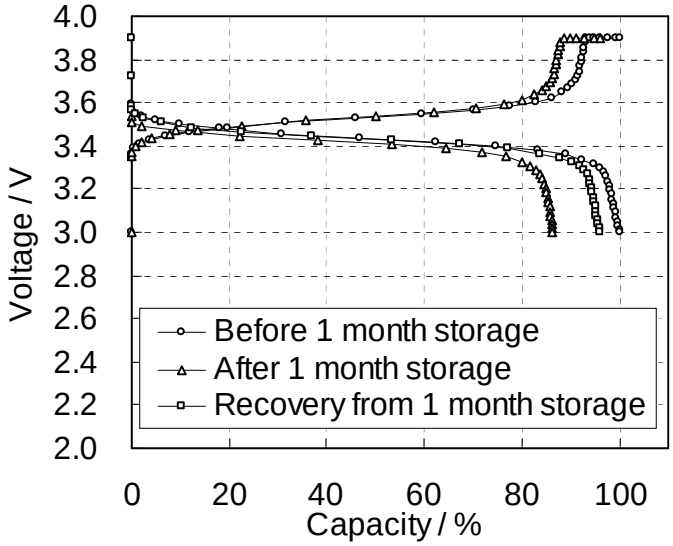

Figure 5.17. Charge and discharge profiles, those were measured before and after 1 month storage at 20°C, of the thin-type organic radical battery with Li^+ pre-doped graphite anode.

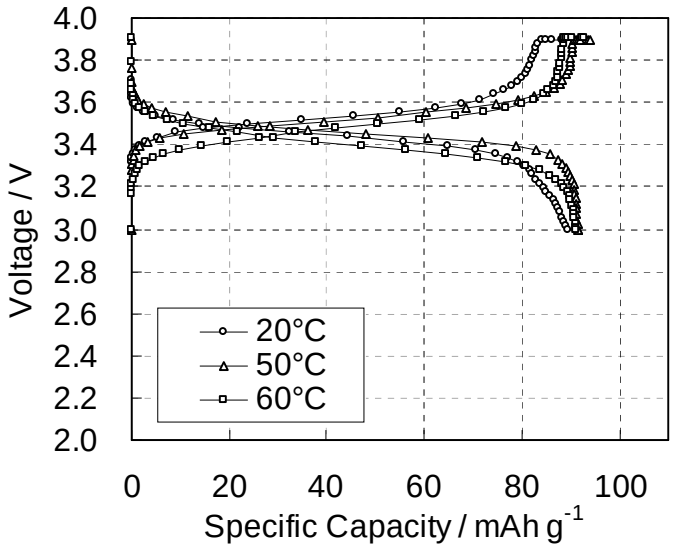

Figure 5.18. Charge/discharge profiles for thin-type organic radical battery with Li^+ pre-doped graphite anode at various temperatures.

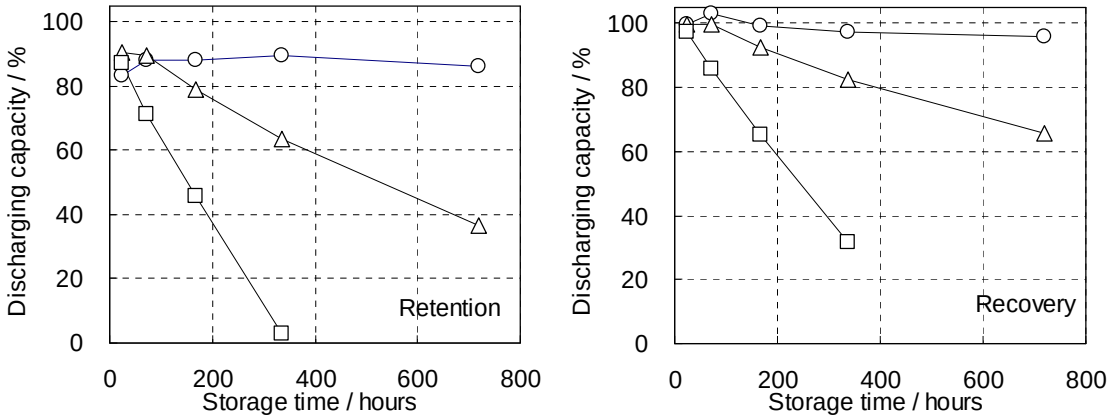

Figure 5.19. Storage evaluation of thin-type organic radical battery with Li^+ pre-doped graphite anode at various temperatures.

5.4. Conclusion of Chapter 5

Water based slurry was applied for PTMA composite electrode making process and we succeeded to make homogeneous electrode. The utilization of active material was improved and almost equal to theoretical capacity (111 mAh g^{-1}) was obtained. Lithium half cells using these PTMA electrodes were fabricated and cycle ability, temperature dependence, rate capability and self-discharge rate were measured in detail. Although they have problems in cycle ability at high temperature and self-discharge rate, they showed relatively good rate capabilities. So we tried to assemble the batteries with graphite anode. Because of graphite anode, they showed 24% of first irreversible capacity. However it was stabilized after second cycle, it would be a good result for the aspect of practical use. Moreover, Li^+ ion pre-doped graphite anode improved stability of organic radical battery, significantly. The technique is a promising for the practical use of the battery, though a deterioration problem at high temperature is still remained.

References

1) F. MacCorquodale, J. A. Crayston, J. C. Walton and D. J. Worsfold, *Tetrahedron Letters*, **1990**, 31, 771.

2) K. Nakahara, S. Iwasa, M. Satoh, Y. Morioka, J. Iriyama, M. Suguro, E. Hasegawa, *Chem. Phys. Lett.* **2002**, 359, 351.

3) H. Nishide, S. Iwasa, Y.-J. Pu, T. Suga, K. Nakahara, M. Satoh, *Electrochim. Acta* **2004**, 50, 827.

4) H. Nishide, K. Oyaizu, *Science* **2008**, 319, 737.

5) H. Nishide, T. Suga, *Electrochem. Soc. Interface* **2005**, 14, 32.

6) J. Iriyama, K. Nakahara, S. Iwasa, Y. Morioka, M. Suguro, M. Satoh, *IEICE Trans.* **2002**, E85-C, 6, 1256.

7) M. Satoh, K. Nakahara, J. Iriyama, S. Iwasa, M. Suguro, *IEICE Trans.* **2004**, E87-C, 12, 2076.

8) K. Nakahara, J. Iriyama, S. Iwasa, M. Suguro, M. Satoh, E. J. Cairns, *J. Power Sources* **2007**, 165, 870.

Chapter 6

Improvement of High-Rate Capability in Organic Radical Batterey

6.1. Introduction of Chapter 6

In the field of electronic devices, demand for low-power consumption is getting bigger and bigger. In case of rechargeable batteries, high-rate capability is getting more and more important. It is considered that high-rate capable rechargeable batteries make it possible not only to achieve smooth acceleration in electric vehicle applications, but also to save the charging time. Many efforts have been done to achieve high-rate capability in lithium ion batteries. K. Zaghib et al., reported that smaller particle size is effective to increase the rate capabilities, but it was also result in increase of irreversible capacity.[1] Thin electrode is also known as a effective way to increase rate capabilities, but it causes decrease of energy density. There is always conflict between high-rate capability and energy density.

In the previous chapter, we reported that an organic radical battery with a PTMA/carbon composite cathode demonstrated quite better rate capability than that of transition metal oxide cathode used in conventional lithium ion batteries.[2,3,4,5] In chapter 6, we reported on the improvement of the rate capability of the Li/PTMA half-cell by employing new composite cathode fabricated by active material solution.

Since PTMA is an organic polymer active material, a new process, which has never been considered in conventional inorganic materials, becomes possible. In this process, PTMA once dissolved in organic solvent completely, and then we made an electrode from active material solutions. Therefore we can fabricate a porous electrode made from conducting additive coating with an active material film. Super large surface area and well dispersion of the active material can be achieved by this process.

6.2. Experimental

Materials

PTMA was synthesized ourselves by a radical polymerization of 2,2,6,6-tetramethylpiperidine-4-yl methacrylate monomer (LA-87, Asahi-denka) using 2'-azobisisobutyronitrile (AIBN) followed by oxidizing it with 3-chloroperoxybenzoic acid (m-CPBA). The synthesis procedure was described somewhere else in detail.[6,7] All electrolytes were obtained from Ube Industries Ltd.

Electrode fabrication

PTMA cathode was prepared by following procedure. To 20 g of *N*-methyl-2-pirrolidone (NMP) solvent, 1.5 g of PTMA and 0.5 g of Poly (vinylidene fluoride) (PVdF, KF#1300, Kureha) were dissolved completely. Then, 3.0 g of vapor grown carbon fiber (VGCF, Showa-denko) was added to the PTMA viscous solution, and stirred extensively. In order to make a thinner film on the surface of VGCF conductive additives, we used an excess amount of VGCF. Resulted slurry was spread on Aluminum foil by doctor blade method. After evaporation of NMP solvent by heating (125^{o}C, 4 min.), a PTMA cathode preparation was completed. This cathode contained PTMA (30 wt%), VGCF (60 wt%) and PVdF (10 wt%). The thickness was adjusted to be 50 μm. Scanning Electron Microscope (SEM) observation was performed by using an S-2400, HITACHI, SEM apparatus.

Cell fabrication

Coin cells (2320-type) were assembled using microporous film separators, Celgard 2400, and 1.4 mm thick lithium metal ingot anodes in dry room (dew point < -50oC). As a liquid electrolyte, we used 1.0M lithium hexafluorophosphate ($LiPF_6$) in ethylene carbonate (EC) and diethyl carbonate (DEC) mixed solvent (EC/DEC=3/7, v/v). Charging and discharging was carried out at voltage range between 3.0 and 4.0 V by using a computer controlled battery measurement system at 20^{o}C.

AC impedance measurements

AC Impedance measurements were carried out using Swagelok cell. At first, the voltage of the cell was set to be 3.0 V and swept up to 3.4 V at the speed of 0.5 mV sec^{-1} controlled by VMP Multi-channel potensiostat, Science Instruments. Then the cell was replaced and AC impedance was measured at room temperature using SI-1260 Impedance / Gain Analyzer, Solartron. Frequency range was 10^{6} to 10^{-2} Hz, and AC amplitude was set to be 10 mV. After the measurement, we connected the cell to the potensiostat again, and swept the voltage up to 3.6 V. We repeated the voltage sweeps

and measurements like this, and obtained the results of AC impedance at 3.4 V, 3.6 V, 3.8 V and 4.0 V.

6.3. Results and Discussion

6.3.1. PTMA/carbon composite cathode fabricated by active materials solution process

Figure 6.1 shows a Scanning Electron microscope (SEM) image of PTMA-carbon composite electrode surface. Since an active material PTMA was once dissolved completely and then electrode was fabricated, it surrounded well the carbon fiber conductive additives. The diameter and the length of carbon fiber were about 150 nm and 10-20 μm, respectively. It looked like PTMA was coating the surface of carbon fibers. Electrode surface was porous, but we found that it was mixed well and relatively homogeneous. The deposited density of the electrode was 0.4-0.5 g cm^{-1}.

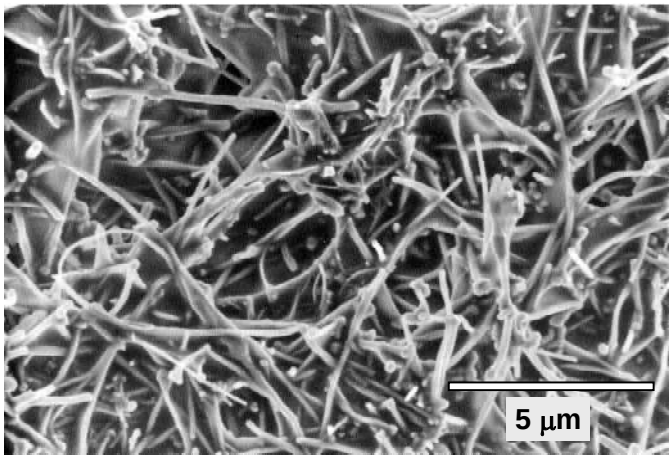

Figure 6.1. A Scanning Electron Microscope (SEM) image of PTMA-carbon fiber composite electrode made from PTMA solution.

6.3.2. Discharge rate capability of a Li/PTMA half-cell with the cathode

Using this PTMA-carbon composite cathode made from a PTMA solution, Li/PTMA half cell was fabricated. Figure 6.2 shows the rate dependence of the discharge curves at the constant current of 1, 5, 10, 20 and 50 C., wherein C corresponds to the capacity of the cell that was 0.04 mAh. The charging and discharging was repeated at 20^{o}C within the voltage range of 3.0-4.0 V. All charging process was carried out at 1 C.

We found that the discharge rate capability of the cell was significantly improved compared with previous reports. Even at high discharge rate 50 C, almost the same capacity as that of 1 C was obtained. Since we always used standard electrolyte solution for Li-ion battery (1.0 M in ED/DEC=3/7, v/v), the drop of the voltage as increase the current was not so much changed. We considered that because of new process using active material solution, the surface area between active material PTMA and carbon fiber conductive additives was remarkably extended. That is why efficiency of the electrode got better and high rate capability would be improved. If we let down the lower limit voltage, extremely high-power rate (several hundred C) could be achieved.

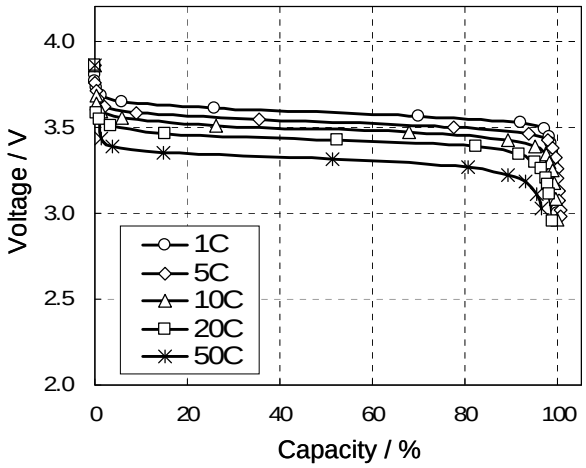

Figure 6.2. Discharge rate capabilities of Li / PTMA half cell at 20oC. All charging process was carried out at 1 C.

6.3.3. Charge rate capability of a Li/PTMA half-cell with the composite cathode

Figure 6.3 shows charging curves measured at constant current of 1, 5, 10, 20 and 50 C. Although upper voltage limit 4.0 V was relatively low, charging process was carried out successfully. Even when it is charged at 50 C, 84% of the capacity at1 C was charged. That means about one minute is required for charging. Figure 6.4 shows the discharge curves at 1 C after rapid charging. It was confirmed that charging energy was stored successfully.

In addition that, it was found that charging rate capability was slightly worse than that of discharging. In case of PTMA electrode employed cells, it was already reported that electrolyte salt concentration is changing continuously while charging and

discharging. And it is already known that the concentration had maximum point at discharged state and started decrease gradually as charging. Therefore, it is considered that charging direction causes polarization and discharge direction releases it. That is why, we think, rate capability of charging process is slightly different from that of discharging.

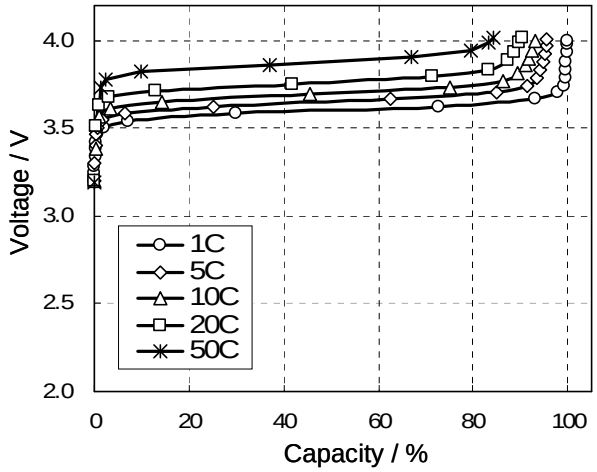

Figure 6.3. Charge rate capabilities of Li/PTMA half cell at 20°C.

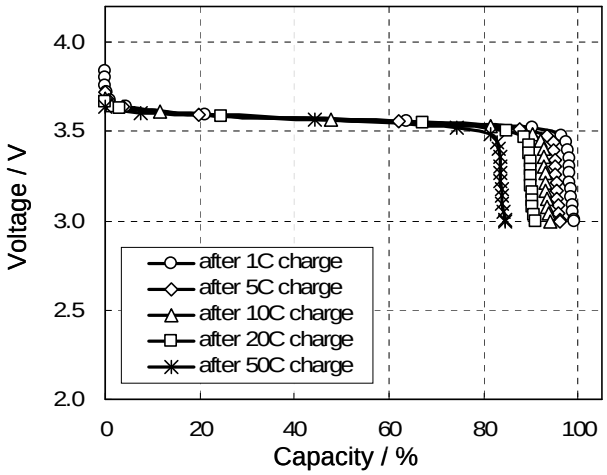

Figure 6.4. Discharge curves of Li/PTMA half cell at 1 C (20°C) after rapid charging at 1, 5, 10, 20 and 50 C rate.

6.3.4. Cyclability of a Li/PTMA half-cell with the composite cathode

Cycle ability at 20°C was shown in Fig. 6.5. The cycle was repeated at constant current of 1 C within the voltage range of 3.0-4.0 V. We found that 89% of initial capacity remained after 1000 cycles. That indicates significant improvement from a previous

report. In previous work, water dispersion slurry was used in electrode making process. Instead of that, NMP solution of PTMA was employed in this process. We think that would be a reason for improvement of cycle ability.

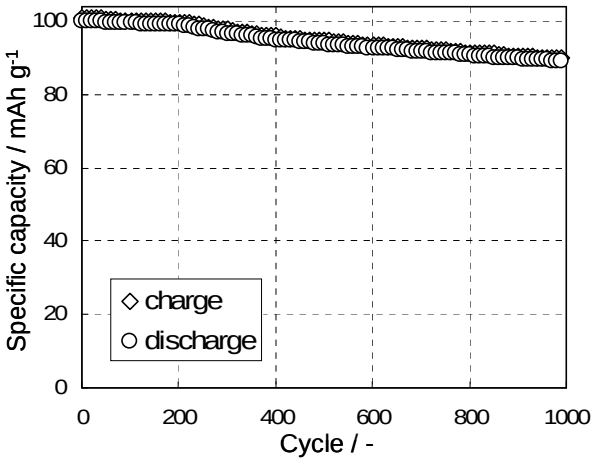

Figure 6.5. Cycle abilities of Li/PTMA half cell at 1 C (20°C).

6.3.5. AC impedance of a Li/PTMA half-cell with the composite cathode

Cole-Cole plots of the cell at various voltages are shown in Fig. 6.6. The x-axis and the y-axis represent the real part (Z') and the imaginary part (Z'') of the impedance, respectively. The high frequency range (10^1-10^6 Hz) of all plots showed semicircles with the diameter of 300-400 Ω, and there was no significant difference among these semicircles obtained at various voltages. These are considered to be made by the Faraday process of the lithium metal anode. However, the low frequency range of the plots significantly differs from the obtained voltage. At discharged state (3.4 V, SOC = 0%), impedance was rising drastically as the frequency lowered and it showed only the early portions of very large semicircles, because of the high resistance. On the other hand, the spectra obtained at 3.6 V (SOC = 8%) and 3.8 V (SOC = 71%) did not increase as the frequency lowered and kept it lower resistance. Then at the charged state (4.0 V, SOC = 100%), the spectrum was rising again as the frequency lowered. This behavior means that although the impedance of the cell is higher and it has insulating nature at completely charged and discharged state, it changes lower suddenly on the way to charging and discharging process. That is why the charging and discharging curves of the cell was very flat and it has extremely good rate capabilities.

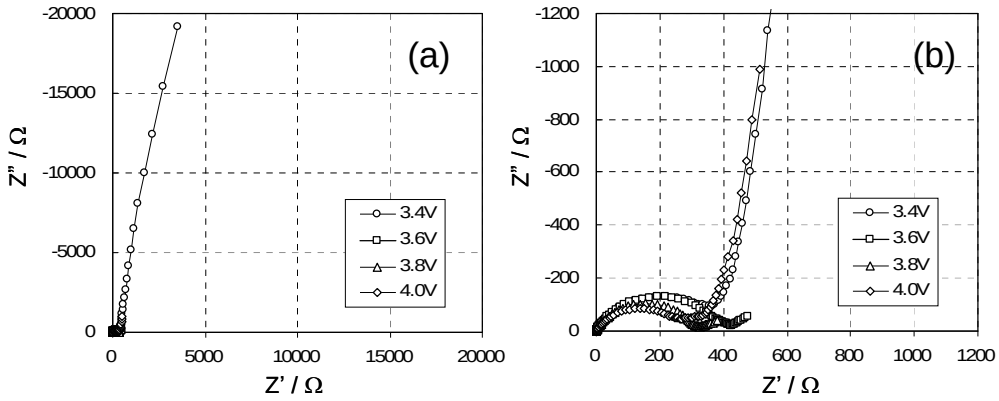

Figure 6.6. Cole-Cole plots of Li/PTMA half cell at 20°C (a) The frequency range was 10^{-2}-10^{6} Hz. (b) is a magnification of low impedance region of (a).

6.4. Conclusion of Chapter 6

An active material, PTMA, was once dissolved in the solvent completely then the electrode was fabricated. In this new process, we could achieve super large surface area between active material and conducting additive. And as a result, power capability of the electrode was improved extremely. Although their capacity was smaller, we can charge and discharge it in a minute. So we can use this battery like an electric double layer capacity. It was also found that the cycle ability is good and 89 % of initial capacity remained after 1000 cycle.

———————————————————————————————

References

1) K. Zaghib, F. Brochu, A. Guerfi and K. Kinoshita, *J. of Power Sources*, 103 (2001)

2) K. Nakahara, H. Oyaizu, H. Nishide, *Chem Lett.*, **2011**, 40, 222.

3) H. Nishide, K. Oyaizu, *Science* **2008**, 319, 737.

4) H. Nishide, T. Suga, *Electrochem. Soc. Interface* **2005**, 14, 32.

5) K. Nakahara, J. Iriyama, S. Iwasa, M. Suguro, M. Satoh, E. J. Cairns, *J. Power Sources* **2007**, 165, 398.

6) K. Nakahara, S. Iwasa, M. Satoh, Y. Morioka, J. Iriyama, M. Suguro, E. Hasegawa, *Chem. Phys. Lett.* **2002**, 359, 351.

7) H. Nishide, S. Iwasa, Y.-J. Pu, T. Suga, K. Nakahara, M. Satoh, *Electrochim. Acta* **2004**, 50, 827.

Chapter 7

Fabrication of Organic Radical Batteries for Practical Applications

7.1. Introduction of Chapter 7

Organic radical battery is now being developed for smart card and sub-battery and applications as the main target at NEC Corporation.[1,2,3,4] Figure 7.1 shows the positions of several energy devices and the organic radical battery prototype cell. The battery overcomes the limitations of the conventional energy devices with regard to high-power density problems. One of the unique features of the battery is its capability to charge large current loads with a good utilization of the capacity. It is clearly observed that the organic radical battery is enabled to charge up to 80% within 1 minute. This result means that the battery can be charged whenever and wherever necessary. Another unique feature of the organic radical battery is the extraordinary cycle life. The organic radical battery is capable of several thousand charging and discharging cycles. Moreover, the battery has been confirmed to be nonflammable and non-thermal runaway cathode active material. Besides these unique properties, the charge storage capacity of the present battery is lower than that of a conventional battery. The synthesis of new radical compounds with higher capacities, i.e., higher radical concentrations, is the greatest challenge in achieving a high power and high capacity type of organic radical battery in the future.

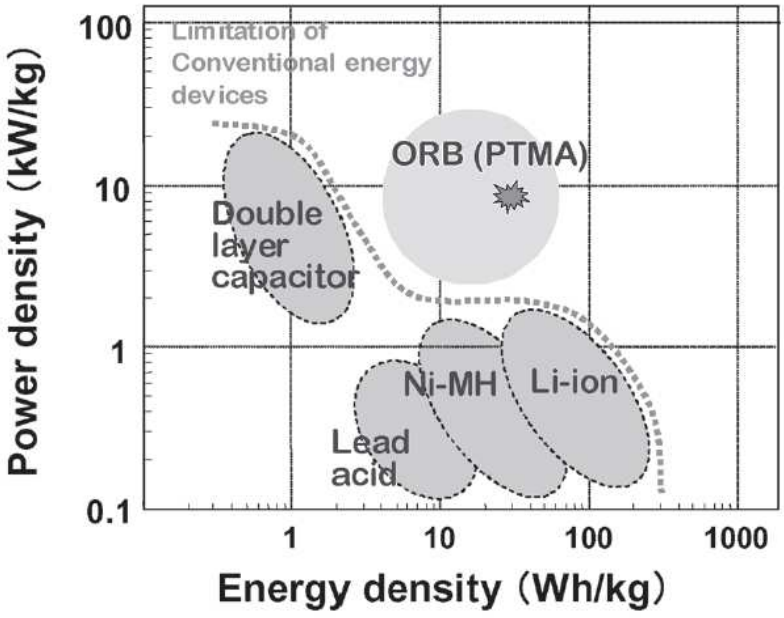

Figure 7.1. positions of the organic radical battery and the other energy storage devices on the plots of energy density and power density.

In chapter 7, we reported on the fabrication of a 100 mAh-class organic radical battery using a PTMA/carbon composite cathode and a graphite anode. Fabrication of practical battery, which is packaged with aluminum laminated film, enables comparative study with conventional batteries. It is also demonstrated that a battery pack consisting of four such batteries connected in series operated a 200 W-class desktop computer without additional power input, so the battery is suitable for emergency use as a sub-battery. The battery pack is compact enough to be installed in an expansion slot of a desktop computer.

7.2. Experimental

Materials

PTMA was synthesized ourselves by a radical polymerization of 2,2,6,6-tetramethylpiperidine-4-yl methacrylate monomer (LA-87, Asahi-denka) using 2'-azobisisobutyronitrile (AIBN) followed by oxidizing it with 3-chloroperoxybenzoic acid (m-CPBA). The synthesis procedure was described somewhere else in detail.[5,6,7] All electrolytes were obtained from Ube Industries Ltd.

Electrode fabrication

PTMA cathode was prepared by following procedure. In order to make viscous solution, we added 5.0 g of Carboxy methyl Cellulose, CMC, (HB9, ZEON Corp.) into 500 g of pure water, and stirred until it was dissolved completely. Then, 1.25 g of PTFE fine powder (60% water dispersion, D-1B, DAIKIN) and 56.25 g of vapor grown carbon fibers (VGCF^{TM}, Showa-Denko) were added into the CMC solution, and kept stirring intensively for 1 hour. We completed to make slurry by adding 62.5 g of PTMA fine powder into well dispersed carbon ink and mixing it well. Resulted slurry was spread on carbon coated Aluminum foil by doctor blade method in one side. And after evaporation of solvent water by heating (100^{o}C, 10 min.), another side was also coated uniformly. This electrode had 180 μm of thickness in each side and contained PTMA (50 wt%), VGCF (45 wt%), CMC (4 wt%) and PTFE (1 wt%). Graphite, mesocarbon microbeads (MCMB#3, Osaka-gas) anode was prepared by normal process using NMP slurry and Doctor Blade method. This anode contained graphite (90 wt%), conductive carbon black (1.0 wt%) and PVdF (9.0 wt%). The thickness was adjusted to be 20 μm in each side.

Cell fabrication

Aluminum-laminated film packaged organic radical batteries were fabricated by the following procedures. PTMA cathodes and graphite anodes were cut into the 45 × 55 mm^2 rectangle pieces with 10 mm width of margin current collectors. And one single side coated and nine both side coated cathodes were setting while we were inserting microporous film separators, Celgard 2400, and graphite anodes. So as a result, nineteen layers of cathodes and the same layers of anodes were facing each other through the separators. After all electrodes were aligned, we connected at the margin part of all aluminum cathode current collectors into an electrode by using supersonic welder and we did same process for cupper anode current collectors. By attaching electric lead tabs, a component for power generation was prepared completely. Then we covered it with formed aluminum-laminated film and sealed three sides of the film by heating. And into the opened pouch of the battery, we put a 1.0 M lithium hexafluorophosphate ($LiPF_6$) in ethylene carbonate (EC) and diethyl carbonate (DEC) mixed solvent (EC/DEC=3/7, v/v) as a liquid electrolyte. After we kept it under weak vacuum condition for a while, we sealed the last side of it to complete a fabrication of the battery. The weight of a fabricated battery was 22 g, and the thickness was 4.3 mm. Charging and discharging was carried out by using a BLS, Tabai espec, automatic battery measurement system under controlled temperature.

7.3. Result and Discussions

7.3.1. Design for a graphite/PTMA battery with the capacity of 100 mAh

Organic radical batteries with graphite anodes and PTMA cathodes were fabricated in dry room. PTMA cathode was prepared adjusting the first charging capacity to the same as anode. Aluminum-laminated film was employed for a packaging material. Figure 7.2 shows an example of appearance. Electrode size was 45 × 55 mm^2 and it corresponds to almost half size of name card. Battery total weight was 22 g and reversible capacity was about 100 mAh.

Figure 7.2. An appearance of Al-laminated film packaged organic radical battery.

7.3.2. Charge/discharge profiles of graphite/PTMA battery with the capacity of 100 mAh

Figure 7.3 shows the first charging and discharging curves for the battery obtain at 20oC. The charging and discharging were carried out at the constant current of 80 mA. Upper and lower limit voltage was set to be 4.2 and 2.5 V, respectively. When charging process, the voltage was going up gradually and the voltage plateau was observed at around 3.5 V. The first charging capacity was 147 mAh. Calculated from the weight of PTMA, the specific capacity of PTMA was found to be 108 mAh g^{-1}. Discharging plateau was also observed around 3.4 V. The first discharging capacity was 109 mAh. Therefore, we found that 38 mAh (26%) of the charging capacity was disappeared during the first cycle. This would be mainly caused by the irreversible capacity of graphite anode. Figure 7.4 shows the second charging and discharging curves. The curves were very flat and the charging and discharging capacities were 103 and 101 mAh, respectively. The change of the capacity was leveled off and there was no significant change in the shape of curves after that until 100 cycles.

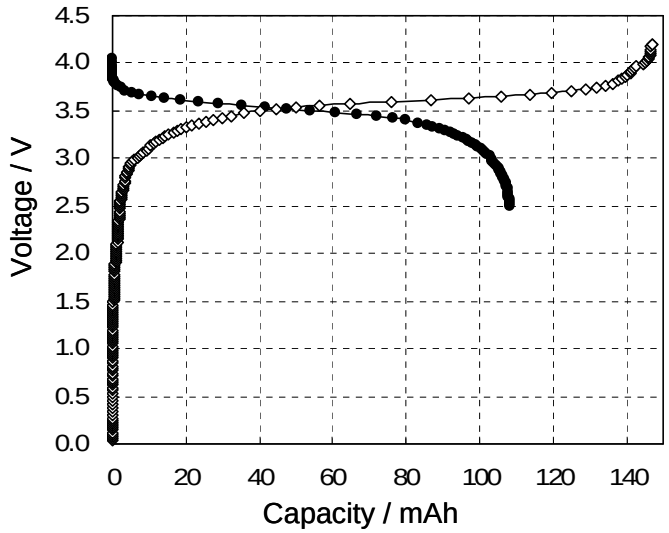

Figure 7.3. The first charging and discharging curves of the organic radical battery at 20°C. Charging and discharging were carried out at the constant current of 80 mA.

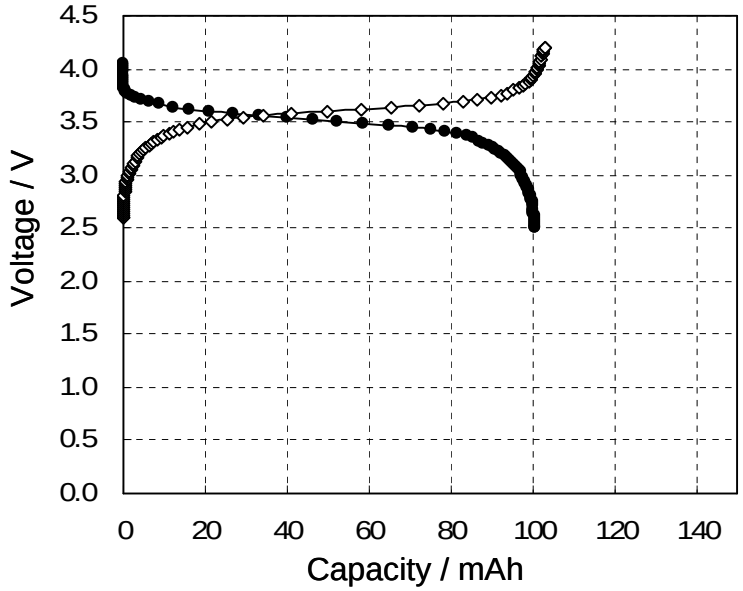

Figure 7.4. The second charging and discharging curves of the organic radical battery at 20°C. Charging and discharging were carried out at the constant current of 80 mA.

7.3.3. Cyclability of graphite/PTMA battery with the capacity of 100 mAh

Cycle abilities at 20°C and 45°C were shown in Fig. 7.5. The capacity decreased gradually during the cycle, and after 100 cycles, 82% of initial capacity was remained (20°C). In case of elevated temperature (45°C), the capacity dropped more rapidly. And we confirmed that the battery was expanded at 45°C, it was slightly detected at 20°C. Gas generation might take place during cycle. As a reason, we doubted the existence of

residual water in PTMA electrode, because we employed water dispersion slurry for making process.

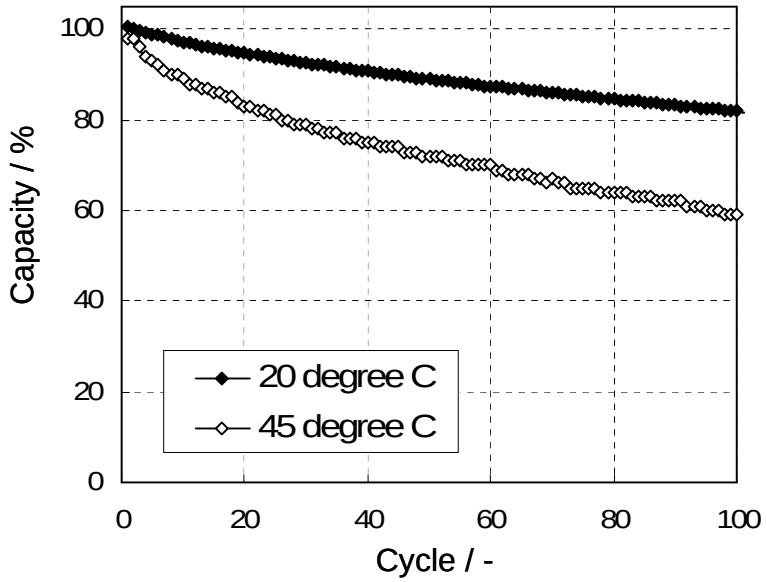

Figure 7.5. Cycle abilities of the battery at 20°C and 45°C. Charging and discharging were repeated at 80 mA between 2.5-4.2 V.

7.3.4. Discharge rate capability of a graphite/PTMA battery with the capacity of 100 mAh

Then we measured the rate capability of the battery. Figure 7.6 shows the discharge curves at constant current of 0.1-5.0 A. Upper and lower limit voltages were set to be 4.2 and 2.4 V, respectively. This experiment was carried out at 20°C, and an exactly same battery was used repeatedly for each measurement. While the current was increased, the voltage was going down and capacity was decreased. However, even at 5.0 A (50 C), 71% of the 0.1 A (1 C) capacity was obtained. And the beginning of charging process at high rate, we observed a slight rise of the voltage. Temperature rise might happen partially because of high current.

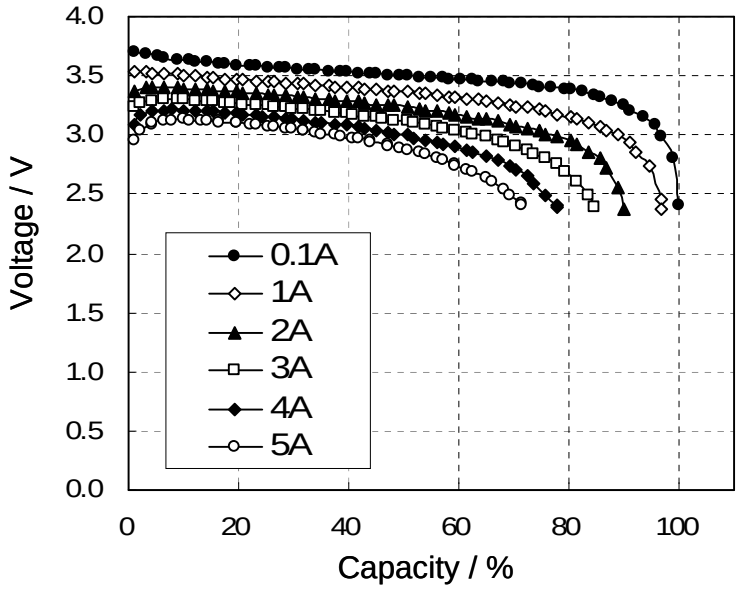

Figure 7.6. Discharge rate capabilities of the organic radical battery at 20°C. All charging process was carried out at 100 mA.

7.3.5. Test of a graphite/PTMA battery pack as a UPS for a high-spec desktop computer

And then, we fabricated a battery pack consist of four series connected cells in order to get sufficient power available for electronic devices, and measured the rate capability. Upper and lower limit voltages were set to be 16.8 and 8.0 V, respectively. Converted to per each cell, they correspond to 4.2 and 2.0 V, respectively. All charging process was carried out at 0.2 A. Figure 7.7 shows the discharge curves at constant current of 1-13 A. As shown here, although the capacity decreased to the half and the voltage dropped significantly, 13 A (130 C) discharge was achieved. Voltage rise was also appeared here at the beginning. Strange to say, the rate capability of the battery pack was better than that of calculated by single cell experiment. When we made a battery pack, we packed it in a case in order to fix it. That is why we considered that a case affected to press the cells, and this effect prevent the gas generation from damaging to the cell properties.

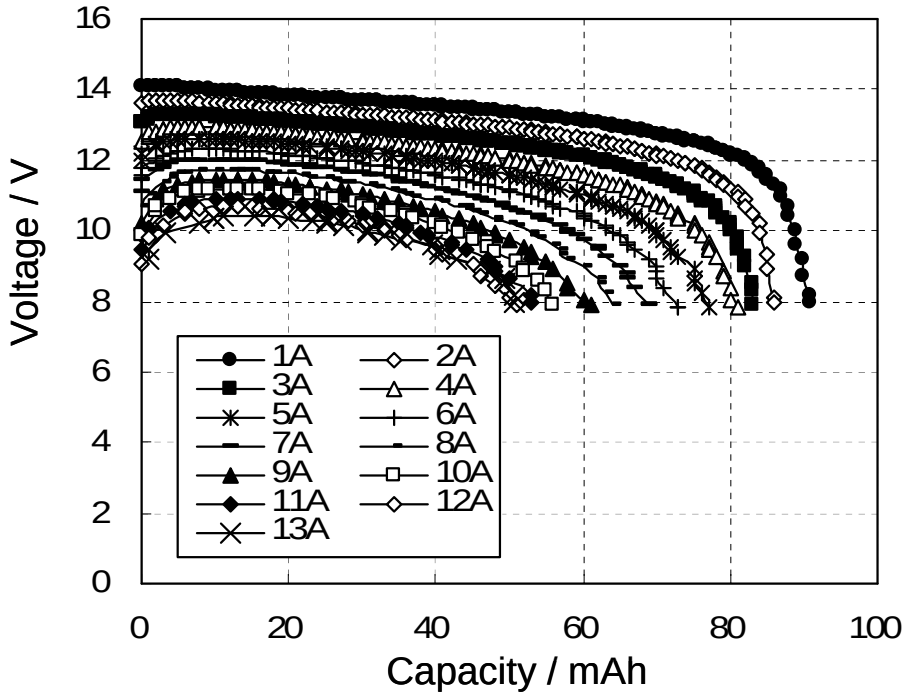

Figure 7.7. Discharge rate capabilities of the organic radical battery pack (4 cells connected in series) at 20^{o}C. All charging process was carried out at 100 mA between 8.0-14.8 V.

The use of organic radical battery pack as an uninterruptable power sources (UPS) for a desktop PC was examined. Generally, data back-up for a PC takese several tens of seconds. Therefore, the battery only has to drive the PC for several tens ofseconds during a power failure. A desktop PC (NEC VALUESTAR, PC/VT5009D, Pentium^{TM}4, 2.8GHz) with maximum output power of 200 W was selected for the UPS demonstration. A four series battery pack was connected with the desktop PC through a control unit, which consists of a charger, a booster, and a signal generator. When a power failure happened, a voltage drop of 4 V occurred. However, it was successfully working by supplying energy from only the organic radical battery pack, during the period (Fig. 7.8).

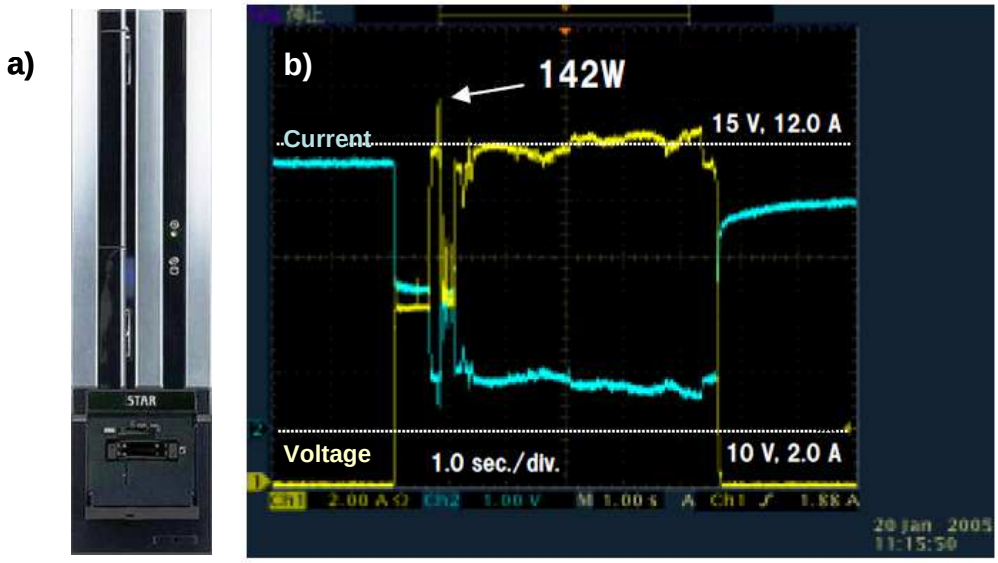

Figure 7.8. a) Desktop PC used for UPS demonstration. b) Voltage and current profiles during power failure.

7.3.6. Comparative study of a graphite/PTMA battery with the other energy devices

This battery consists of PTMA (6.2 wt.%), graphite (1.4 wt.%), conducting additives (6.3 wt. %), electrolyte (28.4 wt. %), current collectors / tab leads (40.2 wt.%), packing film (14.8 wt.%) and porous separator (2.7 wt.%). As described here, the main components of this battery were current collectors, tab leads, electrolyte and packaging film. They occupied over 80% of the battery total weight. Active material PTMA shared only 6.2% of that. In order to make a practical battery, PTMA have to be packed more and more dense. Figure 7.9 shows a Ragone-plot of the battery pack comparing with conventional lithium ion battery.[8] We found that the energy density of organic radical battery was significantly inferior to that of lithium ion battery. However, if we compare the Ragone-plot normalized with active materials weight inside of the battery, the result was different. Figure 7.10 is a result of recalculation of their energy and power density based on the weight of active materials. In that case, we found that although the energy density of organic radical battery was smaller, the power density was quite superior to that of lithium ion battery.

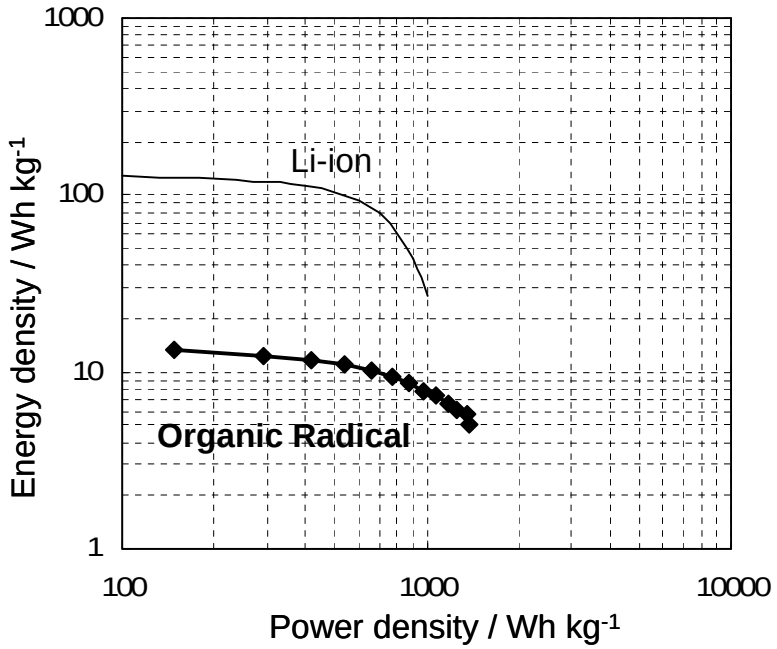

Figure 7.9. Ragone-plot of the organic radical battery compared with a lithium ion battery. The energy density and the power density were obtained based on the battery total weight.

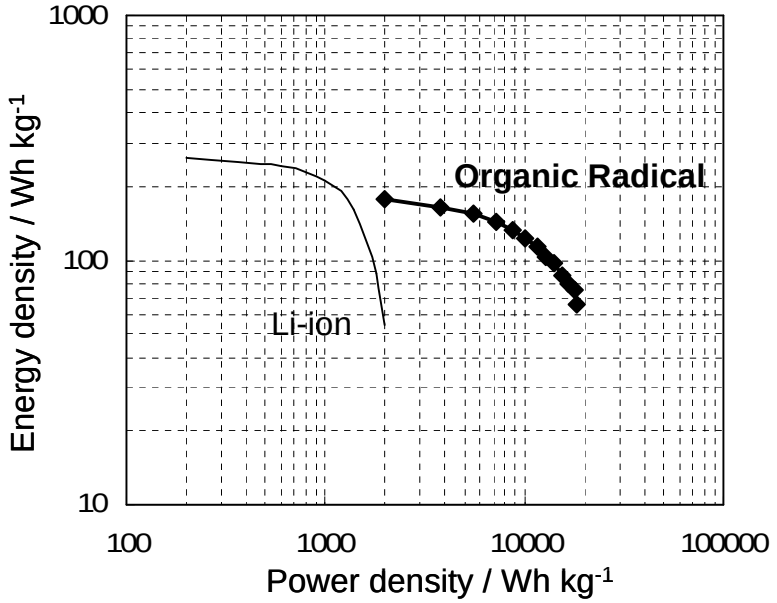

Figure 7.10. Ragone-plot of the organic radical battery compared with a lithium ion battery. The energy density and the power density were obtained based on the active material weight which consists of the battery.

7.4. Conclusion of Chapter 7

A 100-mAh class of organic radical battery with a graphite anode has been fabricated and investigation for practical applications has just begun. This battery has satisfactory rate properties and its cycle ability is adequate for practical use. Although the practical development is in the early stages, it is expected that the performance of the battery will be improved by optimizing the capacity balance and the improvement of fabrication process. The energy density, especially volumetric one, of an organic radical battery is considerably less than that of a lithium ion battery with a transition metal oxide cathode. However, the power density per active material weight was found to be better than that of lithium ion battery. That is why we think, one of the possible applications of it is a high-power energy source such as a sub-battery in electronic devices and motor drive assistance in electric vehicles, replacing electric double-layered capacity and nickel metal hydride batteries. These applications require high-power capability rather than high-energy density, so organic radical batteries would be suitable. Rapid charging would also be an advantage for practical use.

References

1) K. Nakahara, H. Oyaizu, H. Nishide, *Chem Lett.*, **2011**, 40, 222.

2) K. Nakahara, J. Iriyama, S. Iwasa, M. Suguro, M. Satoh, E. J. Cairns, *J. Power Sources* **2007**, 165, 398.

3) K. Nakahara, J. Iriyama, S. Iwasa, M. Suguro, M. Satoh, E. J. Cairns, *J. Power Sources* **2007**, 165, 870.

4) M. Satoh, K. Nakahara, J. Iriyama, S. Iwasa, M. Suguro, *IEICE Trans.* **2004**, E87-C, 12, 2076.

5) K. Nakahara, S. Iwasa, M. Satoh, Y. Morioka, J. Iriyama, M. Suguro, E. Hasegawa, *Chem. Phys. Lett.* **2002**, 359, 351.

6) H. Nishide, S. Iwasa, Y.-J. Pu, T. Suga, K. Nakahara, M. Satoh, *Electrochim. Acta* **2004**, 50, 827.

7) H. Nishide, T. Suga, *Electrochem. Soc. Interface* **2005**, 14, 32.

8) A. D. Pasquire, I. Plitz, S. Menocal and G. Amatucci, *J. of Power Sources* **2003**, 115, 171.

Chapter 8
Future Perspectives

8.1. Approach for Practical Use

Organic radical batteries with a nitroxyl radical polymer composite cathode and a graphite anode are close to becoming practical.[1,2] Because of their low volumetric energy density, they are not suitable as the main battery in mobile phones or laptop computers. However, more specialized applications, such as a sub-battery for desktop computer emergency use and as a smart card power source, are realistic. The remaining issues to be resolved to achieve commercialization are long-term stability for more than years and cost reduction. Our approach to resolving these issues is to modify the production processes.[3,4]

Thin-type organic radical batteries are being developed for application to smart cards. A prototype battery with a thickness of 800 μm was fabricated and tested. It had a composite electrode containing 70 wt% PTVE and a lithium metal anode. The electrode was 24 × 22 mm^2. The discharge capacity of the battery was 6.0 mA·h. The *I–V* characteristics were investigated using the 1 sec. pulse discharge method. The direct current resistance of the battery was only 1.5 Ω, and, as shown in Fig. 8.1(a), the maximum power output was 2.0 W. This output power is considered sufficient for high-power applications such as for the luminescence of an LED flash device. A photograph of the prototype battery embedded in a smart card is shown in Fig. 7.1(b).

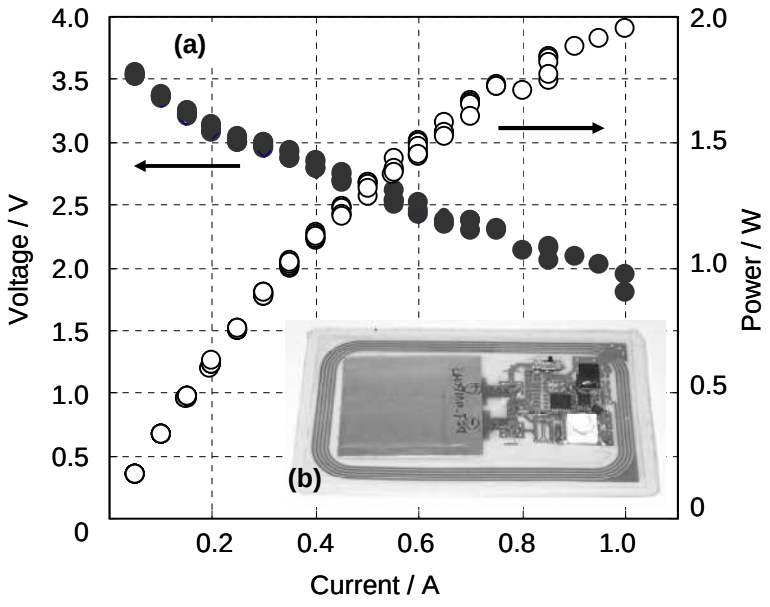

Figure 8.1. (a) *I-V* characteristic of thin-type organic radical battery at 20°C. Voltages obtained at various currents after 1 s discharge(●) and output power of battery(○). (b) Photograph of prototype thin-type organic radical battery embedded in smartcard.

The pulse cyclability of the battery was examined by subjecting it to 5 mA (5 sec.) pulse discharges once a minute (Fig. 8.2). Almost no deterioration was observed up to 10,000 pulse cycles even at 0-40^{o}C. This stability further supports the practical application of the organic radical battery as the power source of smart cards.

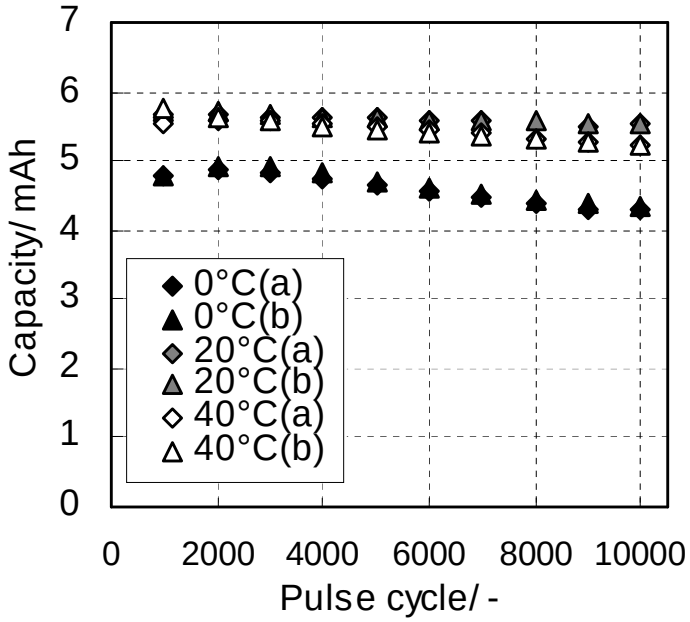

Figure 8.2. Capacity change of thim-type cell during pulse-cyclability test (5 mA-5sec.) at 0-40^{o}C.

Because of its unique features, the organic radical battery has a wide range of potential applications as a power source not only for laptop PCs and PDAs but also for a variety of ubiquitous appliances such as smart cards, sensors, intelligent papers, radio frequency identification tags and micro-sized devices as shown in Fig. 8.3.

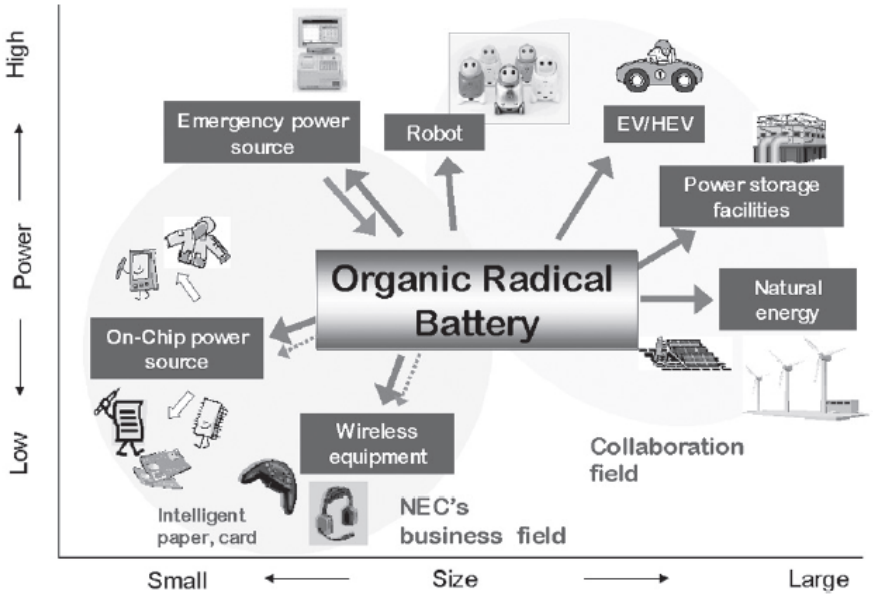

Figure 8.3. Potential applications of organic radical battery

8.2. Materials Innovations

Research on a rocking-chair-type organic radical battery is in progress. Since the electrolyte salt concentration does not change during charging and discharging, the energy density of the battery should be high. The n-type reaction of the radical polymers is critical to the rocking-chair-type battery, but this reaction is more susceptible to side reactions than the p-type reaction. However, the n-type reaction can be controlled by altering the electron-withdrawing characteristics of the substituents on the poly(nitroxylstyrene).[5] Another type of n-type reaction has been demonstrated in poly(galvinoxylstyrene).[6] These polymers are thus attractive as the cathode active material for the rocking-chair type battery.

Radical polymers have been used not only as an alternative to lithium transition metal oxide but also as the electrode active material for various types of rechargeable devices. A totally organic polymer-based rechargeable battery with a poly(TEMPO-substituted norbornene) cathode and a poly(galvinoxylstyrene) anode has been reported[6] as well as an aqueous electrolyte rechargeable battery with a PTVE cathode and a zinc anode.[7] These batteries are attractive as flexible, printable, and green batteries.[8,9,10] Furthermore, radical polymers have been used not only for rechargeable batteries but also for diodes,[11] nonvolatile memories,[12,13] and electrochromic devices.[14]

The use of radical polymers is thus spreading as they become used as electro-active polymers for new functional devices.

Radical polymers are a promising alternative to lithium transition metal oxides in lithium-ion batteries. Nitroxyl radical polymers are a particularly attractive candidate for the cathode active material from the viewpoints of high power density and environmental friendliness. Other radical polymers may be applicable to next-generation batteries, such as an all-plastic battery. The practical use of the polymers in organic radical batteries may thus be near at hand.

References

1) K. Nakahara, H. Oyaizu, H. Nishide, *Chem Lett.*, **2011**, 40, 222.

2) M. Satoh, K. Nakahara, J. Iriyama, S. Iwasa, M. Suguro, *IEICE Trans.* **2004**, E87-C, 12, 2076.

3) K. Nakahara, J. Iriyama, S. Iwasa, M. Suguro, M. Satoh, E. J. Cairns, *J. Power Sources* **2007**, 165, 398.

4) K. Nakahara, J. Iriyama, S. Iwasa, M. Suguro, M. Satoh, E. J. Cairns, *J. Power Sources* **2007**, 165, 870.

5) T. Suga, Y.-J. Pu, S. Kasatori, H. Nishide, *Macromolecules* **2007**, 40, 3167.

6) T. Suga, H. Ohshiro, S. Sugita, K. Oyaizu, H. Nishide, *Adv. Mater.* **2009**, 21, 1627.

7) K. Koshika, N. Sano, K. Oyaizu, H. Nishide, *Macromol. Chem. Phys*. **2009**, 210, 1989.

8) H. Nishide, K. Oyaizu, Science **2008**, 319, 737.

9) H. Nishide, K. Koshika, K. Oyaizu, *Pure Appl. Chem.* **2009**, 81, 11, 1961.

10) K. Koshika, N. Chikushi, N. Sano, K. Oyaizu, H. Nishide, *Green. Chem.* **2010**, 12, 1573.

11) T. Suga, S. Takeuchi, T. Ozaki, M. Sakata, K. Oyaizu, H. Nishide, *Chem. Lett.* **2009**, 38, 12, 1160.

12) Y. Yonekuta, K. Susuki, K. Oyaizu, K. Honda, H. Nishide, *J. Am. Chem. Soc.* **2007,** 129, 14128.

13) Y. Yonekuta, K. Honda, H. Nishide, Polym. *Adv. Technol.* **2008**, 19, 281.

14) Y. Takahashi, N. Hayashi, K. Oyaizu, K. Honda, H. Nishide, *Polym. J.* **2008**, 40, 8, 763.

List of Publications

1. Kentaro Nakahara, Kenichi Oyaizu, Hiroyuki Nishide, "Organic Radical Battery Approaching Practical Use", *Chemistry Letters* **2011**, 40, 3, 222
2. Kentaro Nakahara, Jiro Iriyama, Shigeyuki Iwasa, Masahiro Suguro, Masaharu Satoh, Elton J. Cairns, "High-Rate Capable Organic Radical Cathodes for Lithium Rechargeable Batteries" *Journal of Power Sources* **2007**, 165, 870.
3. Kentaro Nakahara, Jiro Iriyama, Shigeyuki Iwasa, Masahiro Suguro, Masaharu Satoh, Elton J. Cairns, "Cell Properties for Modified PTMA Cathodes of Organic Radical Batteries" *Journal of Power Sources* **2007**, 165, 398.
4. Kentaro Nakahara, Jiro Iriyama, Shigeyuki Iwasa, Masahiro Suguro, Masaharu Satoh, Elton J. Cairns, "Al-Laminated Film Packaged Organic Radical Battery for High-Power Applications", *Journal of Power Sources* **2007**, 165, 398.
5. Kentaro Nakahara, Jiro Iriyama, Shigeyuki Iwasa, Masahiro Suguro, Masaharu Satoh, Elton J. Cairns, "Electrochemical and Spectroscopic Measurements for Stable Nitroxyl Radicals", *Electrochimica Acta* **2006**, 52, 921.

Supplementary Publications

1. Masahiro Suguro, Atsunori Mori, Shigeyuki Iwasa, Kentaro Nakahara, Kaichiro Nakano, "Syntheses and Electrochemical Properties of TEMPO Radical Substituted Silicones: Active Material for Organic Radical Batteries", *Macromolecular Chemistry and Physics* **2009**, 210, 1402.
2. Masahiro Suguro, Shigeyuki Iwasa, Kentaro Nakahara, "Effect of Ethylene Oxide Structures in TEMPO Polymers on High Rate Discharge Properties", *Electrochemical and Solid-State Letters* **2009**, 12, 9, A194
3. Masahiro Suguro, Shigeyuki Iwasa, Kentaro Nakahara, "Fabrication of a Practical and Polymer-Rich Organic Radical Polymer Electrode and its Rate Dependence", *Macromolecular Rapid Communications* **2008**, 29, 1635.
4. Masahiro Suguro, Shigeyuki Iwasa, Yuki Kusachi, Yukiko Morioka, Kentaro Nakahara, "Cationic Polymerization of a Poly(vinyl ether) Bearing a TEMPO Radical: A New Cathode-Active Material for Organic Radical Batteries" *Macromolecular Rapid Communications* **2007**, 28, 1929.
5. Hiroyuki Nishide, Shigeyuki Iwasa, Yong-Jin Pu, Takeo Suga, Kentaro Nakahara, Masaharu Satoh, "Organic Radical Battery: Nitroxide Polymers as a Cathode-Active Material", *Electrochimica Acta* **2004**, 50, 827.
6. Kentaro Nakahara, Shigeyuki Iwasa, Masaharu Satoh, Yukiko Morioka, Jiro Iriyama, Masahiro Suguro, Etsuo Hasegawa, "Rechargeable Battery with Organic Radical Cathodes", *Chemical Physics Letters* **2002**, 359, 351.

List of Presentation on International Conference

1. Kentaro Nakahara, Shigeyuki Iwasa, Masahiro Suguro, Takanori Nishi, Motoharu Yasui, Kaichiro Nakano, "Stability of Organic Radical Battery with PTMA Composite Cathode and Li^+ Pre-Doped Graphite Anode", *International Meeting on Lithium Batteries* **2010**, Montreal, Canada.

2. Kentaro Nakahara, Jiro Iriyama, Shigeyuki Iwasa, Masahiro Suguro, Masaharu Satoh, "Organic Radical Battery: Transition-Metal Free Lithium-ion Battery", *International Meeting on Lithium Batteries* **2004**, Nara, Japan.

3. Kentaro Nakahara, Jiro Iriyama, Shigeyuki Iwasa, Masahiro Suguro, Masaharu Satoh, "A New Architecture of Thin Film Battery with Organic Radical Plastic Cathode", *The Electrochemical Society Meeting* **2005**, Los Angeles, CA, United States.

4. Kentaro Nakahara, Jiro Iriyama, Shigeyuki Iwasa, Masahiro Suguro, Masaharu Satoh, Elton J. Cairns, "Electrochemical and spectroscopic Research on Stable nitroxyl Radicals", *The Electrochemical Society Meeting* **2005**, Los Angeles, CA, United States.

5. Kentaro Nakahara, Jiro Iriyama, Shigeyuki Iwasa, Masahiro Suguro, Masaharu Satoh, "Organic Radical Batteries", *The Electrochemical Society Meeting* **2005**, Quebec city, Canada.

6. Kentaro Nakahara, Jiro Iriyama, Shigeyuki Iwasa, Masahiro Suguro, Masaharu Satoh, "Organic Radical Battery", *The Electrochemical Society Meeting* **2004**, Honolulu, HI, United States.

7. Kentaro Nakahara, Jiro Iriyama, Shigeyuki Iwasa, Yukiko Morioka, Masahiro Suguro, Masaharu Satoh, "Fabrication of 100 mAh-class Organic Radical Battery", *The Electrochemical Society Meeting* **2003**, Paris, France.

8. Kentaro Nakahara, Jiro Iriyama, Shigeyuki Iwasa, Yukiko Morioka, Masahiro Suguro, Masaharu Satoh, "Lithium Batteries with Organic Radical Cathodes", *The Electrochemical Society Meeting* **2002**, Philadelphia, NJ, United States.

9. Kentaro Nakahara, Jiro Iriyama, Shigeyuki Iwasa, Masahiro Suguro, Masaharu Satoh, "High-Power Dischargeable Organic Radical Battery", *International Society of Electrochemistry* **2004**, Thessaloniki, Greece.

10. Kentaro Nakahara, Shigeyuki Iwasa, Masahiro Suguro, Yukiko Morioka, Masaharu Satoh, "Organic Radical Battery", *Advanced Automotive Batteries Conference* **2007**, Long Beach, CA. United State.

11. Kentaro Nakahara, "Organic Radical Battery", *Plastic Electronics Conference Asia* **2008**, Seoul, Korea. *invited*

Acknowledgments

The present thesis is a review of the author's studies that have been carried out at NEC Corporation during 1999-2011 and the Department of Applied Chemistry, Waseda University under the direction of Professor Hiroyuki Nishide and Associate Professor Kenichi Oyaizu during 2002-2011.

The author would like to express the greatest acknowledgement of Professor Hiroyuki Nishide for his invaluable suggestions, discussion, and warmhearted encouragement through the work. The author would also like to express his sincere gratitude of Associate Professor Kenichi Oyaizu for valuable advice, useful discussion, and continuous encouragement. The author would like to thank all members in the Nishide/Oyaizu laboratory for their kind assistance.

The author is sincerely grateful to Professor Kalle Levon (Polytechnic Institute of New York University) and Associate Professor Toshiyuki Momma (Waseda University) for reviewing the thesis.

The author express the special thanks to collaborators in NEC Corporation, Dr. Shigeyuki Iwasa, Dr. Masahiro Suguro, Mr. Jiro Iriyama, Ms. Yukiko Morioka, Mr. Yuki Kusachi, Mr. Takanori Nishi, Mr. Tsuyosi Kato, and Mr. Motoharu Yasui for their useful discussion, advice, and assistance in experimental work. The author would also like to thank Dr. Masaharu Satoh, Dr. Etsuo Hasegawa, Dr. Yoshimi Kubo, Dr. Tsutomu Yoshitake, and Dr. Kaichiro Nakano for their fruitful discussion, advice, and management of the research.

The author is much obliged to Professor Elton J. Cairns (Lawrence Berkeley National Laboratory) for many helpful suggestions and discussions.

Finally, the author wishes to thank his parents Mr. Yutaro Nakahara and Mrs. Sachiko Nakahara, his wife Dr. Mayuko Nakahara those support him to achieve his work.

May 2011

Kentaro NAKAHARA